Tissue Characterization and Cancer Detection Based on Bioimpedance Spectroscopy

by

Sepideh Mohammadi Moqadam

B.Sc., University of Tehran, 2012

Thesis Submitted in Partial Fulfillment of the
Requirements for the Degree of
Master of Applied Science

in the
School of Mechatronic Systems Engineering
Faculty of Applied Sciences

SIMON FRASER UNIVERSITY

Spring 2015

Approval

Name:	**Sepideh Mohammadi Moqadam**
Degree:	**Master of Applied Science**
Title:	***Tissue Characterization and Cancer Detection Based on Bioimpedance Spectroscopy***
Examining Committee:	**Chair:** Siamak Arzanpour Associate Professor

Farid Golnaraghi
Senior Supervisor
Professor

Carolyn Sparrey
Supervisor
Assistant Professor

Woo Soo Kim
Internal Examiner
Assistant Professor
Mechatronic Systems Engineering

Date Defended/Approved: April 21, 2015

Partial Copyright License

Ethics Statement

The author, whose name appears on the title page of this work, has obtained, for the research described in this work, either:

a. human research ethics approval from the Simon Fraser University Office of Research Ethics,

or

b. advance approval of the animal care protocol from the University Animal Care Committee of Simon Fraser University;

or has conducted the research

c. as a co-investigator, collaborator or research assistant in a research project approved in advance,

or

d. as a member of a course approved in advance for minimal risk human research, by the Office of Research Ethics.

A copy of the approval letter has been filed at the Theses Office of the University Library at the time of submission of this thesis or project.

The original application for approval and letter of approval are filed with the relevant offices. Inquiries may be directed to those authorities.

Simon Fraser University Library
Burnaby, British Columbia, Canada

update Spring 2010

Abstract

Current research envisions improvement of breast cancer detection at early stages by adding a non-invasive modality, electrical impedance spectroscopy (EIS) to the detection procedure. The accuracy of clinical breast examination (CBE) is highly dependent on the clinician's experience. EIS enhances the physician's diagnostics capabilities by providing supplementary diagnostic information. Performing CBE besides EIS effects the electrical measurements of soft tissue. In this research the effect of the applied compression during CBE on the electrical properties is studied *in-vitro* and *in-vivo*. EIS is also tested over healthy and tumorous subjects. The correlation between tissue electrical properties and tissue pathologies is identified by offering an analysis technique based on the Cole-Cole model. Additional classification and decision making algorithms is further developed for cancer detection. This research suggests that the sensitivity of tumor detection will increase when supplementary information from EIS as well as the built-in intelligence is provided to the physician.

Keywords: Breast cancer detection; electrical impedance spectroscopy; decision making; classification; Cole-Cole model; non-invasive

To my beloved parents, sisters and brother, for all their supports and encouragements

Acknowledgements

I owe my deepest gratitude to Dr. Farid Golnaraghi, my senior supervisor, whose support, expertise and patience added considerably to my graduate experience. Without his constant and kind encouragement and guidance, this work was simply impossible.

My special thanks to my supervisor, Dr. Carolyn Sparrey, for her time, knowledge and fruitful discussion on this work.

I would also thank Dr. Kirpal Kohli and Dr. Paris Ingeldew for their helpful guidance in the clinical studies.

My special thanks to my parents and siblings, for their endless support, passion and encouragements throughout my academic career and my whole life.

This work has benefited from discussions, comments, and words of support from many colleagues and friends, notably: Pooya Amini, Badia Aghabeigi, Majid Shokoufi, Ehsan Daneshi, Parvind Grewal, Behzad Abdi and Shima Zaeimdar.

Last but not least, I am indebted to my great friends at BCEDL, NeuroSpine and Biomehcatronic research groups for their endless help and support they have given me throughout the whole program.

Table of Contents

Approval ii
Partial Copyright License iii
Ethics Statement iv
Abstract v
Dedication vi
Acknowledgements vii
Table of Contents viii
List of Tables x
List of Figures xi
List of Acronyms xiv

Chapter 1. Introduction 1
1.1. Background 2
1.1.1. Breast Cancer 2
1.1.2. Breast cancer detection techniques 3
1.1.3. Motivation 5
1.2. Literature review 5
1.2.1. Review of tissue electrical characterization 5
1.2.2. Review of tissue mechanical characterization 9
1.2.3. Review of mechanical-electrical properties relationships of soft tissue 10
1.2.4. Review of classification techniques in cancer detection 12
1.3. Research objectives 14
1.4. Thesis outline 15

Chapter 2. Experimental procedure 17
2.1. Experimental setups in *in-vitro* electro-mechanical study 17
2.2. Experimental setup for the *in-vivo* electro-mechanical study 22
2.3. Experimental setups in *in-vivo* cancer detection study 24

Chapter 3. Numerical analysis and classifications of data 27
3.1. Mathematical modeling of admittance data 27
3.1.1. Parameter fitting of three-element RC model in form of admittance 30
3.1.2. Parameter fitting of Cole-Cole model in form of admittance 31
3.2. Mechanical properties (elasticity) extraction method and indentation theory 32
3.3. Classification techniques 33
3.3.1. Naïve Bayes classifier with Gaussian or Kernel distribution 35
3.3.2. Support Vector Machines 37
3.3.3. Cross Validation 39

Chapter 4. Analysis of bioimpedance measurements and displacement-dependency of tissue electrical properties 41
4.1. Bioimpedance measurements 41
4.1.1. Comparison of two electrical impedance models 41
4.1.2. Evaluating the model by bode diagram 45
4.1.3. *In-vitro* measurements 47
4.1.4. *In-vivo* measurements 48
4.2. Mechanical displacements measurements 49
4.2.1. *In-vitro* measurements 49
4.2.2. *In-vivo* measurements 50
4.3. Tissue displacement-dependent electrical features 51

Chapter 5. Tissue classification 61
5.1. Validating the use of contralateral *in-vivo* sites as control 61
5.1.1. Admittance results of contralateral sites in healthy subjects 62
5.1.2. Assessing the use of contralateral extracted electrical features of healthy subjects 68
5.1.3. Admittance results of contralateral sites in tumorous subjects 72
5.1.4. Assessing the use of contralateral extracted electrical features of tumorous subjects 75
5.2. Classification methods 77

Chapter 6. Discussion 82

Chapter 7. Conclusion and future work 91

References 94
Appendix A. Standard operation procedures- preparation of animal tissue samples 102
Appendix B. Standard operating procedures-performing electrical impedance spectroscopy measurements as well as compression testing on animal tissue specimens 104

List of Tables

Table 2.1. Case studies recruited for testing the proposed method on cancerous subjects and their information 26

Table 4.1. Averaged Cole-Cole parameters extracted by the LAD method at the first pressure level and standard deviations, including the error values representing one standard deviation of uncertainty 48

Table 4.2. Averaged Cole-Cole parameters extracted by the LAD method at the first pressure level and standard deviations 49

Table 4.3. The average displacements of chicken and rat breast samples and standard deviations 50

Table 4.4. The average displacements of left and right forearms and biceps of 10 human subjects and standard deviations 51

Table 4.5. The correlation of normalized Cole-Cole parameters 60

Table 5.1. The performance of various classification methods on raw and processed data 81

List of Figures

Figure 1.1. Breast Anatomy....3

Figure 1.2. Electrical impedance measurements: a) bipolar measurement b) tetrapolar measurement....7

Figure 1.3. Schematic of the α, β and γ dispersion regions for biological tissue [21]....9

Figure 2.1. HF2IS Impedance Spectroscope from Zurich Instruments....19

Figure 2.2. HF2TA Current Amplifier from Zurich Instruments....19

Figure 2.3. Left: the chicken sample and the Ag/AgCl electrodes. Right: Finger TPS wearable pressure sensors by PPS....21

Figure 2.4. The exploded view of the probe containing electrical impedance electrodes as well as temperature sensors....23

Figure 2.5. Design of the probe in SolidWorks and the prototype....24

Figure 2.6. Use of probe and the pressure sensors over human tissue....24

Figure 3.1. Three-element RC model circuit....28

Figure 3.2. Imaginary part of admittance versus its real part (three-element RC model)....28

Figure 3.3. Cole-Cole model circuit....29

Figure 3.4. Imaginary part of admittance versus its real part (Cole-Cole arc)....29

Figure 3.5. Paths of high and low frequency currents in a biological tissue....30

Figure 3.6. The optimal hyper-plane marked with a solid line between group A (●) and group B (▲) after support vector machine calibration. The observations on H1 and H2 are called the support vectors as they support the two sub hyper-planes. 38

Figure 4.1. Cole-Cole model and Three-element RC model fitted to admittance data points of 11 healthy subjects (forearms and biceps data) 44

Figure 4.2. Bode diagram of soft tissue resulted from the phase and magnitude of the measured admittance. a) Upper figure: magnitude of admittance over frequency. b) Lower figure: phase of admittance over frequency....46

Figure 4.3. Bode plot of soft tissue generated based on the extracted features and calculated zeros and poles of the system....47

Figure 4.4. Stress versus relative indentation of *in-vitro* chicken sample [55]....50

Figure 4.5. Stress versus relative indentation of *in-vivo* bicep of subject 1 [55]....51

Figure 4.6. Chicken breast tissue, the correlation of compression-dependent Cole-Cole parameters normalized to their values at the first pressure level and tissue displacements: (a) Normalized extracellular resistance versus tissue displacement (b) Normalized intracellular resistance versus tissue displacement (c) Normalized membrane capacitance versus tissue displacement 54

Figure 4.7. Rat breast tissue, the correlation of compression-dependent Cole-Cole parameters normalized to their values at the first pressure level and tissue displacements: (a) Normalized extracellular resistance versus tissue displacement (b) Normalized intracellular resistance versus tissue displacement (c) Normalized membrane capacitance versus tissue displacement 55

Figure 4.8. Left Forearm Tissue, the correlation of compression-dependent Cole-Cole parameters normalized to their values at the first pressure level and tissue displacements: (a) Normalized extracellular resistance versus tissue displacement (b) Normalized intracellular resistance versus tissue displacement (c) Normalized membrane capacitance versus tissue displacement 56

Figure 4.9. Right Forearm Tissue, the correlation of compression-dependent Cole-Cole parameters normalized to their values at the first pressure level and tissue displacements: (a) Normalized extracellular resistance versus tissue displacement (b) Normalized intracellular resistance versus tissue displacement (c) Normalized membrane capacitance versus tissue displacement 57

Figure 4.10. Left Bicep Tissue, the correlation of compression-dependent Cole-Cole parameters normalized to their values at the first pressure level and tissue displacements: (a) Normalized extracellular resistance versus tissue displacement (b) Normalized intracellular resistance versus tissue displacement (c) Normalized membrane capacitance versus tissue displacement 58

Figure 4.11. Right Bicep Tissue, the correlation of compression-dependent Cole-Cole parameters normalized to their values at the first pressure level and tissue displacements: (a) Normalized extracellular resistance versus tissue displacement (b) Normalized intracellular resistance versus tissue displacement (c) Normalized membrane capacitance versus tissue displacement 59

Figure 5.1. Admittance plots of the healthy biceps and their contralateral part 65

Figure 5.2. Admittance plots of the healthy forearms and their contralateral part 67

Figure 5.3. Comparison of the electrical parameters of right and left bicep of healthy subjects 70

Figure 5.4. Comparison of the electrical parameters of right and left forearm of healthy subjects 71

Figure 5.5. Admittance plot of the tumorous subjects and the contralateral healthy part 74
Figure 5.6. Comparison of the electrical parameters of the tumorous tissue and its contralateral healthy tissue in cancerous subjects 76
Figure 5.7. The raw admittance data of healthy and cancerous subjects 78
Figure 5.8. The representation of three extracted electrical properties of 32 subjects (22 healthy subjects and 10 cancerous subjects). Each axis indicates one of the electrical parameters 79
Figure 5.9. The representation of three normalized extracted electrical properties of 32 subjects (22 healthy subjects and 10 cancerous subjects). Each axis indicates one of the normalized electrical parameters to its contralateral values 80
Figure 5.10. Comparison of the performance of 3 classification methods on the data 81

List of Acronyms

Term	Initial components of the term
ANN	Artificial Neural Network
ANOVA	Analysis of Variance
CBE	Clinical Breast Examination
EIS	Electrical Impedance Spectroscopy
ELM	Extreme Learning Machine
GA	Genetic Algorithms
LAD	Least Absolute Deviation
LSM	Least Square Method
MRI	Magnetic Resonance Imaging
PCA	Principal Component Analysis
REIS	Resonance-frequency Electrical Impedance Spectroscopy
STSM	Soft Tissue Stiffness Meter
SVM	Support Vector Machine

Chapter 1.

Introduction

Breast cancer is by far the most common of all cancer types among women [1] and the second most common cancer worldwide. Overall, 10.9% of all cancer patients suffer from breast cancer. Although breast cancer is the fifth cause of mortality due to cancer, it is still the most significant cause of cancer death among women. Breast cancer statistics reveals that in 2012, nearly 1.7 million new cases of breast cancer were diagnosed (World Cancer Research).

Most patients diagnose a lump in their breast when it is already quite large [2]. At this stage the standard screening tool for breast cancer is the X-ray mammogram. Although mammograms can identify the suspicious area, the character of these areas is not conclusive [3]. Therefore, either a fine needle biopsy [4] or a core biopsy [5] is needed to characterize the malignancy. The biopsies have many drawbacks; they are invasive, expensive and a great percentage of biopsies results show that the suspicious tissues are not malignant.

The best defence against cancer is early diagnosis. Some non-invasive techniques such as mammography, ultrasound and Magnetic Resonance Imaging (MRI) play a vital role in early diagnosis. However, there are some limitations which are the barriers for a wider use of such techniques in terms of their size, weight, expenses, sensitivity and specificity. Moreover, due to the subjective nature of the traditional palpation technique, its accuracy can range from good to poor depending on the experience of the clinician. These problems in the common methods of breast cancer detection, considerably supports the demand for developing a new non-invasive and reliable technology for breast cancer diagnosis, which is not physician dependent and has a high sensitivity and specificity.

1.1. Background

1.1.1. Breast Cancer

A woman's breasts extend from approximately the level of the second rib to the level of the sixth rib and sit over the pectoral major muscle. The breasts cover a large part of the chest wall. The human female breast which is an inhomogeneous structure consists mainly of mammary glands, adipose (fat) and connective tissues. As illustrated in Figure 1.1 the mammary gland is usually in a cone shape where the chest wall constructs its base and the nipple forms its peak. A 0.5–2.5 cm layer of subcutaneous fat separates the superficial layer (fascia) from the skin. Fibrous tissue extends in all directions from this fascia to the skin. The breast and the deep fascia are separated by a layer of connective tissue, allowing some degree of motion for the structure.

Cancer is a disease which consists of division of abnormal cells without control. Blood and lymph systems can help cancerous cells spread to other parts of the body. The uncontrolled growth of breast cells is called Breast Cancer. The breast tumors are either benign or malignant. Sometimes the breast cells start to change and no longer grow or behave normally. These changes may lead to benign breast conditions which are not cancerous. The malignant breast tumor is a type of cancer that can spread, or metastasize, to other parts of the body.

The most common types of breast cancer are ductal carcinoma and lobular carcinoma. The ductal carcinoma starts in the cells that line the ducts, which are the tubes that carry milk from the glands to the nipple. While lobular carcinoma starts in the cells of the lobules, which are the groups of glands that make milk. Both ductal carcinoma and lobular carcinoma can be in situ or invasive. This means that these two types of breast cancer either do not spread into surrounding tissue or can spread to other organs. Less common types of breast cancer include inflammatory breast cancer, paget disease of the nipple and triple negative and basal-like breast cancers. Rare types of breast cancer are non-hodgkin lymphoma and sarcoma.

Figure 1.1. Breast Anatomy
(Source: Wikimedia Commons. Patrick J. Lynch and C. Carl Jaffe. Licensed under CC-BY 3.0 http://commons.wikimedia.org/wiki/File:Breast_anatomy_normal.jpg)

1.1.2. Breast cancer detection techniques

Considering the commonality of breast cancer among women worldwide, a large number of breast cancer examination and detection methods have been introduced and commercialized. Breast cancer detection methodologies can be divided into the three categories: screening tests, diagnostic tests and monitoring tests. Women who appear to be healthy, are advised to be given routine screening tests (such as yearly mammograms) in order to detect breast cancer in early stages, when the cancer usually is easier to treat. Thereafter, women who are suspected of having breast cancer are tested by diagnostic tests (such as biopsy). The diagnostic tests are used to detect breast cancer, collect more information about the type of cancer and also determine if the cancer has metastasized. Monitoring tests are used when the breast cancer is diagnosed. They are used during and after treatment to monitor the performance of therapies.

One of the most common and traditional methods of breast examination is clinical breast examination (CBE). This type of examination is performed by physicians who check the normality of the breast by palpation and also by visual inspection. Since the mechanical characteristics of the lesions are different from the healthy tissue, i.e. the lesions are much stiffer than healthy tissue, the physician can feel the abnormality by performing palpation [6]. Due to the subjectivity of this method, the accuracy of this detection technique may vary from poor to good depending on the physician's experience. Once CBE detects a suspicious lesion in a subject, it will be validated through mammography [6].

The best examination tool for breast cancer detection at early stages is mammography [7]. In mammography, the breast is compressed in order to reduce the thickness, so that the emitted X-ray beam can pass through the whole breast tissue. When the X-ray beam is emitted to the tissue, a film placed on the other side of tissue records the response of the breast tissue to the emitted X-ray [6]. Although mammography has been effective in reducing breast cancer mortality rate, there are many drawbacks in using mammography such as its high cost, the high incidence of unnecessary biopsies and the quality of interpretation of mammograms based on the experience of the radiologists [8].

A very sensitive method of breast cancer imaging is magnetic resonance imaging (MRI). In MRI, the alignment of hydrogen nuclei with a magnetic field and radio waves is changed and 2D and 3D images from cross sections of the breast are obtained. MRI has many advantages compared to other breast cancer detection methods while it has its drawbacks as well. One of the most important advantages of MRI is that it has the highest sensitivity among all breast cancer detection techniques and the density of the breast does not reduce its sensitivity. However, this technique is quite expensive and the specificity is low.

The sensitivity and specificity for CBE are recorded as 57.14% and 97.11%. These values for mammography for dense breast examination are 62.9% and 89.1%. MRI has sensitivity of 66.7% and specificity of 64.3%. In spite of high false-positive probability of MRI, it has a high capability of 93.7% in cancer detection [6].

1.1.3. Motivation

Bearing in mind the commonality of Breast Cancer and the high survival rate if diagnosed at early stages, there is a need to develop a new non-invasive, cost effective, reliable and objective methodology to be replaced by the traditional subjective process of CBE. One promising avenue of research for diagnosing breast cancer accurately, non-invasively, and potentially at an earlier stage is electrical impedance (EI). Various studies have shown a statistically significant difference in electrical impedance of cancerous breast and normal breast [9][10][11][12].

Consequently, developing an intelligent device consisting of electrical impedance electrodes was envisioned through this study. The overall purpose of this study is to utilize the multi-frequency electrical impedance spectroscopy (EIS) system as well as decision making algorithms in order to devise a system which can automatically detect the cancerous breast.

1.2. Literature review

1.2.1. Review of tissue electrical characterization

The electrical properties of biological tissue are highly dependent on its structure. Biological tissue which consists of an aggregation of cells surrounded by extracellular fluids exhibit the properties of both conductors and dielectrics. In each cell, the intracellular fluid is surrounded by a membrane. The intracellular and extracellular fluids that consist mainly of water and electrolytes, show resistive behaviours. The semi-permeable membrane, constituted by a thin lipid bilayer, acts like an electrochemical membrane and contains leaky ion-channels [13]. Therefore, it shows both capacitive and resistive behaviours. Since electrical impedance, Z, which is the tissue's opposition to the flow of electric current, contains both resistance and capacitance, it is a complex measure of two components: resistance, R (ohm) and reactance, X (ohm). Electrical impedance which is the inverse of electrical admittance, A, is the ratio between the alternating voltage and the alternating current, described by Ohm's law.

Non-invasive electrical impedance spectroscopy (EIS) is a measure of the electrical properties of tissue made through surface measurements. Bioimpedance measurement is a non-invasive method for investigating tissue structure and physiological changes in soft tissue. The use of electrical impedance spectroscopy as a cancer detection technology has become a topic of great interest for researchers since 1926.

Fricke and Morse observed a higher capacitance in breast malignant tumors in comparison with the healthy breast [14]. Later in 1990, Morimoto *et al.* studied the electrical impedance of breast tumors *in-vivo* and calculated the intracellular resistance, the extracellular resistance and cell membrane capacitance of normal and pathological tissue based on the impedance spectra at a frequency range of 0 to 300 kHz and a circuit model [9]. They reported a statistically significant increase in the intra- and extracellular resistances and a statistically significant decrease in the membrane capacitance in the pathological tissue. Jossinet *et al.* performed an experiment on 64 subjects with normal, benign and carcinoma breast tissues [15]. Jossinet compared the complex impedance loci of normal and carcinoma in a frequency range of 488 Hz to 1 MHz and an obvious difference was observed in the shape and location of the loci at frequencies above 125 kHz. Keshtkar *et al.* performed electrical impedance measurements on 38 *in-vivo* benign and malignant subjects at a frequency range of 2-348 kHz [12]. The results revealed that the impeditivity of the malignant subjects were significantly higher than the impeditivity of benign subjects which was in contrast to the results presented by Brown *et al.* [16] and Gonzales-Correa [17].

Kim *et al.* [11] developed a new analysis technique on the admittance of freshly-excised malignant breast tissue and its surrounding normal tissues which resulted in a clear distinction between the pathological and normal tissues. In a study conducted by Laufer *et al.* [10], the Cole-Cole model, which is an electrical circuit equivalent model consisted of one resistor in parallel with a resistor and a capacitor which are in series [18], was fitted to the impedance data and the four parameters of Cole-Cole model were compared in the cancerous and normal liver tissue. Obtaining the parameters of the Cole-Cole model gave a better understanding of the tissue in cellular level. The results

illustrated that the conductivity of cancerous tissue was much higher than that of normal tissue.

A common conclusion can be drawn from these in-vitro and in-vivo electrical impedance studies; it can be concluded that the electrical properties of normal tissue differ significantly from the electrical properties of malignant tissue. Electrical impedance of biological tissue could thus be a potential indicator for cancer detection.

The electrical properties of tissue can be measured by two different electrode setups: bipolar and tetrapolar techniques (Figure 1.2). In bipolar technique, the electrical current is applied to the tissue by the reference electrode (A1) and the resultant voltage is measured by the other electrode attached to the tissue (A2). In the tetrapolar measurement method, the current from the source passes through the two outer electrodes (A1 and A2) and then to the tissue. The two inner electrodes are placed on the tissue between the current electrodes and measure the voltage (R1 and R2). In both methods, one can determine the impedance and admittance of tissue, by measuring the current and the voltage drop.

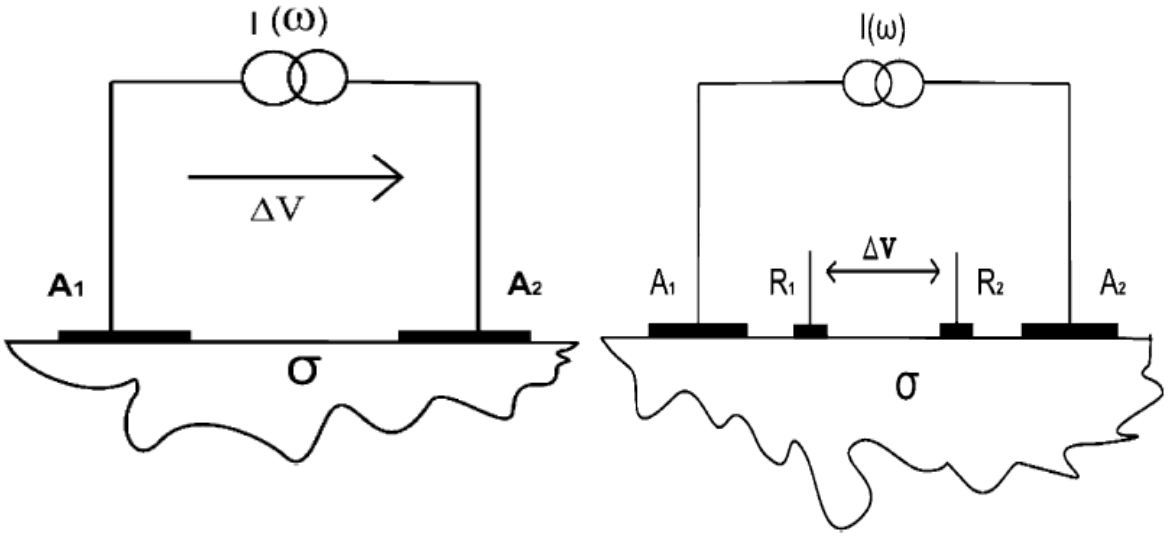

(a) (b)

Figure 1.2. Electrical impedance measurements: a) bipolar measurement b) tetrapolar measurement

Bioimpedance measurement is also performed either by multi frequency or single frequency methods. The multi frequency parameter mapping compared to the single frequency parameter mapping provides a novel vision to study bioimpedance signals [19]. Frequency sweeping is a better technique, since it results in identifying the points of interest in the frequency spectrum such as poles and zeros of the system. Knowing these points are of utmost importance, since they are used to characterize the system. Frequency sweeping consists of applying a stimulus signal at various frequencies and then measuring the systems response to the frequencies. Various types of frequency sweeps are available: linear frequency sweep, logarithmic frequency sweep, segmented frequency sweep and harmonic frequency sweep.

In electrical impedance spectra of biological tissue, the electrical impedance generally decreases with increasing frequency except for some regions where the electrical impedance remains constant with increasing frequency. These constant electrical impedance areas in the spectra, creates three major frequency regions, shown in Figure 1.3. In impedance spectra, the areas where the impedance is decreasing, i.e. the steep slopes in Figure 1.3 are called dispersion regions. Schwan identified three major dispersion regions in bioimpedance spectra, the α-, β- and γ-dispersions [20]. The α-dispersion (Hz to tens of kHz) reflects mainly polarisation of ionic clouds around the cells. The β-dispersion (kHz to hundreds MHz) contributes to the structural membrane changes, oedema, and polarisation of the cell membranes affect. The γ- dispersion (over hundreds MHz) reflects relaxation of water and other small molecules. Therefore, the β-dispersion often contains most of the clinically relevant information.

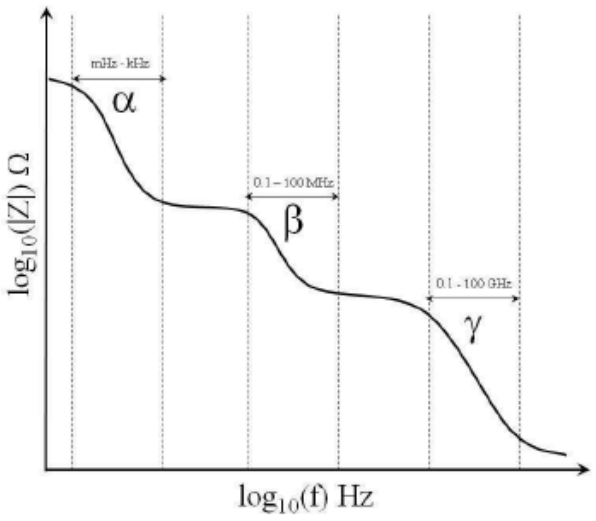

Figure 1.3. Schematic of the α, β and γ dispersion regions for biological tissue [21]

1.2.2. Review of tissue mechanical characterization

The alteration of soft tissue elastic stiffness in abnormal breast tissue was identified long ago [22]. In clinical examinations, the alteration of soft tissue elasticity is mostly evaluated by manual palpation which is clinician-dependent and subjective. However, several researchers have proposed new objective techniques for evaluating the soft tissue consistency. Fischer introduced a device to quantify palpation of tissue in an objective manner [23]. He suggested the use of tissue compliance meter in order to monitor the variation in soft tissue elasticity when there is a malignancy in the tissue. Other researchers suggested techniques based upon pressure distribution measurements made at the surface of the tissue [24] [25]. In these techniques, an array of pressure sensors is mounted on a rigid scanhead to record the surface pressures resulting from pressing the scanhead into the tissue. Geometric distribution of the stiffness of the pressed underlying tissue is quantified by these methods [26].

Although these methods provide useful information on the elastic features of the tissue, some researchers were looking for the elasticity of the tissue by means of imaging techniques. Many techniques have been proposed for examining abnormal breast tissue based on imaging the elastic contrast [27] [28]. Most imaging techniques record the images of the tissue at two different applied forces and then the displacement

of the tissue is measured. Given the applied force and the displacement of soft tissue, its stiffness can be computed. In other studies conducted by Zhang *et al.*, the indentation stiffness of soft tissue was assessed by an ultrasound indentation pen-size probe [29]. MRI is also a promising non-invasive technique which contributes to measurement of tissue stiffness by measuring the propagation of elastic shear waves [30].

Soft tissue behavior is mostly close to behavior of viscoelastic materials. However, in order to develop a mathematical model for behavior of soft tissue using a single elastic or shear modulus, most researchers have assumed that soft tissue is isotropic, elastic [31] [32] [25] [29] and nearly incompressible [33].

Under these assumptions, Sarvazyan *et al.* reported a study of 150 specimens of normal and cancerous tissues which showed that cancer can be as much as 7 times stiffer than normal tissue [25]. Wellman *et al.* demonstrated that there is a correlation between elastic modulus in compression and histological diagnosis [24]. They computed the elastic moduli of both normal and abnormal breast tissues from the nominal stress–nominal strain data resulting from force displacement data measured during punch indentation tests. In another study, a novel, easy-to-use soft tissue stiffness meter (STSM) which is based on the principle that the resistance of tissue to the applied force by the indenter, is an indicator of the tissue compressive stiffness is introduced [34]. However, the principle of this stiffness measuring system is similar to the indentation instrument developed earlier for the measurement of cartilage stiffness under arthroscopic control [35].

1.2.3. Review of mechanical-electrical properties relationships of soft tissue

Electrical and mechanical properties of tissue play a prominent role in tumor detection [24], [36]–[38]. Pathology in soft tissue changes the stiffness of its local area [39]. Stiffness of soft tissue which is different in tumor and its surrounding healthy tissue can be estimated by measuring the applied external load to the body surface and its resultant displacement [40]. Besides, Jossinet *et al.* and Stuchly *et al.* have shown that anomaly conductivity is significantly different from normal tissues conductivity [38], [41].

However, the link between tissue mechanical and electrical properties and, their correlation to pathological fluctuations remains unclear.

Much research has been performed independently on the mechanical and electrical properties of soft tissue and the effect that tissue pathology has on these properties. In the majority of breast examinations, the palpation method is used to examine the breast [6], thus characterizing the compressive behavior of soft tissue provides insight into the mechanisms of tissue pathology. Fung *et al.* [33] identified the effect of pathological fluctuations on the elastic characteristics of the microscopic and macroscopic structural organization of tissue. Moreover, Fricke and Morse found that the capacitance of pathological tissue is significantly different from normal tissue [42]. Recently new electrical impedance imaging technologies for breast cancer detection have been proposed which detect tissue tumors by means of measuring electrical properties of tissue. Although a lot of studies have focused on electrical and mechanical properties of healthy and cancerous tissue, the correlation of electrical and mechanical properties in healthy and tumorous tissue were not established and compared.

Soft tissue properties change due to tissue compression [43]. Different types of tissue have diverse compressive behaviors. Little within the literature has been published regarding the effect of compressive behavior of soft tissue on the changes of electrical properties. Gonzalez *et al.* [44] showed that not only by increasing the applied pressure the resistivity increases, but also the difference in the changes of properties of two types of tissue was sizeable. Belmont's test [45] on a soft tissue mimicking phantom showed a decrease in the admittance of phantom under compression. Dodde *et al.* [43] studied the electrical properties of tissue under compression in the cellular level. A non-linear behavior was reported by Dodde *at al* compression level around 60%.

The purpose of the present study is to find the variation in tissue electrical properties with varying soft tissue displacements. We postulate that electrical properties of tissue are related to the mechanical properties and also any type of tissue has a specific electrical-mechanical properties based model. Since tumors in soft tissues change both electrical and mechanical properties of tissue, it is also postulated that healthy and tumorous tissues have different electrical-mechanical correlation. Thus by

finding this relationship and model, the structure, type and abnormality of tissue can be estimated. Therefore presence of inhomogeneity in soft tissue and its effect on the electrical-mechanical behaviour of tissue may help to develop a tumour detection technique.

To test the validity of this claim, various types of *in-vivo* and *in-vitro* tissues are mechanically and electrically tested. As compared by [46], one model which fits to the measured data well is the Cole-Cole model [47]. The elasticity of the tested tissues is calculated from the linear relationship of engineering stress-strain graphs. The effect that compression has on the electrical properties of tissue and also the relationship between electrical features and tissue displacement is elaborated in this study.

1.2.4. Review of classification techniques in cancer detection

As explained in the previous sections, EIS is a non-invasive technique capable of assisting the physician in the process of abnormality detection in patients. However, classification techniques are needed in order to assist the healthcare professionals in the diagnostic decision-making process.

There are two major steps in the intelligent anomaly diagnosis process: the feature extraction and selection or data reduction, and the decision-making (diagnosis). The feature extraction or data reduction is used to reduce the large set of variables into a small set of variables which account for most of the information in the measurements. Common methods for feature extraction and data reduction include modeling the tissue as an electrical equivalent model or computationally transforming the data into a set of uncorrelated components using principal component analysis (PCA). [48] The decision-making process includes using various classification methods such as artificial neural networks (ANN), support vector machines (SVM), linear discriminant analysis, naïve Bayes (NB) methods and many other techniques.

Several studies have proposed methods for tissue classification based on EIS. Esterla da Silva *et al.* reduces the data by extracting 9 features from the electrical impedance spectra and used a linear discriminant analysis for classification. This linear classifier performed better than approaches such as neural nets or K-nearest neighbor

classifiers, since the latter methods are quite demanding on the size of the training sets [49]. Ledermn *et al.* assessed the performance of resonance-frequency electrical impedance spectroscopy (REIS) by means of ANN, SVM and Gaussian mixture model (GMM). The electrical impedance data of 140 breast cancerous women in the frequency range of 200-800 kHz were measured and afterwards data reduction was performed by means of genetic algorithms (GA). These reduced features as well as participant's age and breast density were used for training the ANN and classification of the subjects. The results of this study showed that ANN yielded the highest performance among the three classification methods [50].

In a study conducted by Bharati and Natarajan, an efficient classification technique combining SVM) and extreme learning machines (ELMs) was proposed [51]. In this proposed method, the important genes were ranked by means of analysis of variance (ANOVA) and then used for training SVM. Afterwards, the ELM was used to increase the classification accuracy. Also Daliri proposed a hybrid classification system based on AVM and ELM classifiers. However, he presented his approach for breast cancer classification based on features extracted from EIS [52]. He extracted 9 features from electrical impedance spectra and selected some of these features which were more relevant in breast cancer classification in the feature selection phase. Several ELMs were trained based on these selected features and the outputs were combined using SVM in order to classify the data.

Amin *et al.* performed electrical impedance spectroscopy on 19 patients who had single or multiple tumors in one or both breasts [53]. The 12 features selected by this group displayed considerable overlap between malignant and benign cases which were separated by dividing each feature by their respective subjects' ages. Using K-NN classification method a sensitivity of 75% and a specificity of 87% was resulted. The results presented by Wu *et al.* reveal that Naïve Bayes fusion effectively reduces the mean-squared errors and the classification accuracy is improved by 15% [54].

The purpose of this study is to distinguish between the EIS data of cancerous and healthy subjects. In order to achieve this goal, the data reduction and feature extraction is performed by describing the electrical properties of both anomaly and

normal tissue by an electrical equivalent circuit, Cole-Cole model. Afterwards, several classifiers were trained for malignancy diagnosis and the SVM and naïve Bayes methods appeared to give more reasonable discrimination; however, the data set in this study is quite small.

1.3. Research objectives

The primary objective of the present study is to find the variation in soft tissue electrical properties with varying tissue displacements. In other words the purpose is to characterize the electrical properties of tissue under compression and correlate the changes in electrical properties to the mechanical displacements of tissue resulting from the applied pressure. We postulate that the electrical properties of tissue are related to the mechanical properties and also any type of tissue has a specific electrical-mechanical properties based model. The electrical properties of tissue as well as the mechanical properties of tissue play a significant role in diagnosis and monitoring of cancer. Much research has been performed independently on the mechanical and electrical properties of soft tissue and the effect that tissue pathology has on these properties. Although a lot of studies had focused on electrical and mechanical properties of healthy and tumorous tissue, the correlation of electrical and mechanical properties in healthy and tumorous tissue were not established and compared. Since tumours in soft tissues change both electrical and mechanical properties of tissue, it is also postulated that healthy and tumorous tissues have different electrical-mechanical correlation. Thus by finding this correlation and model, the structure, type and abnormality of tissue can be estimated. Therefore presence of inhomogeneity in soft tissue and its effect on the electrical-mechanical behaviour of tissue may help to develop a tumour detection technique.

Another key objective of this study is to characterize the electrical properties of cancerous subjects and accordingly develop an intelligent method for the purpose of cancer detection based on the electrical properties of abnormality. Previous studies within literature [9] [10] [12] have proven that there is a significant variation in the electrical properties of malignant tissue and healthy tissue. In order to achieve this goal, the electrical properties of malignant and healthy subjects are extracted from the multi-

frequency electrical impedance measurements and then classified into two groups by means of various classification methods.

The secondary objectives accomplished throughout this process include:

- Development of an electrical impedance measuring probe
- Modeling the electrical impedance data of tissue and extracting electrical features of measured tissue
- Comparing the lesion electrical impedance and its contra-lateral healthy tissue electrical impedance as the control
- Training, testing and evaluating various classifier methods for the purpose of malignancy classification and evaluating the accuracy of each method

1.4. Thesis outline

Chapter one gives an overview of breast cancer and the detection techniques utilized for diagnosis of the breast cancer and also the motivation of this study in section 1.1. Section 1.2 is focused on the literature review of this thesis. This study includes four parts; electrical, mechanical, electro-mechanical and the classifications. Therefore, the literature review has been divided into four sections. The chapter ends with the research objectives and the outline of this thesis.

Chapter two expands the experimental procedures of the *in-vitro* and *in-vivo* experiments. The experimental setups for the mechanical and bioimpedance measurements are explained in this chapter.

The mathematical modeling and also the classification methods used in this study are explained in chapter three. The two models used for bioimpedance data are introduced in section 3.1. Section 3.2 gives an overview of the mechanical part of this study and elasticity extraction methods are explained. The final section of this chapter, section 3.3, introduces the classification techniques used in this study.

Chapter four represents the electrical results, mechanical results and finally electro-mechanical results of both *in-vitro* and *in-vivo* experiments. In section 4.1, the bioimpedance results are represented and the best model is selected. Thereafter, the

elasticity of *in-vitro* and *in-vivo* samples and subjects are extracted (section 4.2). This chapter ends with a section explaining the correlation of electrical and mechanical properties of soft tissues tested.

Chapter 5 represents validating the idea proposed within this study in which the contralateral sites of body can be used as the controls for the purpose of cancer detection. In section 5.2, the classification techniques are implemented on the bioimpedance data of contralateral sites and the performance of each technique are discussed.

Finally the conclusion, discussion and future work of the research work has been elaborated in chapter six and seven.

Chapter 2.

Experimental procedure

This study follows two overall objectives. The first objective is to characterize soft tissue response to the electrical impedance spectroscopy under compression and benefit from the resultant response for the purpose of cancer detection. In this chapter, the experimental setups, devices and procedures for electrical and mechanical measurements in both *in-vitro* and *in-vivo* studies are explained. Bioimpedance of *in-vivo* and *in-vitro* tissue were measured during electrical experimental procedures with two different setups, which will be explained in the following sections of this chapter. The second objective of this study is to perform *in-vivo* measurements on healthy and cancerous human subjects and distinguish the cancerous subjects from the healthy subjects by means of classification techniques. The details of each experimental procedure will be discussed in this chapter.

2.1. Experimental setups in *in-vitro* electro-mechanical study

This section describes the experimental setup used for the *in-vitro* electro-mechanical study. The electro-mechanical study was performed with two different setups, a bioimpedance measurement setup arranged in this study and a mechanical setup utilized in a previous study by Zaeimdar [55]. Twenty chicken samples from ten chicken breasts and two rat samples from two rat breasts were dissected for the *in-vitro* electro-mechanical study. Although the tested samples in the two bioimpedance and mechanical setups were dissected from the same animal tissue to assure consistency in results, the size of the samples were not the same in both types of experiments because of the limits in each experimental setup. The electrical study will be elaborated in this section and the mechanical results from the study conducted by Zaeimdar [55] will be

utilized for the electro-mechanical analysis. In this section the sample dissection procedure is also explained.

The bioimpedance measurements of this study were conducted by incorporating an impedance spectroscope HF2IS, along with a transimpedance amplifier HF2TA (TA) by Zurich instrument (Zurich Instrument Inc., Switzerland).

- **Impedance spectroscope HF2IS**

The Zurich instruments HF2IS which is a high-frequency impedance spectroscope with 2 inputs , has a frequency range from 0.7 μHz to 50 MHz with 210 MSamples/s (mega samples /sec). This sampling rate is 4 times the analog bandwidth to ensure full capture of signal and avoid aliasing, 14 bit AD conversion, and allows 8 frequencies mapping simultaneously. With up to 8 demodulators the HF2IS allows simultaneous measurements at 8 frequencies and with 2 physical input channels accommodates readily for 2/3/4-terminal configurations. This device is capable of performing dynamic multi-frequency measurements with very high sensitivity and precise static impedance measurements in applications where precision and speed matter. HF2IS has two differential measurement units with a wide frequency range and 4 dual-phase demodulators, along with a high precision 128-bit DSP engine. This enables HF2IS to analyze the frequency response of noisy and low-voltage systems. The 2 input paths of the HF2IS are optimized for very-low noise operation and the 2 high-frequency outputs are generated as a linear combination of up to 8 sinusoids in the range from DC to 50 MHz. The amplitude and the frequency can independently be set for each component. Configurable filter properties include time constant from 1 μs to 500 s (corresponding to bandwidths from 80 μHz to 200 kHz) and filter order from 1st to 8th. The advantages of this device over common analog instruments are higher dynamic reserve, zero drift, and accurate phase shifts. An integrated oscilloscope with memory for 2048 samples provides direct signal versus time and spectral views on the input signal. Moreover a frequency-response sweeper provides accurate signal versus frequency plots.

Figure 2.1. HF2IS Impedance Spectroscope from Zurich Instruments
(Source: Zurich Instruments has all rights, http://www.zhinst.com/products/hf2is)

- **HF2TA current amplifier**

The HF2TA is a current amplifier which converts the input current from the tissue to the output voltage that is measured in the impedance spectroscope in a frequency range of up to 50MHz. Since this device is an active probe, it can be placed close to the measurement setup. Providing 2 input and 2 output connectors, the HF2TA features transimpedance architecture with a variable precision resistor as gain parameter (R). The transimpedance architecture matches the current through the feedback resistor and keeps the input at virtual ground. The second amplification stage provides decoupling from the first stage and an additional gain (G). The resulting output voltage corresponds to U = R * G * I. The combination of HF2TA current amplifier along with HF2IS ensures stability, high performance measurements, insensitivity to interference and a smooth operation over the entire frequency range.

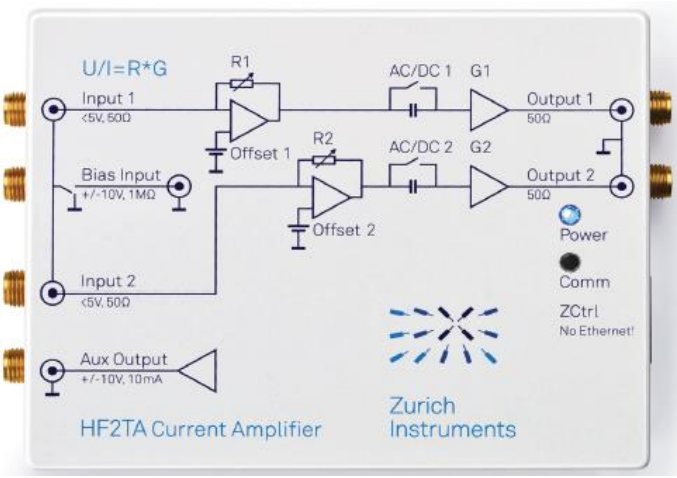

Figure 2.2. HF2TA Current Amplifier from Zurich Instruments
(Source: Zurich Instruments has all rights, http://www.zhinst.com/products/hf2preamps/hf2ta)

A frequency response sweeper was integrated into the HF2IS. The H2FIS Impedance Spectroscope along with the HF2TA current amplifier was used to take EIS readings in terms of complex admittance over a selected frequency sweep. The admittance data points over the frequency sweep are further used to perform the post-processing and analysis.

The tissue bioimpedance can be measured by means of this impedance spectroscope via two methodologies: two-point measurement and four-point measurement. In the current study, the two-point measurement was selected for data collection. In the two-point measurement, the current is applied to the tissue by one electrode and the other electrode measures the resulting voltage. In this study a different type of two-point measurement was incorporated; the HF2IS generated a voltage signal of 1V pick-to-pick and transferred this voltage to the tissue by means of the reference electrode. The measuring electrode attached to the other side of tissue measured the resulting current and transfers it to the HF2IS by means of a HF2TA current amplifier. Considering the advantages of multi-frequency mapping in EIS, multi-frequency bioimpedance measurement was incorporated in this study.

In the *in-vitro* experiment, twenty chicken samples excised from 10 chicken breasts and two rat samples excised from two rat breasts were chosen. Samples were cut in a cubic form using a sharp cutter from the same parts of the animals' breast to assure consistency in the results. The size of samples was 4cm, 3.5cm and 2cm in length, width and thickness respectively. All the *in-vitro* measurements were performed within 1-2 hours after excitation at ambient temperature consistent with other studies [56]. For *in-vitro* bioimpedance measurements, two Ag/AgCl pre-gelled electrodes from Vermed (Vermed Inc., USA) were placed at two opposite sides of the cubic samples (one electrode at the bottom and one electrode at the top sides of the samples). By means of wearing finger wearable capacitive pressure sensors on the examiner's fingers, 6 constant force levels (0.5, 1, 1.5, 2, 2.5 and 3lb) were applied to the electrodes. While keeping the pressure constant at each level, the multi-frequency bioimpedance data was collected in three trials.

Figure 2.3. Left: the chicken sample and the Ag/AgCl electrodes. Right: Finger TPS wearable pressure sensors by PPS
(Source: PPS has all the rights with the picture on the right: http://www.pressureprofile.com/finger-tps/)

As previously mentioned, the 1V signal, generated by impedance spectroscope, was applied to the tissue via the reference electrode and the current flow through the tissue was measured with the measuring electrode. Knowing the applied voltage and the measured current, the tissue impedance or admittance was calculated. This procedure was performed at various frequencies, considering the advantages of multi-frequency measurements. The frequency sweep performed in this study was from 10 kHz to 1MHz. Using shielded cable greatly reduced the high frequency noise pickups from the surrounding environment. Measuring electrode was virtually grounded, so that the impedance of the tissue could be easily calculated by dividing the applied voltage to the measured current, and the tissue admittance, which is the inverse of the tissue impedance, was also calculated.

In order to determine the effect of compression on the electrical properties of soft tissue and finding the electrical-mechanical relationship in various types of tissue, bioimpedance measurements of two types of tissue were conducted while incremental pressure levels were applied to the *in-vitro* tissue. The bioimpedance measurements were conducted using a two point measurement technique [57] at 50 frequencies in the frequency range of 10 kHz to 1 MHz under incremental compression levels. One finger wearable force sensors FingerTPS by Pressure Profile Systems (Pressure Profile Systems Inc., LA, USA) were worn over the examiner's finger. Before performing the

test, force sensors were calibrated using a load sensor and the customized software “Chameleon TVR”, available with PPS sensors. The examiner placed her finger over the electrodes and applied constant pressure to the electrode over the tissue. The applied pressure was held constant by the examiner monitoring the pressure value from Chameleon TVR software. This procedure was repeated at 6 force levels (0.5-3lb) for chicken and rat samples. Therefore, the admittance of twenty chicken samples and two rat samples were collected and further mathematical analysis was conducted on them which will be presented in the proceeding chapters.

2.2. Experimental setup for the *in-vivo* electro-mechanical study

This section describes the experimental setup used for the *in-vivo* electro-mechanical study. This study was performed with two different setups, a bioimpedance measurement setup arranged in this study and a mechanical setup utilized in a previous study by Zaeimdar [55]. In order to assure consistency in the results, the same subjects are tested in the two bioimpedance and mechanical setups. The bioimpedance and mechanical measurements have been performed on the both left and right forearms and biceps of eleven subjects.

In-vivo experiment was performed on left and right forearm and bicep of 11 healthy human subjects. The subjects were three females and eight males aged 24 to 45. For the *in-vivo* bioimpedance experiment, two Ag/AgCl electrodes were integrated into a probe. Electrical impedance electrodes, along with temperature sensors, were integrated into an enclosure by the computer aided design software SolidWorks. Thereafter the prototype was developed by means of 3D printer and rapid prototyping technique. In this design which is shown in Figure 2.5, two Ag/AgCl electrodes, as well as six temperature sensors, were integrated into the probe. The temperature sensors were used for another study, therefore the results of the temperature sensors are not presented in this study. The probe was designed in a way that the electrodes were at 2-centimeter distance. An especial area was considered for the gels so that the used gels of each electrode is not mixed with the gel of the other electrode. The area designed for the gels also prevents the contact of the gels with the temperature sensors. The

existence of gels on top of the temperature sensors changes the measured temperature of the tissue. In spite of the design of the electrode positions in such a way that the gels cannot be mixed, the electrodes were in a good contact with the tissue. The details of the probe design can be seen in Figure 2.4.

In order to have consistency in results, the tests were conducted on the same places of both hands. For bicep and forearm tests, the probe was placed at a distance 8cm from elbow and wrist respectively and the examiner wearing the FingerTPS pressure sensors over her finger, applied constant pressure over the probe (see Figure 2.6). The applied pressure was held constant by the examiner monitoring the pressure value from Chameleon TVR software. The *in-vivo* data collection procedure was the same as the *in-vitro* testing. The only difference was that in the *in-vivo* experiments, the force levels were chosen in a way that the pressure values were tolerable by human subjects. Thus just three force levels (2.5N, 5N and 7.5 N) were applied to the probe placed over the subjects' forearms and biceps. The *in-vivo* admittances were measured at various force levels in three trials and recorded for further analysis.

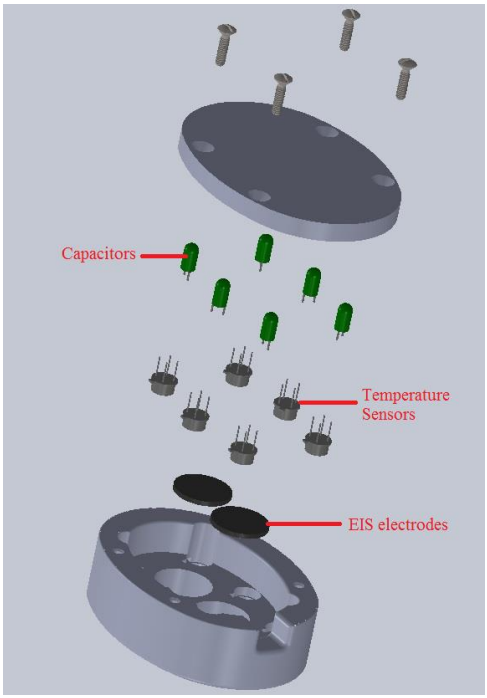

Figure 2.4. The exploded view of the probe containing electrical impedance electrodes as well as temperature sensors

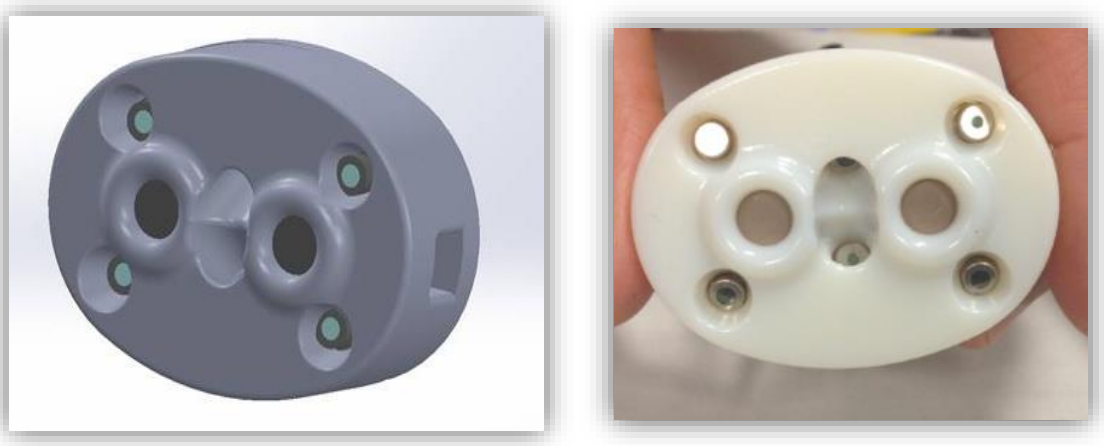

Figure 2.5. Design of the probe in SolidWorks and the prototype

Figure 2.6. Use of probe and the pressure sensors over human tissue

2.3. Experimental setups in *in-vivo* cancer detection study

This section describes the experimental setup used for the *in-vivo* cancer detection study. The main purpose of this study was to utilize the electrical impedance spectroscopy as a means for cancer detection. Since the malignancy changes the tissue structure, the tissue electrical properties in the malignant tissue will also be different from the electrical properties of healthy tissue. In previous sections, the use of electrical

impedance over healthy samples and subjects were explained and in this section, the use of this method on cancerous subjects will be elaborated.

This study was a collaborative research project with BC cancer agency (BCCA). The primary purpose of this study was to test EIS over breast cancerous subjects. However, the team oncologists' suggestion was to test the method on skin tumors due to the sensitivity involved in breast cancer patients.

This study was performed under the UBC BCCA Research Ethics Board under Dr. Paris Ann Ingledew as the Principal Investigator and REB Number H13- 02887. Ethics approval for conducting this study was taken from the UBC BCCA Research Ethics Board and from SFU Ethics Board. The title of the ethic approval is: "Electrical Impedance Analysis of Malignant and Benign Skin Tissue: Effects of Temperature and Pressure".

In this study, the same probe as the one used in the *in-vivo* electro-mechanical study was used. Ten cancerous subjects were recruited for this study. This study was preformed over malignant skin tumors with their contralateral healthy tissue as the control. The details of skin cancerous subjects, their age, sex, type of tumor and tumor position are listed in Table 2.1 .

As it will be explained in the results chapter, the electrical properties of tissue change with compression. Thus in this study, the force sensors will be utilized in order to monitor the amount of applied pressure over the tissue, so as to apply the same amount of pressure on all subjects and have consistency in results.

Additionally, in the data analysis and classification, it was also benefited from the results of biceps and forearms of eleven healthy subjects obtained in section 4.1.4. In other words, the bioimpedance results of cancerous subjects as well as the bioimpedance results of biceps and forearms of healthy subjects -at the first pressure level- were utilized for data classification.

Table 2.1. Case studies recruited for testing the proposed method on cancerous subjects and their information

Case Study No.	Age	Sex	Tumor Type	Tumor Position
Subject 1	90	Female	BCC (Basal Cell Carcinoma)	Left side of nose along sidewall
Subject 2	97	Female	SCC (Squamous Cell Carcinoma)	Left cheek center
Subject 3	81	Male	SCC (Squamous Cell Carcinoma)	Right Temple of head
Subject 4	93	Female	SCC (Squamous Cell Carcinoma)	Left cheek
Subject 5	87	Female	BCC (Basal Cell Carcinoma)	Left cheek under the eye
Subject 6	93	Female	BCC (Basal Cell Carcinoma)	Left mid neck
Subject 7	87	Male	BCC (Basal Cell Carcinoma)	Right cheek
Subject 8	92	Male	SCC (Squamous Cell Carcinoma)	Forearm
Subject 9	66	Female	BCC (Basal Cell Carcinoma)	Upper left cheek
Subject 10	65	Male	BCC (Basal Cell Carcinoma)	Left nasal wing

Chapter 3.

Numerical analysis and classifications of data

In this chapter, the incorporated numerical data analysis methods in this study are presented. Thereafter, the main concept contributing to electrical characterization of soft tissues is presented by introducing different models. The theory of Boussinesq indentation is also explained for the mechanical characterization part of this study and integration to the changes in electrical properties of tissue. Moreover, the main concepts of various classifier methods contributing in tissue classification are introduced.

3.1. Mathematical modeling of admittance data

Various models and circuit theories have been proposed for modeling the multi-frequency electrical impedance data. These models consider the tested tissue as a circuit containing some resistances and capacitances. In this study parameter mapping of EIS will be presented using the two most popular models: the “three-element RC model” in the form of admittance and the “Cole-Cole model” in the form of admittance. Each of these multi frequency circuit theories provides the mapping of four parameters, which represent a better vision of tissue. The structure of these circuits and their constitutive mathematical equations are explained as follows:

- **Three-element RC model (in the form of admittance)**

The three-element RC circuit is illustrated in Figure 3.1. The whole admittance of tissue can be expressed by the following equation in the three-element RC model:

$$Y = G + jB = G_s \,||\, (G_p + j\omega C_p) \tag{1}$$

where *Y*, *G* and *B* are the whole admittance, the whole conductance and the whole susceptance respectively. G_p is the parallel conductance, C_p is the parallel capacitance and G_s is the serial conductance. Liu *et al.* [46] showed that plotting the imaginary part of admittance (susceptance) versus the real part of admittance (conductance) in a complex plane results in a semicircle as shown in Figure 3.2. Considering the three-element RC circuit theory, the following circle equation can be obtained:

$$[G - \frac{G_s(2G_p+G_s)}{2(G_s+G_p)}]^2 + B^2 = [\frac{G_s^2}{2(G_s+G_p)}]^2 \quad (2)$$

As stated by Liu *et al.* [46] for human tissue, B is greater than 0, so that the semi-circle plot of human tissue admittance will be in the positive section of complex plane, illustrated in Figure 3.2.

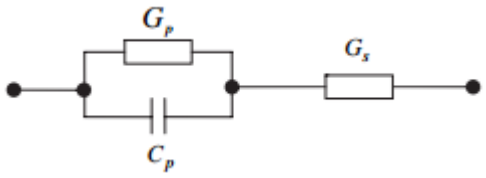

Figure 3.1. Three-element RC model circuit

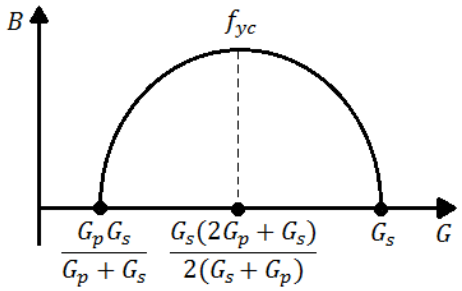

Figure 3.2. Imaginary part of admittance versus its real part (three-element RC model)

- **Cole-Cole model (in the form of admittance)**

The circuit of the Cole-Cole model is illustrated in Figure 3.3. The admittance of human tissue can be expressed by the Cole-Cole equation in the form of admittance proposed by Liu *et al.* [46]:

$$Y = G + jB = G_\infty + \frac{G_0 - G_\infty}{1+(\frac{jf}{f_{yc}})^\alpha} = \frac{1}{Z} \quad (3)$$

where *Y* is the whole admittance, *G* is the conductance and *B* is the susceptance. G_0 is the admittance at zero driving frequency, G_∞ is the admittance when the driving

frequency is infinity, *f* is the driving frequency, f_{yc} is the frequency at which the imaginary part of the admittance reaches its maximum and α is the dispersion parameter.

As stated by Liu *et al.* [46], equation of admittance can form the equation of a circle, and thus plotting the imaginary part of admittance (susceptance) versus the real part of admittance (conductance) in a complex plane, results in a semicircle as shown in Figure 3.4. The difference of the semicircle in the Cole-Cole model and the three-element RC model is that in Cole-Cole model, the semicircle is depressed below the real axis.

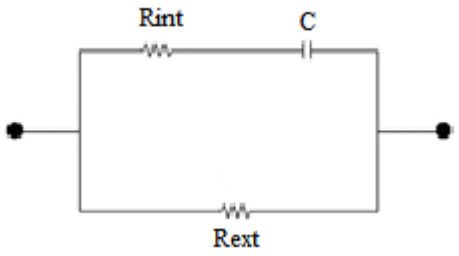

Figure 3.3. Cole-Cole model circuit

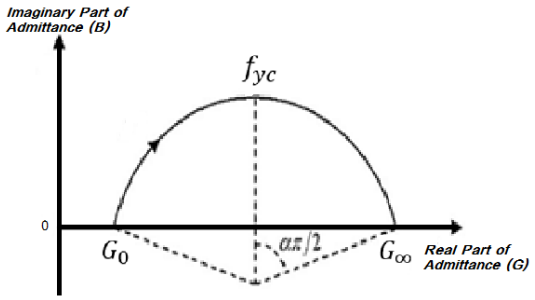

Figure 3.4. Imaginary part of admittance versus its real part (Cole-Cole arc)

Generally, the low-frequency region is affected by the extracellular environment and the high-frequency region is influenced by the intracellular space. In other words, since the cell membranes have a high capacitance, currents at low frequency cannot penetrate into the cell and must pass around the cells and go through the extracellular area. According to the Cole-Cole circuit, in low frequencies, open circuit occurs in the branch containing capacitance. Therefore, current flows only through the resistor called extracellular resistance. High frequency currents, on the other hand, have the ability to penetrate through cell membranes and other electronic barriers in the cell structure by polarisation. In Cole-Cole circuit, the same behavior is observed in high frequencies in which the capacitor short circuit occurs and thus current flows through both resistances in parallel. Based on these facts, Cole-Cole model may represent the cellular properties of biological tissue in a better way.

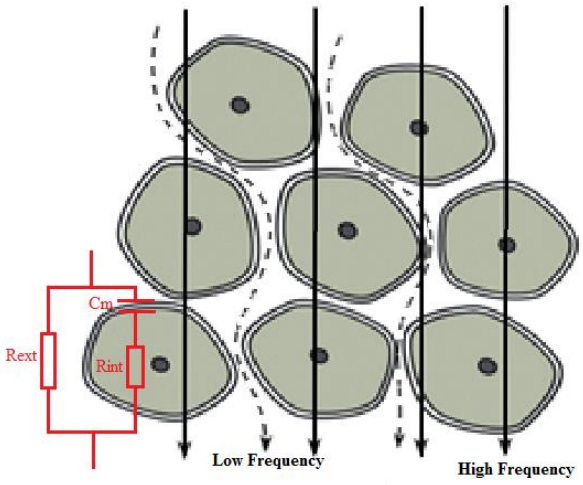

Figure 3.5. Paths of high and low frequency currents in a biological tissue

3.1.1. Parameter fitting of three-element RC model in form of admittance

In this model, it is considered that the center of the circle is located on the real axis of the complex plane [19]. Thus the center of the circle will be (m,0) and the radius will be r. Consequently, the circle equation will be:

$$(G - m)^2 + B^2 = r^2 \tag{4}$$

In the multi frequency measurement, N bioimpedance data points are measured. In the least square method (LSM), the error function, which must be minimized, will be the following equation:

$$F = \sum_{k=0}^{N-1}[(g_k - m)^2 + b_k^2 - r^2]^2 \tag{5}$$

Optimizing this error function will result in the radius and the center of the circle. Therefore, by knowing the center (m) and radius (r) of the semicircle, G_p, G_s and C_p can be obtained:

$$m = \frac{G_s(2G_p + G_s)}{2(G_s + G_p)} \tag{6}$$

$$r = \frac{G_s^2}{2(G_s+G_p)} \tag{7}$$

$$G_p = \frac{m^2-r^2}{2r} \tag{8}$$

$$G_s = m + r \tag{9}$$

$$C_p = \frac{1}{2N}\sum_{k=0}^{N-1}\left[\frac{(G_s+G_p)g_k - G_sG_p}{2\pi f_k b_k} + \frac{b_k(G_s+G_p)}{2\pi f_k(G_s-g_k)}\right] \tag{10}$$

3.1.2. Parameter fitting of Cole-Cole model in form of admittance

Yang *et al.* proposed an improved least absolute deviation (LAD) method for data fitting and Cole-Cole feature extraction which is an alternative to LSM [58]. The LAD method is an optimization method which minimizes the summation of the absolute errors which can be found by subtracting each data point from the fitted data [59].

$$Fitness\ Func. = \min\sum_{i=1}^{n}|e_i| = \sum_{i=1}^{n}\left|Y_{raw} - Y_{fitted}\right| \tag{11}$$

In the MATLAB optimization toolbox, the *fminunc* function uses the BFGS quasi-newton method in order to fit the data to the Cole-Cole model in the form of admittance as discussed by [58]. Four Cole-Cole features (G_0, G_∞, α and f_{yc}) are extracted by this method.

The Cole-Cole model, Figure 3.3, models the tissue as a circuit including one resistor in series with one capacitor, and both in parallel with a resistor. The resistor and capacitor which are in series mimic the intracellular resistance (R_{int}) and bulk membrane capacitance (C_m) and the resistor in parallel with these two components mimics the extracellular resistance of tissue (R_{ext}). All these three Cole-Cole circuit parameters can be calculated by the following equations:

$$R_{ext} = R_0 \tag{12}$$

$$R_{int} = \frac{R_0\,R_\infty}{R_0 - R_\infty} \tag{13}$$

$$C_m = \frac{1}{2\,\pi\, f_c\,(R_{int}+R_{ext})} \tag{14}$$

where $R_0 = \frac{1}{G_0}\mathrm{R}_0 = \frac{1}{\mathrm{G}_0}$, $R_\infty = \frac{1}{G_\infty}$ and $f_c = f_{yc}\sqrt[\alpha]{\frac{G_0}{G_\infty}}$.

3.2. Mechanical properties (elasticity) extraction method and indentation theory

In the present work, the indentation theories were applied for the *in-vivo* experiments considering soft tissue as an elastic layer bounded to a rigid body which is deformed by flat-ended cylindrical punch in normal direction. Elastic modulus at each point of the indentation test was calculated in a study performed by Zaeimdar [55] on the same subjects used in the present study. The elastic modulus of the tissue, within 10% relative indentation, was obtained from the slope of stress distribution versus relative indentation curve. The obtained elastic modules of tissues in [55] were utilized for calculating the tissue displacements based on Hayes's theoretical solution [60]:

$$E = \frac{P\,(1-\upsilon^2)}{2\,D\,a\,\kappa(\upsilon,\frac{a}{h})} \tag{15}$$

where *P* is the indentation load, *D* is the indentation displacement, υ is Poisson's ratio, *a* is the radius of the indenter, *h* is the thickness of the tissue and κ is a factor which is a function of material properties and geometry of the tissue. The κ values corresponding to relative indentation and aspect ratios of the current study were calculated by doing some interpolations on the provided tables for different indentation levels [29].

Regarding the unconfined compression testing of chicken and rat breast tissues, elastic moduli of the samples are acquired from Hooke's law. Hooke's law is a first order linear approximation to the real response of elastic materials to applied forces. Since the chicken and rat samples were compressed to 10% strain, the Hooke's law can still be used on these samples and the elastic modulus of these samples were obtained from the slope of the engineering stress versus strain.

$$E = \frac{\sigma}{\varepsilon} \tag{16}$$

The elasticity of the chicken and rat samples as well as biceps and forearms of human subjects were calculated by equations 16 and 15 respectively [55]. The displacements of all samples and subjects at each pressure level can be acquired by knowing the elasticity values calculated in [55] and by employing equations 15 and 16.

3.3. Classification techniques

In the classification procedure of the data from cancerous and healthy subjects and intelligent anomaly diagnosis process, there are two major steps. The first step includes the feature extraction and selection. In multi-frequency EIS, a large number of data points are needed in order to have a better perspective of properties and condition of the tissue. In bio-impedance frequency sweeps, the data can be reduced into lower number of variables by data reduction methods or model based approaches. The small sets of variables resulted from data reduction or model based methods can provide most of the needed information in the measurements. Accordingly, two data reduction methods are the principal component analysis (PCA) and modeling the tissue by an electrical equivalent circuit like Cole-Cole model. The disadvantage of the former is that the PCA is a “black-box” and the principal components do not represent any special information about the tissue, while modeling tissue into Cole-Cole model provides some information in the cellular level of tissue and gives us a perspective about the intra- and extra-cellular properties of tissue [48]. The second step of the anomaly diagnosis process is the decision-making procedure, which is the process of classifying the extracted features into different categories. Tissue classification, based on the electrical impedance properties of tissue, has been performed by various classification techniques [54] [3] [61] [53] [52].

Classification refers to identifying to which categories or “classes” a new observation belongs, on the basis of training sets of data containing observations (or instances) whose category membership is known. Each classification process involves separating data into training sets and testing sets. Each instance in the training set

contains a “target value” or “class label” and several “attributes” or “features” or “observed variables”.

Many classification methods such as decision tree, Bayesian classifiers, support vector machine (SVM), genetic algorithms (GA), fuzzy logic, artificial neural network (ANN) and a combination of some of these methods are used for the purpose of classification. To date, ANN is one of the most promising techniques because of its good learning and noise handling abilities. In spite of great performance and popularity of ANN, it has some disadvantages which encouraged the researcher of this study to implement other classification techniques. One of the disadvantages of ANN is that it needs a great number of training data sets to be provided to it; otherwise the training process cannot be reliable. Unfortunately in this study, according to all of the limitations in performing the experiments on human subjects, the number of subjects tested is too few. Since the size of training set is extremely small, simpler classification methods are selected in order to prevent over fitting. However, classification by means of ANN or ANFIS is the long term purpose of this study. Therefore, three classification techniques: Naïve Bayes with Gaussian distribution, Naïve Bayes with Kernel distribution and SVM are conducted on the raw data, extracted and normalized features and their results are compared according to each method’s sensitivity, specificity, accuracy, resubstitution error and the cross validation error.

Sensitivity, specificity and accuracy are statistical measures of the performance of a binary classification test. Sensitivity, or the true positive rate, measures the proportion of actual positives which are correctly identified. Specificity, or the true negative rate, measures the proportion of negatives which are correctly identified. The accuracy of a classifier refers to the ability of a given classifier to correctly predict the class label of new or previously unseen data. The resubstitution error is the percentage of incorrectly classified samples. The cross-validation error return the average of errors across all k trials in k-fold cross validation.

$$Sensitivity\ (TPR) = \frac{True\ Positive}{True\ Positive + False\ Negative} \tag{17}$$

$$Specificity\ (SPC) = \frac{True\ Negative}{True\ Negative + False\ Positive} \tag{18}$$

$$Accuracy\ (ACC) = \frac{True\ Positive + True\ Negative}{All\ data} \quad (19)$$

$$\%\ Resubstitution\ Error = \frac{Number\ of\ samples\ classified\ incorrectly}{Total\ number\ of\ samples} \times 100 \quad (20)$$

3.3.1. Naïve Bayes classifier with Gaussian or Kernel distribution

Naïve Bayes is a simple technique for constructing classifiers. Naïve Bayes is not a single algorithm for training classifiers, but a family of algorithms based on a common principle: all Naïve Bayes classifiers assume that the value of a particular feature is independent of the value of any other feature, given the class variable.

For some types of probability models, Naïve Bayes classifiers can be trained very efficiently in a supervised learning setting. In many practical applications, parameter estimation for Naïve Bayes models uses the method of maximum likelihood; in other words, one can work with the Naïve Bayes model without accepting Bayesian probability or using any Bayesian methods. An advantage of Naïve Bayes is that it only requires a small amount of training data to estimate the parameters necessary for classification, which makes it a very appropriate choice in this study due to the small number of training data sets.

The training step in Naïve Bayes classification involves estimating the parameters of a probability distribution using the training samples, while it is assumed that the features are conditionally independent. Subsequently, in the prediction step, the posterior probability of the unseen samples belonging to each class is computed by the method. Afterwards, the test sample is classified according to the largest posterior probability [62].

In other words, the Naive Bayes classifier can be considered as a simple Bayesian network with one root node representing the class and *n* leaf nodes representing the features or attributes. Class label of *C* is assumed to have *k* possible values and a $\{X_1,\ldots, X_n\}$ is assumed to be a set of attributes or features of the environment. The combination of the Bayesian probabilistic model with a maximum a

posteriori (MAP) rule, also called discriminant function, gives the classifier [63]. The Naive Bayes classifier is defined as follows:

$$Naive\ Bayes\ (a) = argmax_{c \epsilon C}\ P(c) \prod_{i=1}^{n} P(x_i|c) \tag{21}$$

where a $=\{X_1 = x_1, \dots, X_n = x_n\}$ is a complete assignation of attributes. This equation assumes that the attributes are conditionally independent.

When dealing with continuous data in the Naïve Bayesian classification, a typical assumption is that the continuous values associated with each class are distributed according to a Gaussian (normal) distribution to represent the likelihoods of the features conditioned on the classes [64]. The normal distribution is appropriate for predictors that have normal distributions in each class. For each predictor you model with a normal distribution, the naive Bayes classifier estimates a separate normal distribution for each class by computing the mean and standard deviation of the training data in that class. Thus each attribute is defined by a Gaussian probability density function (PDF) as:

$$X_i \sim N(\mu\ ,\ \sigma^2) \tag{22}$$

The Gaussian probability density function is bell-shaped and is defined by the following equation:

$$P(X_i|C) \sim N(\mu, \sigma^2)(x) = \frac{1}{\sqrt{2\pi\sigma^2}} e^{-\frac{(x-\mu)^2}{2\sigma^2}} \tag{23}$$

where μ and σ^2 are the mean and the variance respectively and can be calculated by the following formulas [65]:

$$\mu_{X_i|C=c} = \frac{1}{N_c} \sum_{i=1}^{N_c} x_i \tag{24}$$

$$\sigma^2{}_{X_i|C=c} = \frac{1}{N_c} \sum_{i=1}^{N_c} x_i^2 - \mu^2 \tag{25}$$

Another common technique for handling continuous values is to use kernel density distribution. This is a Bayesian network which estimates the true density of the

continuous variables using kernels. The kernel distribution is appropriate for predictors that have a continuous distribution. It does not require a strong assumption such as a normal distribution and you can use it in cases where the distribution of a predictor may be skewed or have multiple peaks or modes. It requires more computing time and more memory than the normal distribution. For each predictor you model with a kernel distribution, the naive Bayes classifier computes a separate kernel density estimate for each class based on the training data for that class. Kernel density estimation is a non-parametric method for estimating the probability density function population [66]. Using kernel density estimation on a set of labeled training data $\{X_1,\ldots, X_n\}$, given class C, the probability that the feature value in the *i*-th position is equal to *xi,* can be estimated by the following equation:

$$P_i(x_i|C = c) = \frac{1}{N_c h} \sum_{j=1}^{N_c} K\left(x_i, x_{j|i|c}\right) \tag{26}$$

$$K(x, \mu) = \frac{1}{\sqrt{2\pi}} e^{-\frac{(x-\mu)^2}{2h^2}} \tag{27}$$

where N_c is the number of the input data *X* belonging to class c, and h is a bandwidth, or a smoothing parameter [67].

3.3.2. Support Vector Machines

SVM or support vector machine is a highly principled supervised learning method. It follows the structural risk minimization rather than least mean square error. The structural risk minimization is based on the fact that the sum of the training error rate bounds the error rate of the learning machine on the test data [62]. The goal of SVM is to produce a model based on the training data, which predicts the target values of the test data, given only the test data attributes. The main concept in SVM is based on the decision boundaries which are in the form of hyper-planes (generalization of a plane in a multidimensional space). These hyper-planes perform as boundaries between objects which have various class labels.

In this study, the simplest form of SVM classifier, binary classification, has been used to classify the data in two classes: healthy and cancerous classes. In binary

classification, a support vector machine constructs a hyper-plane with the best possible boundary between the two groups to be classified in an often high-dimensional space. The best hyper-plane for an SVM is the one with the largest margin between the two classes. The support vectors are the data points that are closest to the hyper-planes. In Figure 3.6 a hyper-plane is shown separating two groups with a best margin between the two groups.

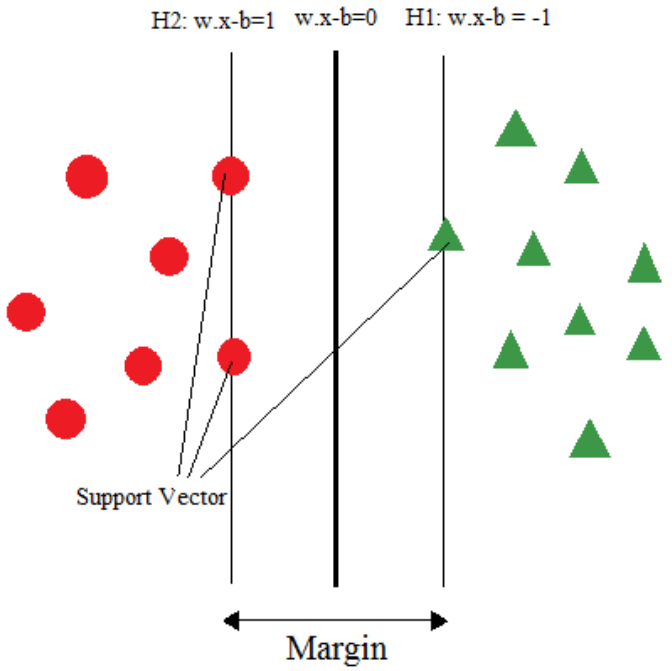

Figure 3.6. The optimal hyper-plane marked with a solid line between group A (●) and group B (▲) after support vector machine calibration. The observations on H1 and H2 are called the support vectors as they support the two sub hyper-planes.

For a training set $\{(x_1, y_1), (x_2, y_2), \dots, (x_m, y_m)\}, x_i \in \mathbb{R}^n, y_i \in \{-1, +1\}$, we consider a hyper-plane defined by (w, b), where w is a weight vector and b is a bias. The SVM requires the solution to the following optimization problem [180]:

$$\min \frac{1}{2} w^T w + C \sum_{i=1}^{m} \gamma_i \tag{28}$$

subject to

$$y_i(w^T \emptyset\,(x_i) + b) \geq 1 - \gamma_i; \qquad \gamma_i \geq 0 \tag{29}$$

The SVM maps the training vectors x_i into a higher dimensional space by the function ∅. Then a linear separating hyperplane with the maximum margin in this higher dimensional space is found by SVM. The penalty parameter of the error term is C>0.

The advantage of SVM is that by applying a kernel, even non-linearly separated groups in which no plane can be drawn in the input space, can easily be solved. A kernel maps the input space into a higher dimensional feature space where the groups "suddenly" are separable by a hyper-plane once more [21].

3.3.3. Cross Validation

In all classification and learning techniques, the data sets should be divided into the training set, testing set and validation set. According to the number of data sets, the division of data into these three groups varies. If a large sample size is provided, 60% of the data sets should be considered as the training set, 20% of the data set as the test set and 20% of the data set as the validation set. If a medium sample size is provided to the classification algorithm, 60% of data set should be allocated for the training set and 40% of data set as the testing. Finally, if the sample size is too small, having the training set and the testing set may not be a good idea. In this situation the cross validation method is used.

In cross validation some of the data is removed, before the training begins. Then when training is completed, the data that was removed can be used to test the performance of the learned model on the "new" data. This is the basic idea for a whole class of model evaluation methods called cross validation. There are various methods of cross validation such as the holdout method, K-fold cross validation method and leave-one-out cross validation method.

The holdout method is the simplest kind of cross validation. In the holdout method, the data set is separated into two sets, called the training set and the testing set. The function approximator fits a function using the training set only. Then the function approximator is asked to predict the output values for the data in the testing set (it has never seen these output values before). The errors it makes are accumulated as before to give the mean absolute test set error, which is used to evaluate the model. The

advantage of this method is that it is usually preferable to the residual method and takes no longer to compute. However, its evaluation can have a high variance. The evaluation may depend heavily on which data points end up in the training set and which end up in the test set, and thus the evaluation may be significantly different depending on how the division is made.

K-fold cross validation is one way to improve over the holdout method. The data set is divided into k subsets, and the holdout method is repeated k times. Each time, one of the k subsets is used as the test set and the other k-1 subsets are put together to form a training set. Then the average error across all k trials is computed. The advantage of this method is that it matters less how the data are divided. Every data point will be in a test set exactly once, and will be in a training set k-1 times. The variance of the resulting estimate is reduced as k is increased. The disadvantage of this method is that the training algorithm has to be rerun from scratch k times, which means it takes k times as much computation to make an evaluation. A variant of this method is to randomly divide the data into a test and training set, k different times. The advantage of doing this method is that you can independently choose how large each test set is and how many trials you average over.

Leave-one-out cross (LOO) validation is K-fold cross validation, with K equal to N, the number of data points in the set. That means that N separate times, the function approximator is trained on all the data except for one point and a prediction is made for that point. As before the average error is computed and used to evaluate the model. The evaluation given by leave-one-out cross validation error (LOO-XVE) is good, but at first pass, it seems very expensive to compute. Fortunately, locally weighted learners can make LOO predictions just as easily as they make regular predictions. That means computing the LOO-XVE takes no more time than computing the residual error and it is a much better way to evaluate models.

In this study, the 10-fold cross validation, which is a more common method, is used to minimize the bias produced by random sampling of the training and test data samples.

Chapter 4.

Analysis of bioimpedance measurements and displacement-dependency of tissue electrical properties

Following the introduced experimental procedures, mathematical modeling and analysis methods in previous chapters, this chapter presents the results of *in-vitro* and *in-vivo* (healthy subjects) bioimpedance measurements and the tissue displacement-dependent electrical features.

4.1. Bioimpedance measurements

This section compares the two electrical impedance models introduced in the previous chapter by applying both methods to the same admittance data. Having compared the value of the fitting error of both models to the data points, the model with the lower fitting error was chosen to be used in the data fittings of the whole study. Thereafter, the chosen model was evaluated by the Bode diagram and the transfer function of the tissue. Finally, the bioimpedance results in the *in-vitro* and *in-vivo* studies are presented.

4.1.1. Comparison of two electrical impedance models

The admittance data of one subject is fitted to the three-element RC model and the Cole-Cole model by means of the LSM and the LAD methods, respectively. The averages of errors calculated by the LSM for the three-element circuit model fitted to the data of forearm and bicep of 11 healthy subjects are 6.22e-5 and 4.12e-5 and the averages of the errors obtained by the LAD for the Cole-Cole circuit model for forearm and bicep of 11 healthy subjects are 1.32e-12 and 7.13e-12. According to the obtained

errors by fitting the data points to the two models and by comparison of the two models illustrated in Figure 4.1 and also as concluded in [19], the Cole-Cole model is a much more accurate model for the purpose of admittance data fitting.

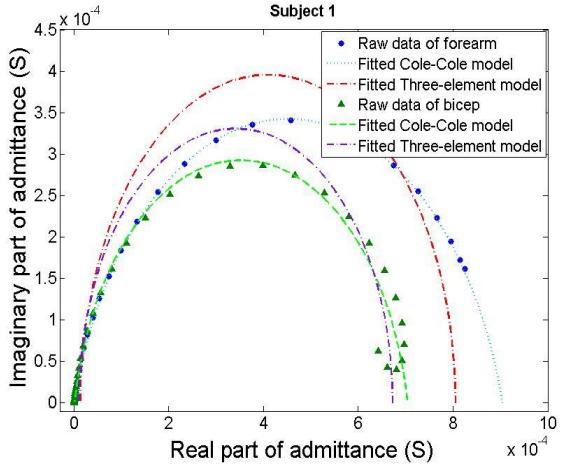
Subject 1
Raw data of forearm
Fitted Cole-Cole model
Fitted Three-element model
Raw data of bicep
Fitted Cole-Cole model
Fitted Three-element model
Imaginary part of admittance (S)
Real part of admittance (S)
x 10^-4
x 10^-4

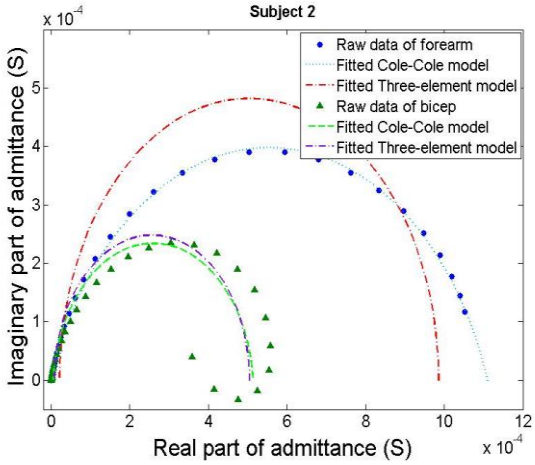
Subject 2
Raw data of forearm
Fitted Cole-Cole model
Fitted Three-element model
Raw data of bicep
Fitted Cole-Cole model
Fitted Three-element model
Imaginary part of admittance (S)
Real part of admittance (S)
x 10^-4
x 10^-4

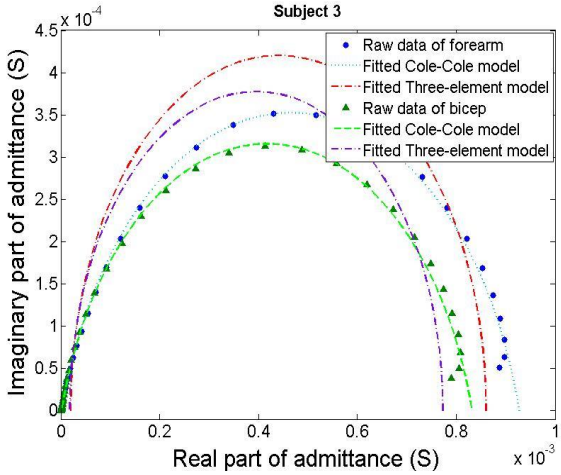
Subject 3
Raw data of forearm
Fitted Cole-Cole model
Fitted Three-element model
Raw data of bicep
Fitted Cole-Cole model
Fitted Three-element model
Imaginary part of admittance (S)
Real part of admittance (S)
x 10^-4
x 10^-3

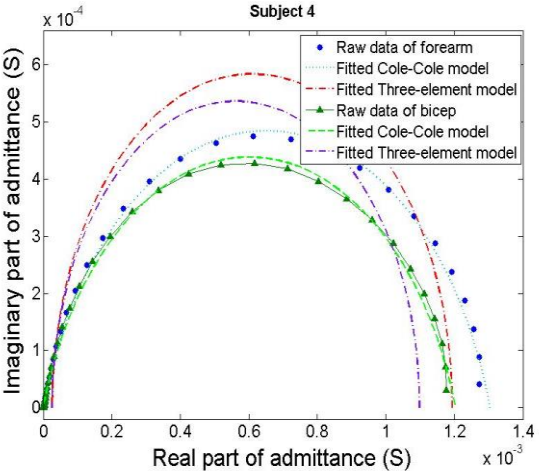
Subject 4
Raw data of forearm
Fitted Cole-Cole model
Fitted Three-element model
Raw data of bicep
Fitted Cole-Cole model
Fitted Three-element model
Imaginary part of admittance (S)
Real part of admittance (S)
x 10^-4
x 10^-3

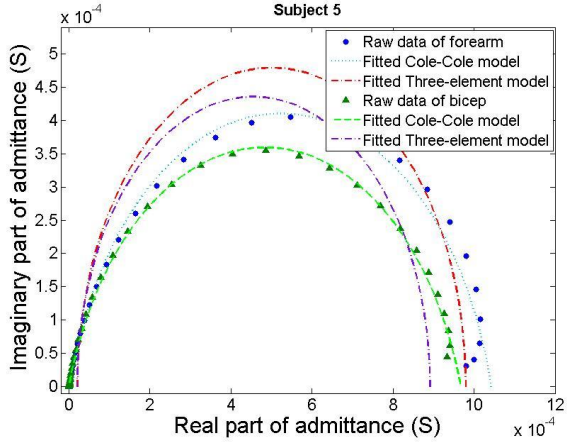
Subject 5
Raw data of forearm
Fitted Cole-Cole model
Fitted Three-element model
Raw data of bicep
Fitted Cole-Cole model
Fitted Three-element model
Imaginary part of admittance (S)
Real part of admittance (S)
x 10^-4
x 10^-4

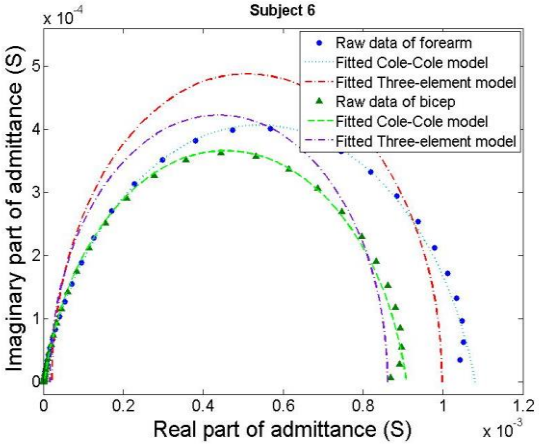
Subject 6
Raw data of forearm
Fitted Cole-Cole model
Fitted Three-element model
Raw data of bicep
Fitted Cole-Cole model
Fitted Three-element model
Imaginary part of admittance (S)
Real part of admittance (S)
x 10^-4
x 10^-3

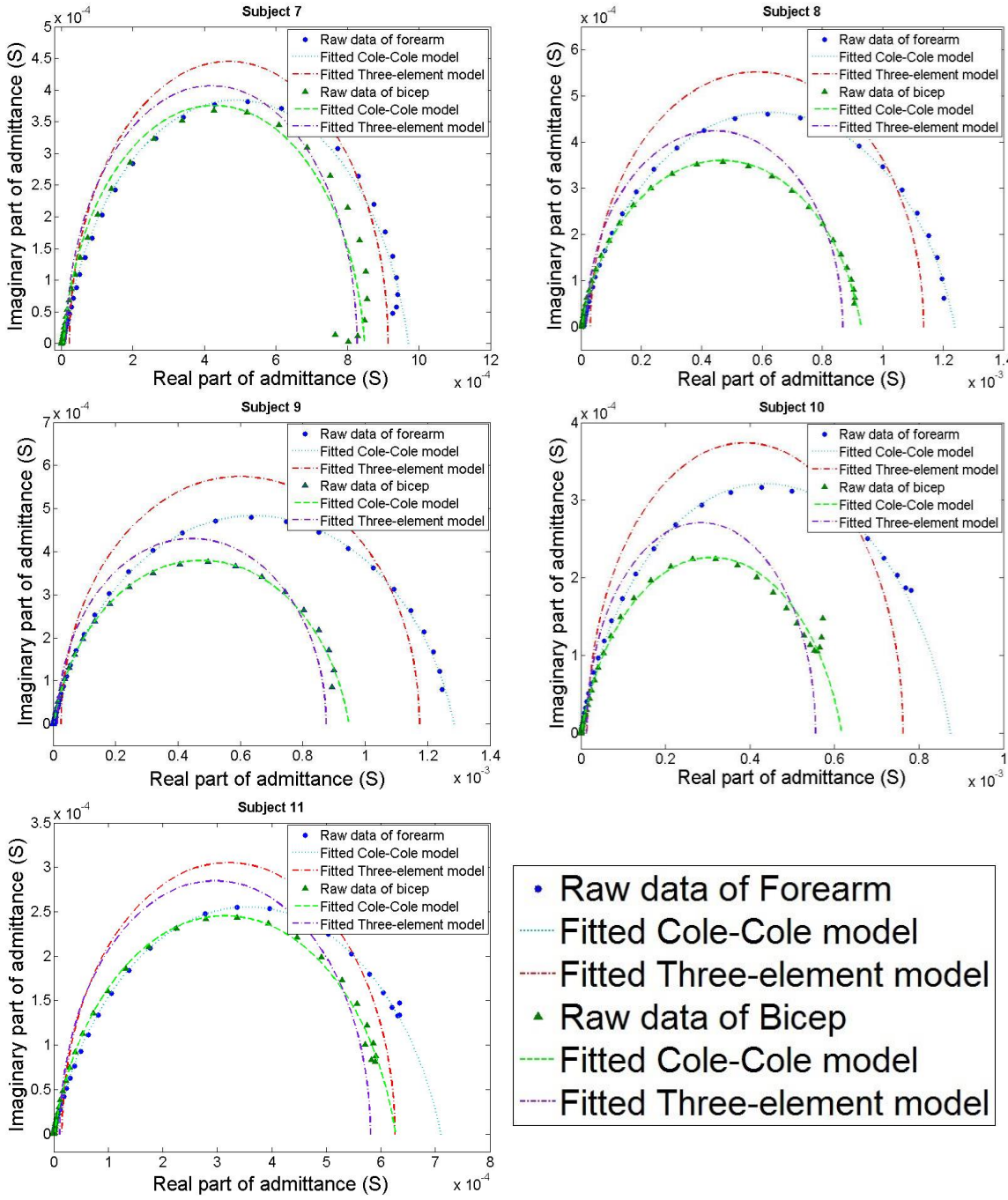

Figure 4.1. Cole-Cole model and Three-element RC model fitted to admittance data points of 11 healthy subjects (forearms and biceps data)

4.1.2. Evaluating the model by bode diagram

In order to evaluate the chosen model and confirm the transfer function of the system of soft tissue, Bode plot of soft tissue has been compared to the Bode plot generated based on the zeros and poles of the fitted Cole-Cole model to the data points. Bode plot is usually a combination of a Bode magnitude plot, expressing the magnitude of the frequency response (see Figure 4.2a), and a Bode phase plot, expressing the phase shift (see Figure 4.2b). Both magnitude and phase values are plotted against the logarithm of frequency.

In Figure 4.2a, the magnitude of the admittance measured at various frequencies is plotted against frequency and in Figure 4.2b, the phase of admittance measured at various frequencies is plotted versus frequency. Consequently, the Bode diagram of soft tissue resulted from the phase and magnitude of the measured admittance data points is illustrated in Figure 4.2. This figure shows that soft tissue has one pole at a frequency of about 3e5 Hz and one zero at a frequency of about 5e2 Hz. According to one pole and one zero of the system, the tissue can be considered as a first order system. Moreover, modeling human tissue by means of Cole-Cole model results in the following admittance equation, which considers the tissue as a first order system:

$$Y = \frac{1}{R_{ext}} \frac{1+(R_{ext}+R_{int})C_m\, s}{1+R_{int}\, C_m\, s} \tag{30}$$

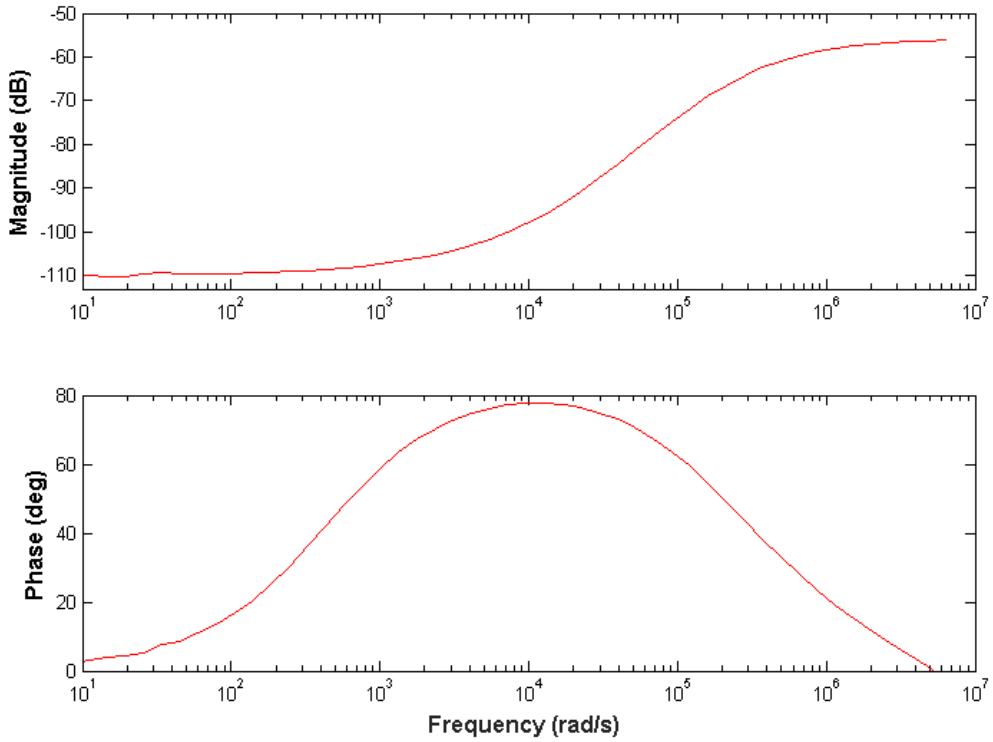

Figure 4.2. Bode diagram of soft tissue resulted from the phase and magnitude of the measured admittance. a) Upper figure: magnitude of admittance over frequency. b) Lower figure: phase of admittance over frequency

In order to have a better comparison of the actual Bode plot of soft tissue and the Bode plot based on the poles and zeros calculated from the fitted Cole-Cole model, it is needed to extract the Cole-Cole model features from the Nyquist plot of admittance. By means of LAD method explained in Chapter 3, the electrical features of the Cole-Cole model (R_{ext}, R_{int} and C_m) are extracted from the Nyquist plot of one subject. According to equation 31, the poles and zeros of admittance in human tissue based on the Cole-Cole model are:

$$\text{Zero} = -\frac{1}{R_{int}\, C_m} \qquad \text{Pole} = -\frac{1}{(R_{ext}+R_{int})\, C_m} \tag{31}$$

The extracted electrical properties of one subject based on its admittance Nyquist plot and the subsequent pole and zero are as follows:

R_{ext}= 212 Ω R_{int}= 222 Ω C_m= 12 nF

Zero = -426.4276 Pole = -375380

Considering the extracted features as well as calculating the soft tissue pole and zero, alongside the definition of the Bode diagram, the Bode diagram of the tissue is plotted in Figure 4.3. Comparison of bode plots in figures Figure 4.2 and Figure 4.3, proves that the soft tissue is a first order system and confirms that the Cole-Cole circuit is a good model for modeling soft tissue.

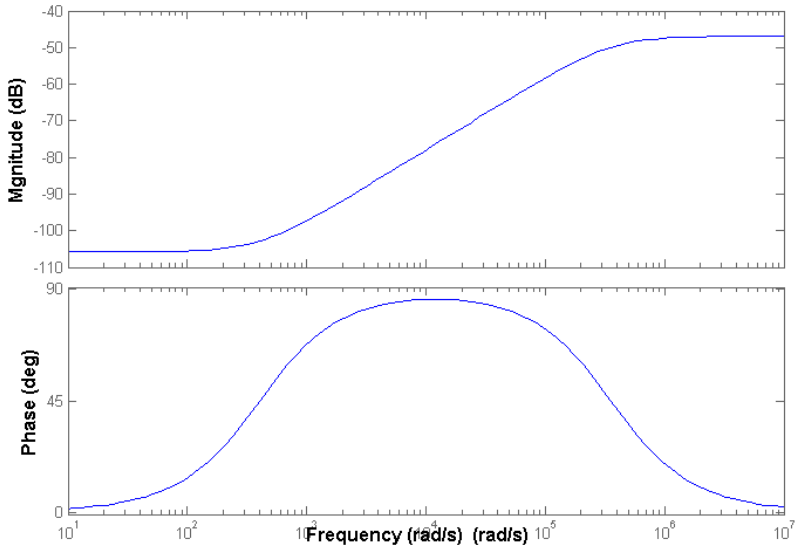

Figure 4.3. Bode plot of soft tissue generated based on the extracted features and calculated zeros and poles of the system

4.1.3. *In-vitro* measurements

Knowing the applied current, the received voltage and the sweeping frequency, the admittance of the tested samples and subjects were calculated at each compression level. By fitting equation 3 to the admittance Nyquist plots at each trials, the Cole-Cole features (G_0, G_∞, α and f_{yc}) were extracted within each pressure level. Cole-Cole circuit equivalent parameters (R_{ext}, R_{int} and C_m) were then calculated from equations 12 to 14. Thus, for all twenty chicken samples and two rat samples, R_{ext}, R_{int} and C_m were acquired at 6 pressure levels and at each trial. For each sample, the electrical parameters of three trials were averaged within each compression level. These

averaged electrical parameters will be utilized later in section 4.3 for correlating the electrical properties of the chicken and rat tissue to their mechanical properties. The averaged values of R_{ext}, R_{int} and C_m at the first pressure level for both chicken and rat samples are listed in Table 4.1, including the error values representing one standard deviation of uncertainty.

Table 4.1. Averaged Cole-Cole parameters extracted by the LAD method at the first pressure level and standard deviations, including the error values representing one standard deviation of uncertainty

Samples	Fitting Results		
	R_{ext} (Ω)	R_{int} (Ω)	C_m (nF)
Chicken Breasts	537.85 ± 23.19	512.34 ± 24.32	7.91 ± 0.50
Rat Breasts	565.54 ± 18.19	675.83 ± 98.93	30.7 ± 14.9

4.1.4. *In-vivo* measurements

In the *in-vivo* section of this study, the procedure of calculating admittance and extracting the features is the same as was explained in section 4.1.3 (the *in-vitro* study). Thus as explained, the admittance of the tested forearms and biceps of subjects are calculated by knowing the applied current, the voltage and the sweeping frequency. Fitting equation 3 to the admittance Nyquist plots, extracted the Cole-Cole features (G_0, G_∞, α and f_{yc}) within each pressure level. The Cole-Cole circuit equivalent parameters (R_{ext}, R_{int} and C_m) were then calculated from equations 12 to 14. Thus for all eleven human subjects' left and right biceps and forearms, R_{ext}, R_{int} and C_m were acquired at 3 pressure levels and 3 trials. For each subject, the electrical parameters of three trials were averaged within each compression level. The averaged values of R_{ext}, R_{int} and C_m at the first pressure level are presented in Table 4.2, including the error values. These averaged electrical parameters will be utilized later in section 4.3 for correlating the electrical properties of the chicken and rat tissue to their mechanical properties.

Table 4.2. Averaged Cole-Cole parameters extracted by the LAD method at the first pressure level and standard deviations

Subjects	Fitting Results		
	R_{ext} (Ω)	R_{int} (Ω)	C_m (nF)
Left Forearms	2612508.42 ± 359731.87	986.46 ± 189.34	16.46 ± 6.19
Right Forearms	2125924.31 ± 189807.62	970.02 ± 183.89	18.45 ± 8.99
Left Biceps	7577699.16 ± 180562.62	1386.3 ± 299.1259	14.83 ± 7.65
Right Biceps	7563298.20 ± 121059.83	1252.9 ± 437.72	15.26 ± 8.53

4.2. Mechanical displacements measurements

The mechanical experiments resulted in the correlation of engineering stress versus the strain (elasticity modulus) in the unconfined tissues, chicken and rat samples, and relative indentations in the confined tissues, human subjects, in a previous study performed by Zaeimdar [55]. In the current study, the displacements of the tested tissues were acquired by the corresponding formulations, theories and the elastic moduli presented in [55]. The averaged displacements of the left and right forearms, the left and right biceps of eleven human subjects, the chicken and rat breast samples at each pressure level are presented in Table 4.3 and Table 4.4, respectively. These acquired displacements will be used in section 4.3 for correlating the changes of electrical properties in regard to tissue displacements.

4.2.1. *In-vitro* measurements

As explained in section 3.2 in small deformations, soft tissue exhibits linear elasticity and can be described by a linear relationship between the stress and strain. Thus, the elastic moduli of the samples can be obtained from the slope of the engineering stress versus strain; as an example, the unconfined compression testing of the one chicken sample performed by Zaeimdar is illustrated in Figure 4.4. The elasticity of each sample, which was extracted from fitting a straight line to the stress-strain plots, was utilized for the displacements calculations. The averages of the displacements of the chicken and rat breast samples are presented in Table 4.3.

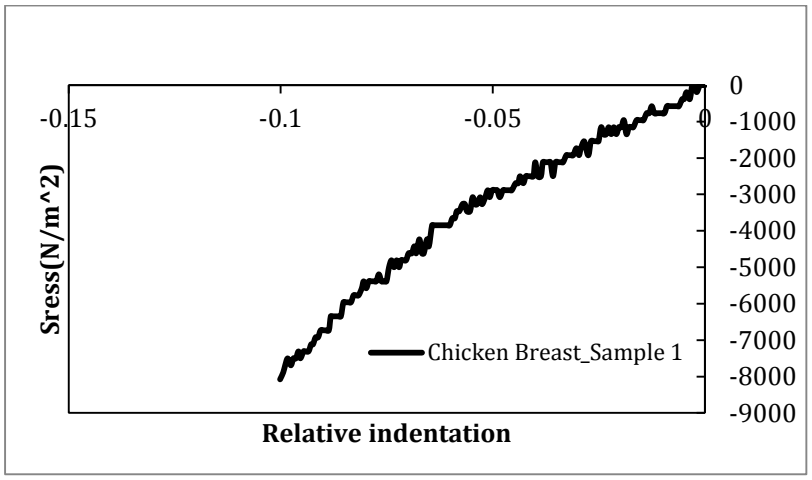

Figure 4.4. Stress versus relative indentation of *in-vitro* chicken sample [55]

Table 4.3. The average displacements of chicken and rat breast samples and standard deviations

Force (lb)	**0.5**	**1**	**1.5**	**2**	**2.5**	**3**
Chicken Samples Average Displacements (mm)	0.4 ± 0.03	0.9 ± 0.05	1.4 ± 0.11	1.9 ± 0.14	2.4 ± 0.18	2.9 ± 0.21
Rat Samples Average Displacements (mm)	0.45 ± 0.02	0.89 ± 0.03	1.34 ± 0.06	1.78 ± 0.09	2.23 ± 0.12	2.67 ± 0.16

4.2.2. *In-vivo* measurements

The elastic moduli of the right and left biceps and forearms of 10 human subjects were obtained in [55]. The stress-strain plot of one subject is illustrated in Figure 4.5. The indentation theory was applied for the *in-vivo* experiments considering soft tissue as an elastic layer bounded to a rigid body which is deformed by flat-ended cylindrical punch in normal direction. The displacements of the bicep and forearm tissues at each pressure level were calculated using equation 15. The average of the displacements of

the ten subjects' right and left forearm and biceps are presented in Table 4.4, including the error values representing one standard deviation of uncertainty.

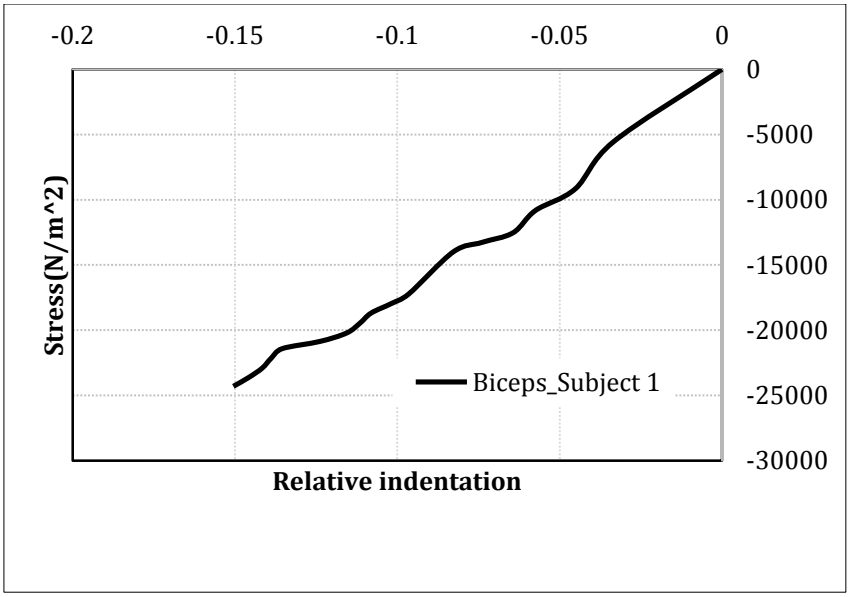

Figure 4.5. Stress versus relative indentation of *in-vivo* bicep of subject 1 [55]

Table 4.4. The average displacements of left and right forearms and biceps of 10 human subjects and standard deviations

	Displacements (mm)			
	Forearm		Bicep	
Force (N)	Right	Left	Right	Left
2.5	1.89 ± 0.36	1.93 ± 0.24	2.11 ± 0.42	2.12 ± 0.45
5	3.78 ± 0.46	3.87 ± 0.51	4.23 ± 0.62	4.24 ± 0.59
7.5	5.67 ± 0.78	5.81 ± 0.69	6.34 ± 0.85	6.36 ± 0.87

4.3. Tissue displacement-dependent electrical features

Knowing the elasticity of each type of tissue and by incorporating the Hayes's equation and Hooke's law, the displacements of each samples and subject at each pressure level was calculated in previous sections. The displacement of the unconfined tissues, chicken and rat, were measured by the Hooke's equation and the displacement of the confined human subjects were calculated by the indentation theory. The extracted

Cole-Cole features and subsequently the Cole-Cole circuit equivalent parameters at each pressure level for each trial were obtained in section 4.1.3 and 4.1.4. Because of the high variability between samples and subjects, the average values of extracellular resistance, intracellular resistance and membrane capacitance at the 3 trials were normalized to their values at the first compression level (listed in Table 4.3 to Table 4.4). These averaged normalized parameters measured at each pressure level were plotted against the pressure corresponding displacement in Figure 4.6 to Figure 4.11. These figures illustrate a linear relationship between the normalized Cole-Cole parameters and the displacement of tissue.

As Figure 4.6 illustrates, at the maximum displacement of chicken tissue under compression, when the maximum force, 3lb, is applied to the tissue samples, the normalized extracellular resistance increases 45% relative to its first value. Normalized intracellular resistance decreases 20% and normalized membrane capacitance increases 48% in the chicken tissue. The changes in rat tissue includes an increase of 6% in the normalized extracellular resistance, 7% decrease in the normalized intracellular resistance and 17% increase in the normalized membrane capacitance (Figure 4.7). Figure 4.8 to Figure 4.11 indicate that at the maximum force applied to the human subjects, 7.5N, the normalized extracellular resistance has an increase of 39.7% and 38.5% in the left and right forearms and an increase of 294% and 297% in the left and right biceps, respectively. At this point the normalized intracellular resistance increases 8.8% and 8.9% in the left and right forearms and 12.4% and 12.5% in the left and right biceps, respectively. The decrease of normalized membrane capacitance in the left and right forearms is 11.8% and 12.3% and in the left and right biceps is 26.9% and 24.0%, respectively.

Figure 4.6 to Figure 4.11 illustrate the correlation of the compression-dependent Cole-Cole parameters and tissue displacements. The Cole-Cole parameters are normalized to their values at the first pressure level. Part (a) of these figures shows the compression-dependent extracellular resistance versus tissue displacement. The correlation of the normalized intracellular resistance and the normalized cell membrane capacitance to their displacements are also presented in part (b) and (c) of the figures, respectively. The correlation of the normalized extracellular resistance, the normalized

intracellular resistance and the normalized cell membrane capacitance to the tissue displacement and the corresponding Pearson product values of all experiments are represented in Table 4.5.

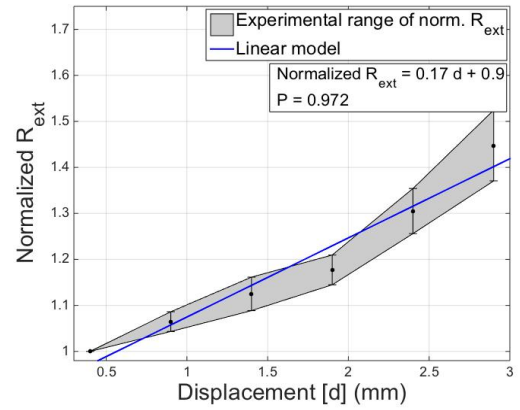

(a)

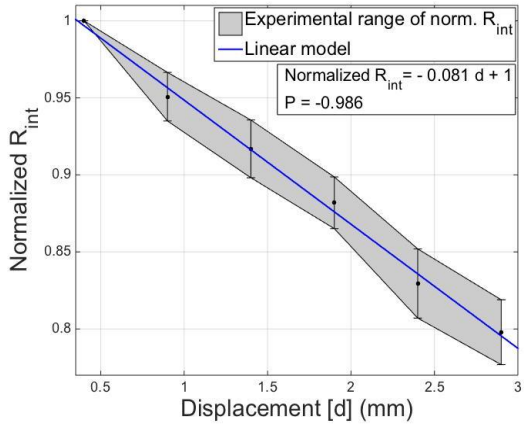

(b)

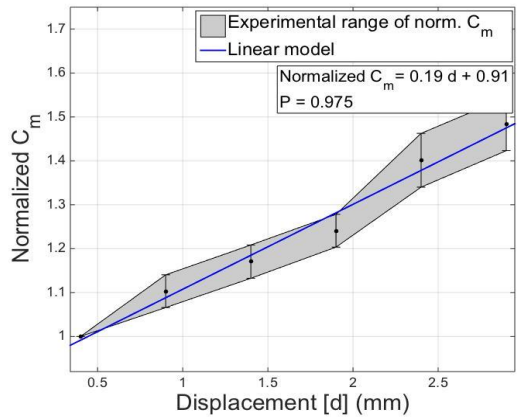

(c)

Figure 4.6. Chicken breast tissue, the correlation of compression-dependent Cole-Cole parameters normalized to their values at the first pressure level and tissue displacements: (a) Normalized extracellular resistance versus tissue displacement (b) Normalized intracellular resistance versus tissue displacement (c) Normalized membrane capacitance versus tissue displacement

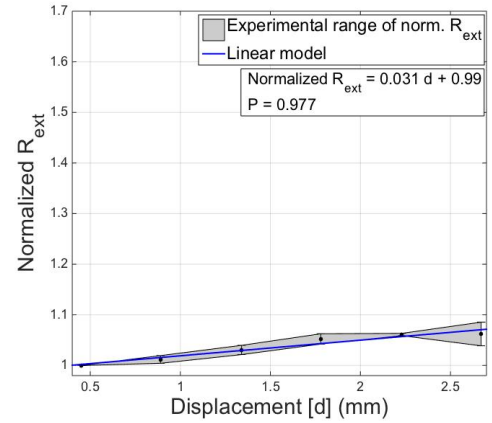

(a)

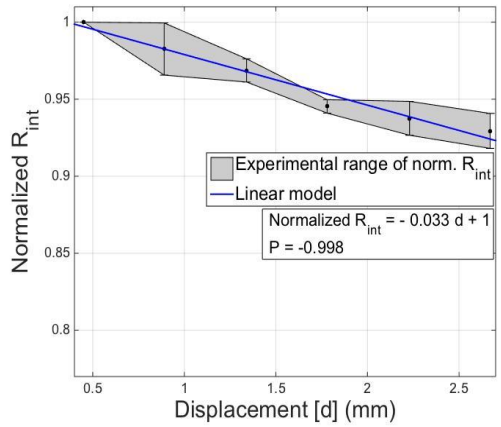

(b)

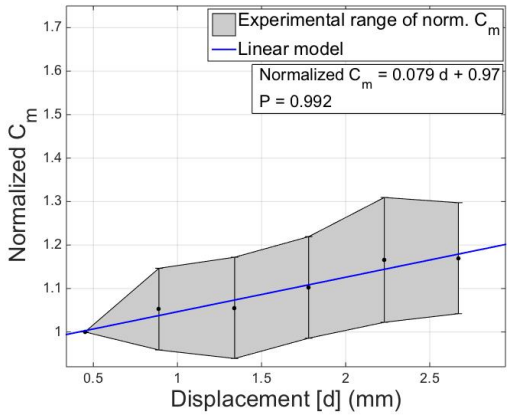

(c)

Figure 4.7. Rat breast tissue, the correlation of compression-dependent Cole-Cole parameters normalized to their values at the first pressure level and tissue displacements: (a) Normalized extracellular resistance versus tissue displacement (b) Normalized intracellular resistance versus tissue displacement (c) Normalized membrane capacitance versus tissue displacement

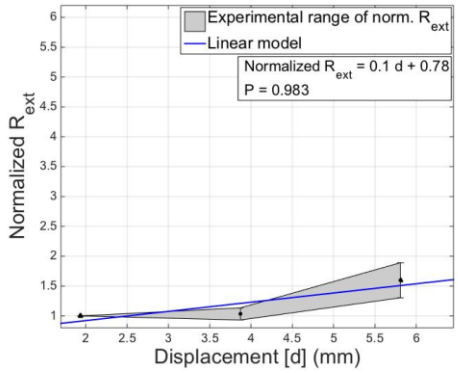

(a)

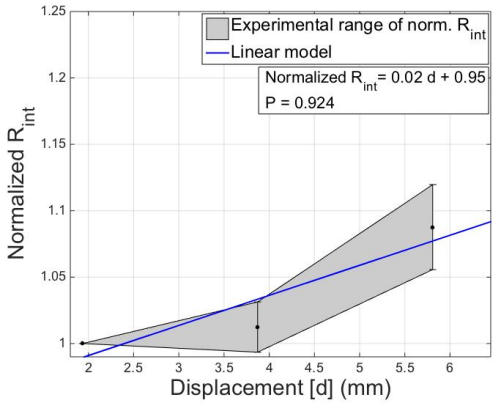

(b)

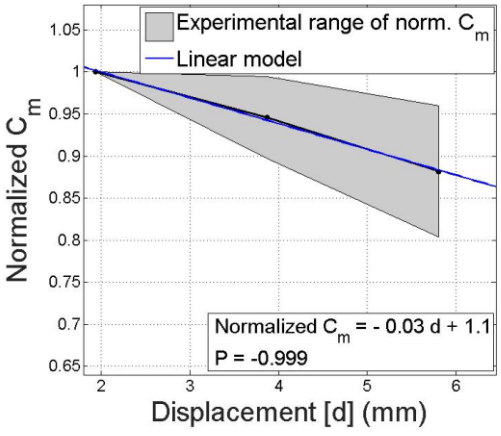

(c)

Figure 4.8. Left Forearm Tissue, the correlation of compression-dependent Cole-Cole parameters normalized to their values at the first pressure level and tissue displacements: (a) Normalized extracellular resistance versus tissue displacement (b) Normalized intracellular resistance versus tissue displacement (c) Normalized membrane capacitance versus tissue displacement

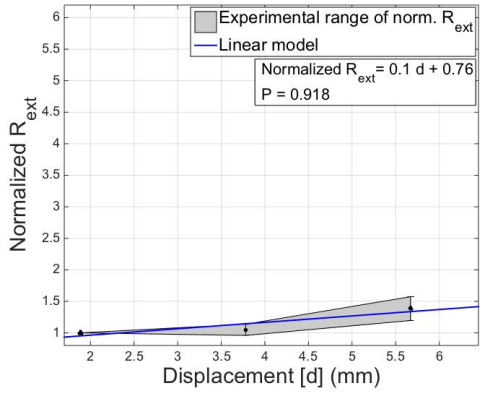

(a)

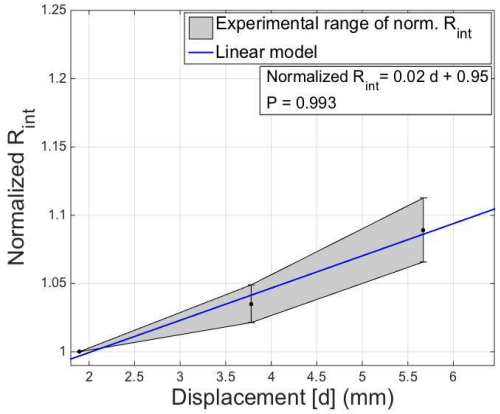

(b)

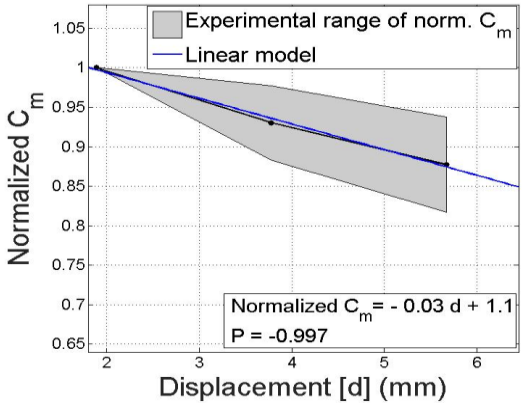

(c)

Figure 4.9. Right Forearm Tissue, the correlation of compression-dependent Cole-Cole parameters normalized to their values at the first pressure level and tissue displacements: (a) Normalized extracellular resistance versus tissue displacement (b) Normalized intracellular resistance versus tissue displacement (c) Normalized membrane capacitance versus tissue displacement

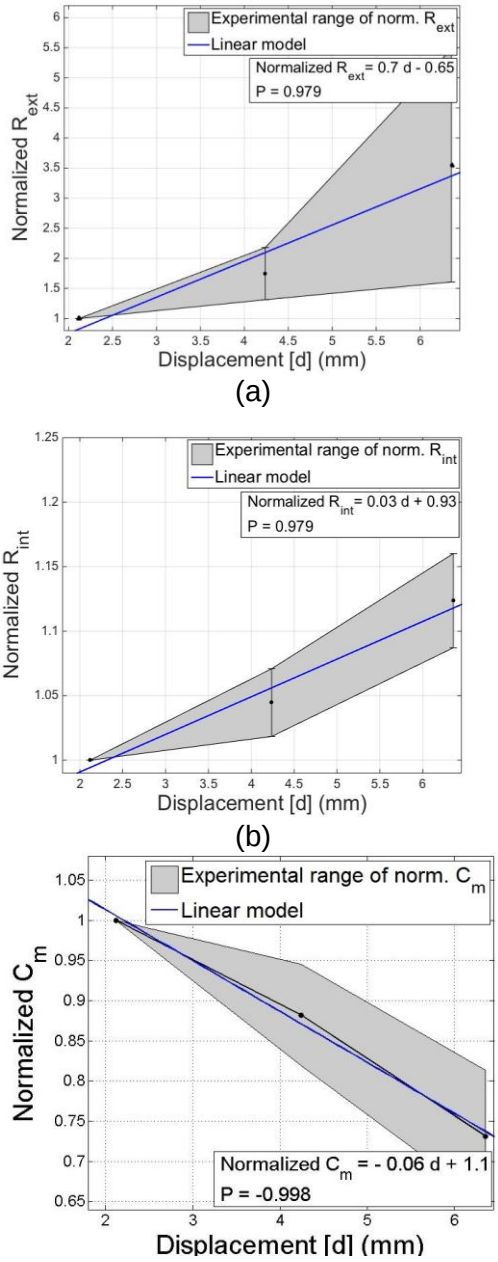

Figure 4.10. Left Bicep Tissue, the correlation of compression-dependent Cole-Cole parameters normalized to their values at the first pressure level and tissue displacements: (a) Normalized extracellular resistance versus tissue displacement (b) Normalized intracellular resistance versus tissue displacement (c) Normalized membrane capacitance versus tissue displacement

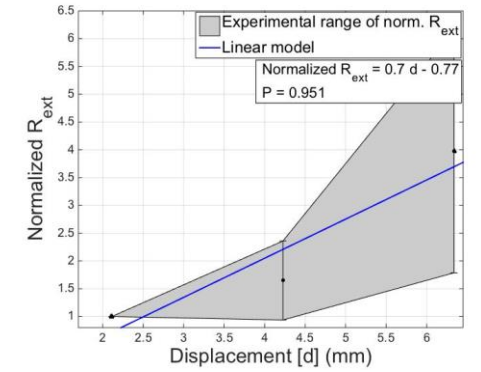

(a)

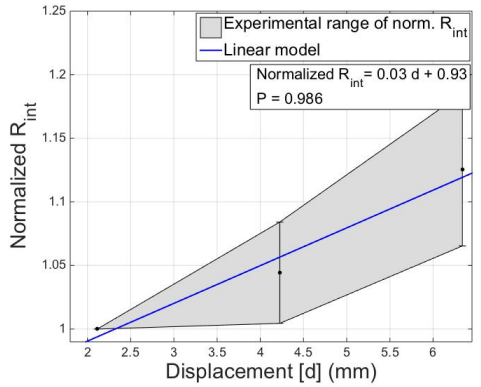

(b)

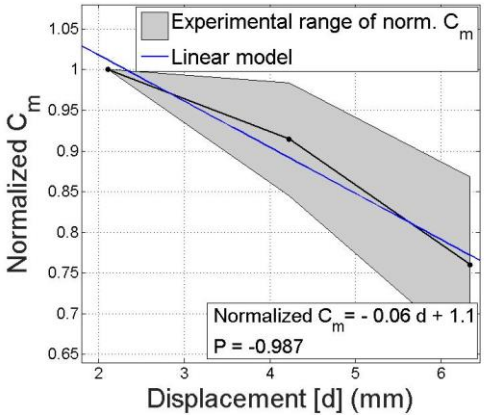

(c)

Figure 4.11. Right Bicep Tissue, the correlation of compression-dependent Cole-Cole parameters normalized to their values at the first pressure level and tissue displacements: (a) Normalized extracellular resistance versus tissue displacement (b) Normalized intracellular resistance versus tissue displacement (c) Normalized membrane capacitance versus tissue displacement

Table 4.5. The correlation of normalized Cole-Cole parameters

Samples and Subjects	Linear Correlation of Normalized R_{ext} to Displacement Pearson Product	Linear Correlation of Normalized R_{int} to Displacement Pearson Product	Linear Correlation of Normalized C_m to Displacement Pearson Product
Chicken Samples	Norm R_{ext}=0.17 d+0.9 0.972	Norm R_{int}=-0.081 d+1 -0.986	Norm C_m=0.19 d+0.91 0.975
Rat Samples	Norm R_{int}=-0.033 d+1 0.977	Norm R_{int}=-0.033 d+1 -0.998	Norm C_m=0.079 d+0.97 0.992
Left Forearms	Norm R_{ext}=0.1 d+0.78 0.983	Norm R_{int}=0.023 d+0.95 0.924	Norm C_m=-0.031 d+1.1 -0.999
Right Forearms	Norm R_{ext}=0.1 d+0.76 0.918	Norm R_{int}=0.024 d+0.95 0.993	Norm C_m=-0.032 d+1.1 -0.997
Left Biceps	Norm R_{ext}=0.69 d-0.65 0.979	Norm R_{int}=0.029 d+0.93 0.969	Norm C_m=-0.063 d+1.1 -0.998
Right Biceps	Norm R_{ext}=0.7 d-0.77 0.951	Norm R_{int}=0.03 d+0.93 0.986	Norm C_m=-0.057 d+1.1 -0.987

Chapter 5.

Tissue classification

Based on the experimental procedures in 2.3Chapter 2 and the mathematical modeling methods explained in Chapter 3, this chapter presents the results of experiments and further mathematical analysis on the results. The experimental results of healthy and cancerous subjects are presented and compared in this chapter. Furthermore, the classification methods for the purpose of cancer detection are applied on the healthy and cancerous subjects' results.

5.1. Validating the use of contralateral *in-vivo* sites as control

In this study, the use of contralateral sites of body is proposed to be used as the control. Soft tissue is conductive, and the tissue conductivity is different in various types of tissues. Thus it is postulated that the contralateral sites of healthy human body, which have almost the same tissue structures, have the same conductivities. Moreover, the electrical properties of malignant tissues alter with respect to healthy tissue due to the increased cellular water and sodium content, altered membrane permeability, and changed packing density and orientation of cells [68] [69]. As a result, in this study it is proposed to use the contralateral sites of the body as control. This idea suggests that if the tested tissue is healthy, the changes in electrical properties of that tissue with respect to its contralateral site will not be significant and if the tested tissue is tumorous, a significant change in the electrical properties of both sites will be observed. In this section, the changes of the electrical properties of healthy and cancerous human tissues, with regard to their contralateral parts, are studied.

In order to validate this postulation, the data collected from two ethical studies were analyzed. The studies included: "*In-vivo* data collection of dielectric, thermal and elastic properties of human tissue, APPL. #2011s0523" which was taken from the Office of Research Ethics, Simon Fraser University and "Electrical Impedance Analysis of Malignant and Benign Tissue: Effects of Temperature and Pressure" which was performed under the UBC BCCA Research Ethics Board under Dr. Paris Ann Ingledew as the Principal Investigator and REB Number H13-02887.

In the first study, the collection of *in-vivo* data from healthy subjects was involved. Tissue admittance at various compression levels and elastic properties of biceps and forearms of eleven healthy human subjects were measured. However, in this section, only the admittance data of subjects at the first pressure level are used. In the second study which was a collaborative research with the BC Cancer Agency, the admittance data collection was performed on ten malignant skin tumors with the healthy contralateral skin as the control in order to observe the variation of the admittance in healthy and tumorous human tissue.

5.1.1. Admittance results of contralateral sites in healthy subjects

In this study, 11 healthy subjects were recruited. The electrical impedance measuring probe was tested on these healthy subjects' forearms and biceps at three various compression levels and in three trials per each compression level. As illustrated in Chapter 4, the electrical properties of soft tissue vary with the applied pressure. Therefore it can be concluded that for cancer detection purposes based on the electrical impedance spectroscopy, in order to have consistent results the experiments should either be performed at a fixed pressure level or the used pressure levels should be recorded and then the results should be scaled. The first sets of bioimpedance data, i.e. the bioimpedance data at the first compression level (2.5 N) was analysed in this section. The bioimpedance measurement was conducted on the biceps and the forearms of each subject; therefore the number of healthy data can be considered to be 22 healthy subjects. In order to have a comparison, the bioimpedance measurements were conducted on the contralateral sites on biceps and forearms. The imaginary part of the admittance of each subject was plotted versus the real part of the admittance, thus

the Nyquist plot of each subject was obtained. The Nyquist plot of each subject's contralateral body sites were represented in the same plot, so that a visual comparison can be made on the Nyquist plots of the contralateral sites of each subject. Thereafter, the raw data were fitted into the Cole-Cole model and the corresponding electrical parameters were calculated. In Figure 5.1, the Nyquist plots of eleven subjects' bicep as well as their contralateral Nyquist plots are illustrated and similarly in Figure 5.2, the Nyquist plots of contralateral sites on healthy forearms are compared.

As illustrated by Figure 5.1 and Figure 5.2, the contralateral sites of body have almost the same Nyquist bioimpedance results. In order to have a more detailed comparison, the electrical properties of contralateral sites are extracted and compared in section 5.1.2.

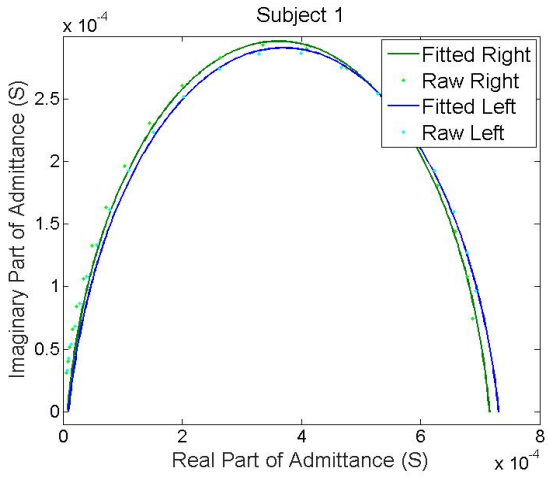
Subject 1
x 10^-4
Imaginary Part of Admittance (S)
Real Part of Admittance (S)
x 10^-4
Fitted Right
Raw Right
Fitted Left
Raw Left

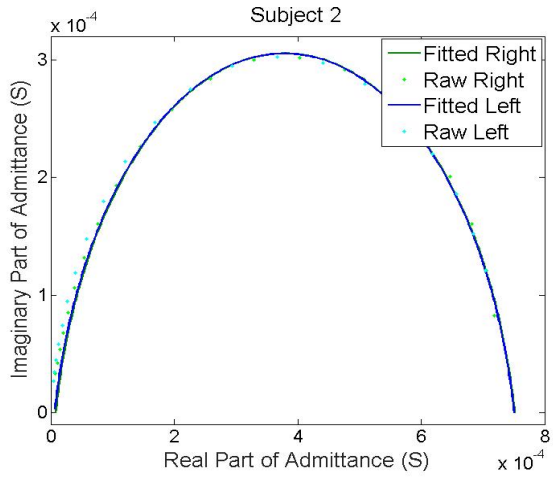
Subject 2
x 10^-4
Imaginary Part of Admittance (S)
Real Part of Admittance (S)
x 10^-4
Fitted Right
Raw Right
Fitted Left
Raw Left

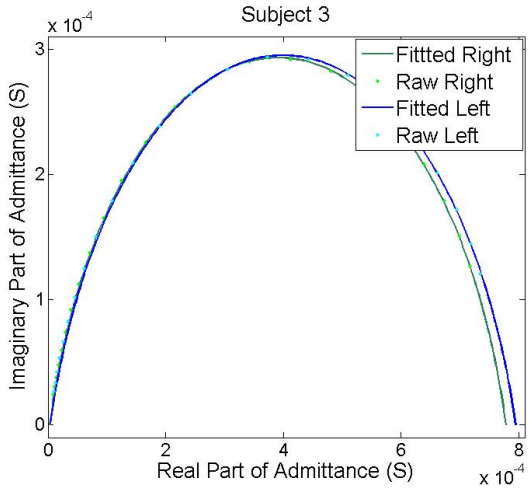
Subject 3
x 10^-4
Imaginary Part of Admittance (S)
Real Part of Admittance (S)
x 10^-4
Fittted Right
Raw Right
Fitted Left
Raw Left

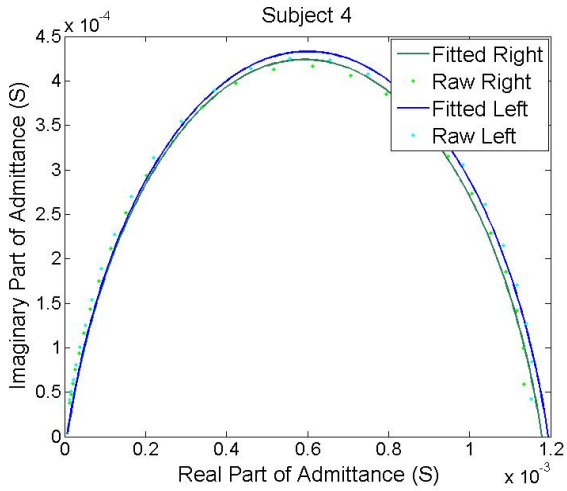
Subject 4
x 10^-4
Imaginary Part of Admittance (S)
Real Part of Admittance (S)
x 10^-3
Fitted Right
Raw Right
Fitted Left
Raw Left

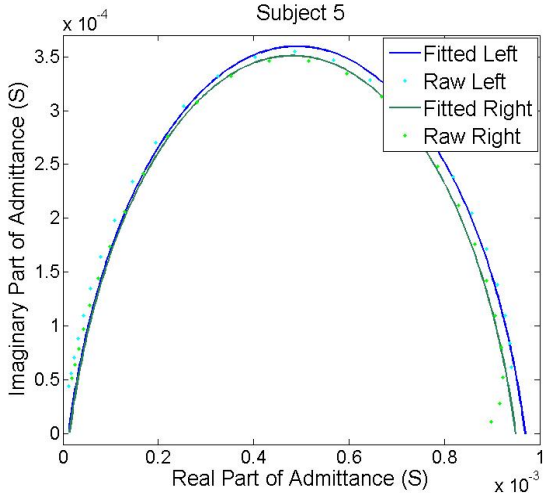
Subject 5
x 10^-4
Imaginary Part of Admittance (S)
Real Part of Admittance (S)
x 10^-3
Fitted Left
Raw Left
Fitted Right
Raw Right

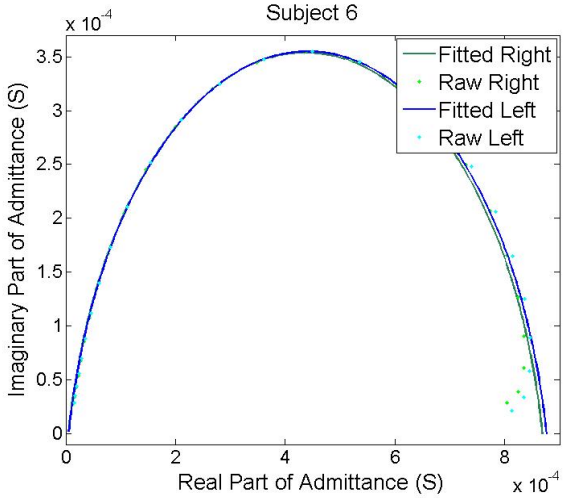
Subject 6
x 10^-4
Imaginary Part of Admittance (S)
Real Part of Admittance (S)
x 10^-4
Fitted Right
Raw Right
Fitted Left
Raw Left

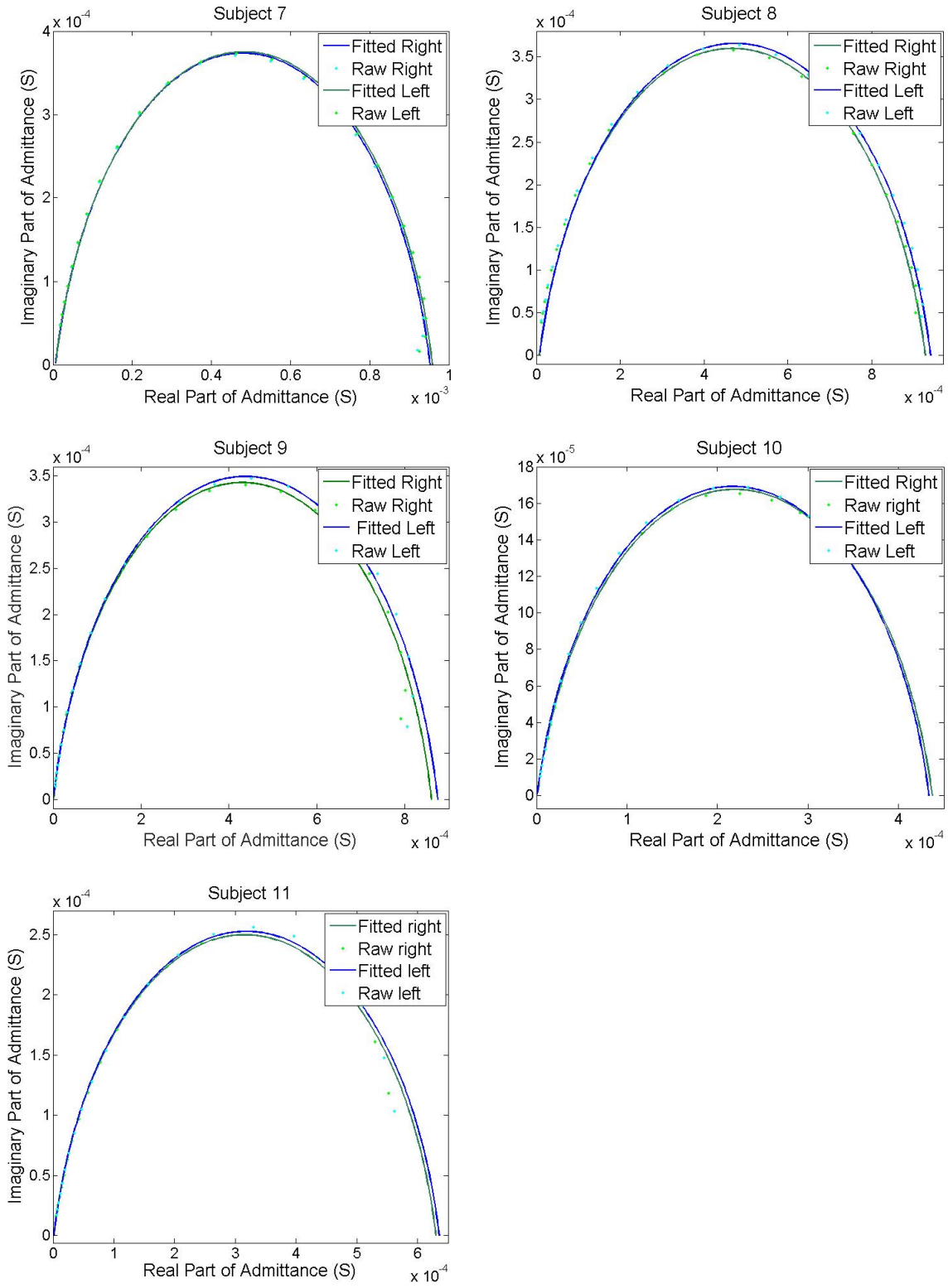

Figure 5.1. Admittance plots of the healthy biceps and their contralateral part

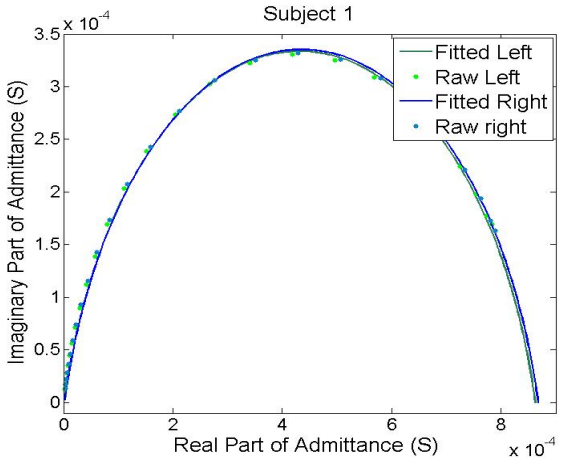
Subject 1
x 10^-4
Imaginary Part of Admittance (S)
Real Part of Admittance (S)
x 10^-4
Fitted Left
Raw Left
Fitted Right
Raw right

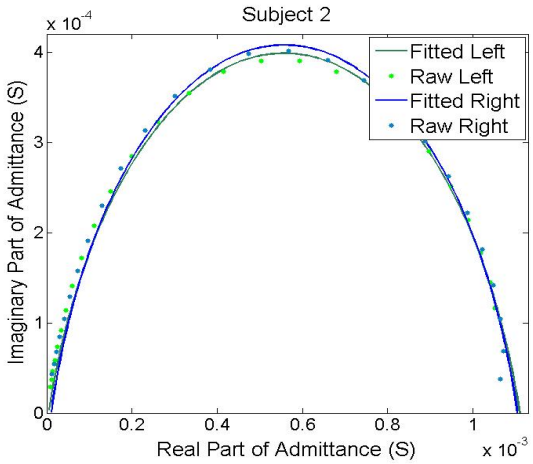
Subject 2
x 10^-4
Imaginary Part of Admittance (S)
Real Part of Admittance (S)
x 10^-3
Fitted Left
Raw Left
Fitted Right
Raw Right

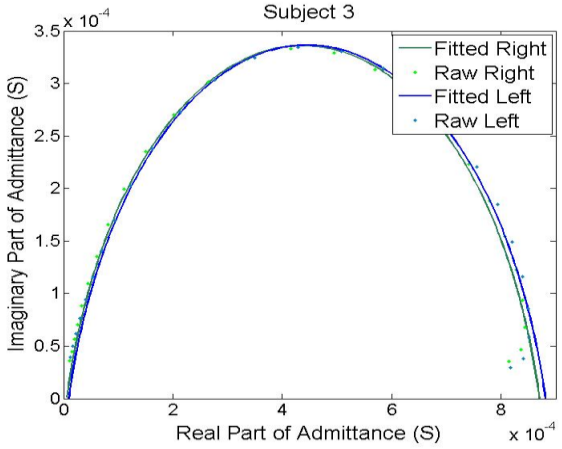
Subject 3
x 10^-4
Imaginary Part of Admittance (S)
Real Part of Admittance (S)
x 10^-4
Fitted Right
Raw Right
Fitted Left
Raw Left

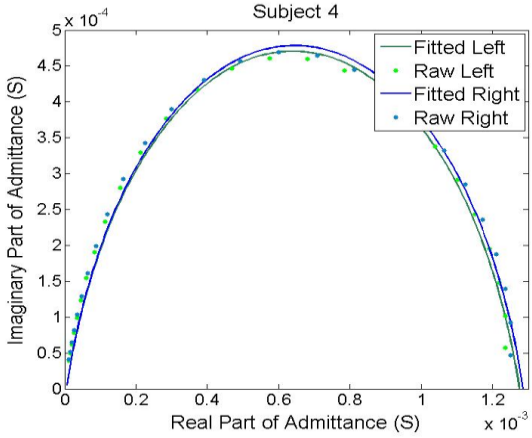
Subject 4
x 10^-4
Imaginary Part of Admittance (S)
Real Part of Admittance (S)
x 10^-3
Fitted Left
Raw Left
Fitted Right
Raw Right

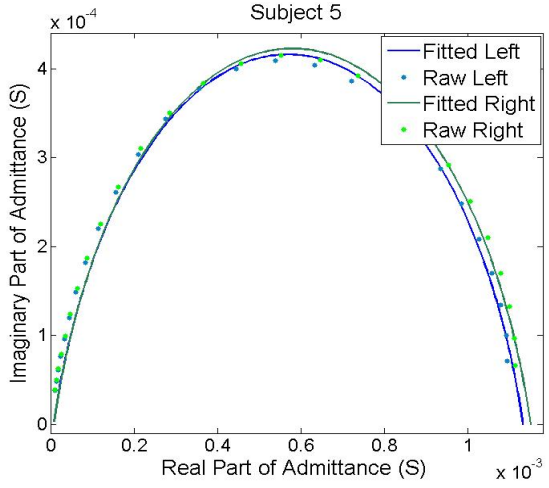
Subject 5
x 10^-4
Imaginary Part of Admittance (S)
Real Part of Admittance (S)
x 10^-3
Fitted Left
Raw Left
Fitted Right
Raw Right

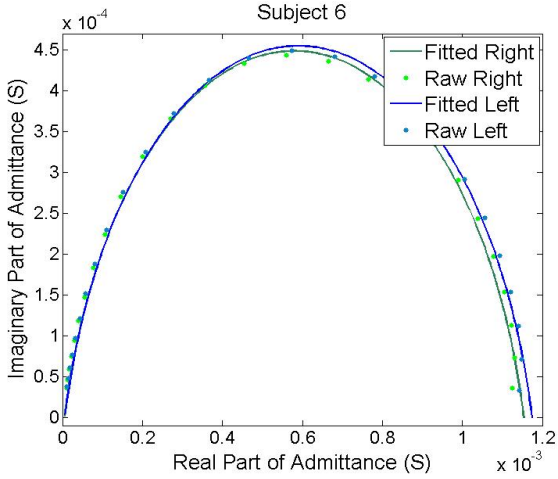
Subject 6
x 10^-4
Imaginary Part of Admittance (S)
Real Part of Admittance (S)
x 10^-3
Fitted Right
Raw Right
Fitted Left
Raw Left

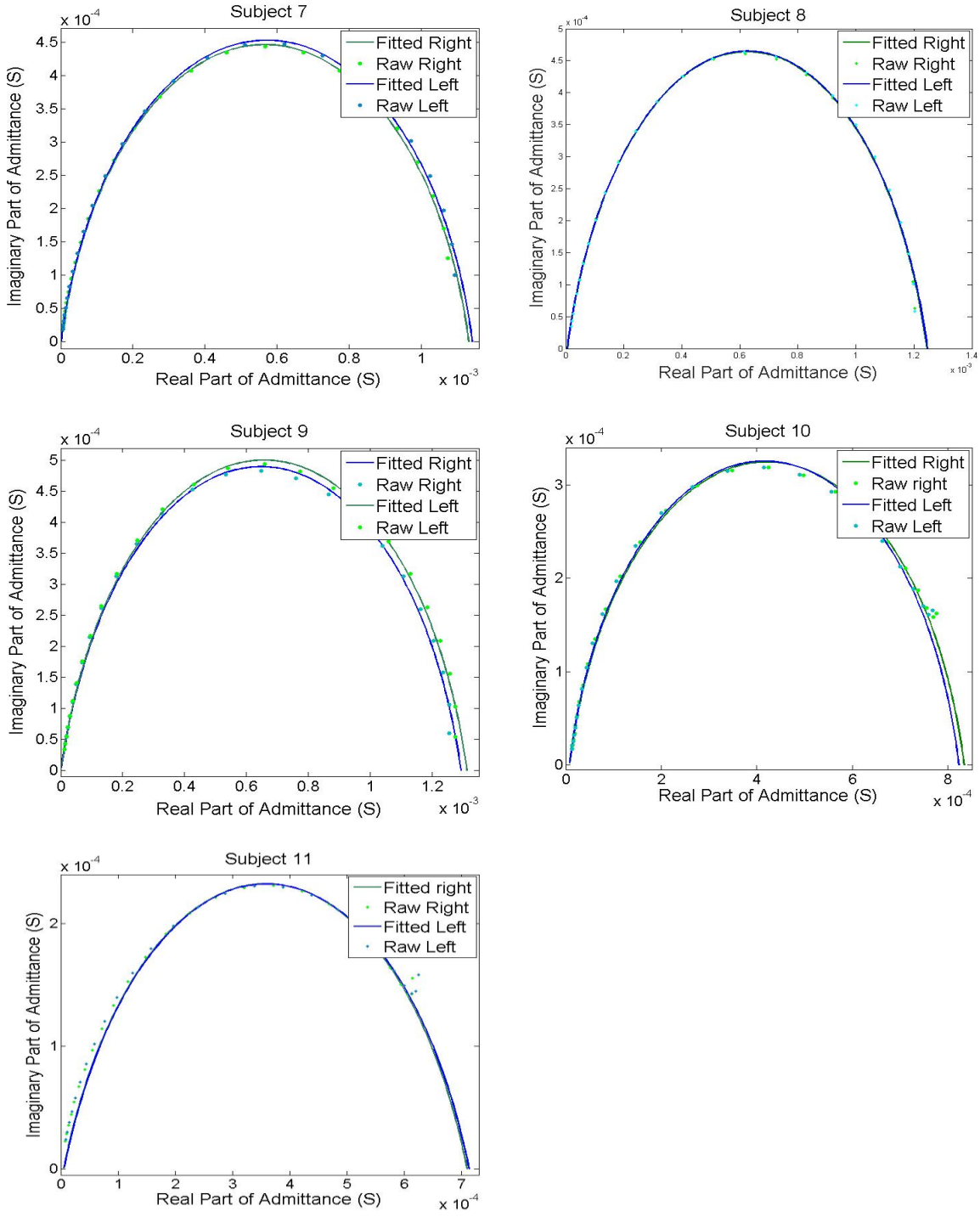

Figure 5.2. Admittance plots of the healthy forearms and their contralateral part

5.1.2. Assessing the use of contralateral extracted electrical features of healthy subjects

The visual comparison of Nyquist plots of admittances of contralateral sites of the biceps and forearms of eleven subjects were illustrated in section 5.1.1. In order to have a more detailed comparison, the electrical properties of each subject are extracted and compared according to the statistical analysis methods in this section.

Many parametric statistical methods such as ANOVA, t-test and f-test require that the dependent variable is approximately normally distributed for each category of independent variable. In order to check if the data are normally distributed, there are some tests which should be conducted on the data. There are a set of values in each test which have a desirable range. If these values are in the desirable range, the data are normally distributed. The first test is the Skewness and Kurtosis test, in which the z-value should be between -1.96 and +1.96. It should be better if the z-value is as close as zero. The Shapiro-Wilk test is considered as the second test. In this type of test, the null hypothesis is that the data are normally distributed and a p-value is obtained based on this test. If this p-value is below 0.05, the null hypothesis will be rejected and the data will not be normally distributed.

In addition, there are some visual inspections which should be performed for testing the normally distribution of data. The first visual inspection of data is checking the histogram of data for each category. The histogram of each category of data should have the approximate shape of a normal curve. The other visual inspection method is the Q-Q plots in which the data points should be along the line. The final visual inspection method is the box plots which should be symmetrical. It should be mentioned that the data do not need to be perfectly distributed. The main goal is that the data should be approximately normally distributed and each category of independent variables should be checked to be normally distributed.

Thus the first step for this purpose is to check if the electrical properties of healthy subjects are normally distributed. Checking the normality of variables was performed in SPSS. The calculated skewness and kurtosis z-values were between -1.96 and +1.96, so the requirement of this test has been met [70] [71]. The data were a little

skewed and kurtotic for the three electrical properties of both right and left sides of body but they did not differ significantly from normality. Thus we can assume that the data were approximately normally distributed in terms of skewness and kurtosis.

A Shapiro-Wilk's test [72] [73] was also performed and the p-values were above 0.05. Therefore, the null hypothesis of the Shapiro-Wilk's test was not rejected and the data were normally distributed.

Finally the visual inspection of their histograms, normal Q-Q plots and box plots showed that the electrical properties were approximately normally distributed for each subject's left and right forearm and bicep.

Since the electrical properties were normally distributed and there were two groups of data to be compared (contralateral parts of body), the statistical analysis method which was chosen for this study was the independent sample t-test.

Being normally distributed, an independent t-test was conducted to assess the use of the contralateral sites as the control. The null hypothesis was: there is no statistically significant difference between the mean electrical properties of the tested tissue of each healthy subject and the mean electrical properties of its contralateral tissue. In order to see if this null hypothesis is rejected or not, an independent t-test was performed on each subject's electrical properties extracted from each measurement individually. The t-test results on each subject's 3 electrical properties showed $p>0.05$. Thus the null hypothesis was not rejected and there was no statistically significant difference between the mean electrical properties of the contralateral sites of body. Therefore, the contralateral sites of healthy subjects can be considered as the control.

The extracted electrical properties of each subject are illustrated in Figure 5.3 and Figure 5.4. In these figures the electrical properties of the left and right tissues of each subject are plotted side by side in order to compare the results. Figure 5.3 illustrates the electrical parameters of the healthy subjects' biceps while Figure 5.4, compares the electrical parameters of healthy subjects' forearms.

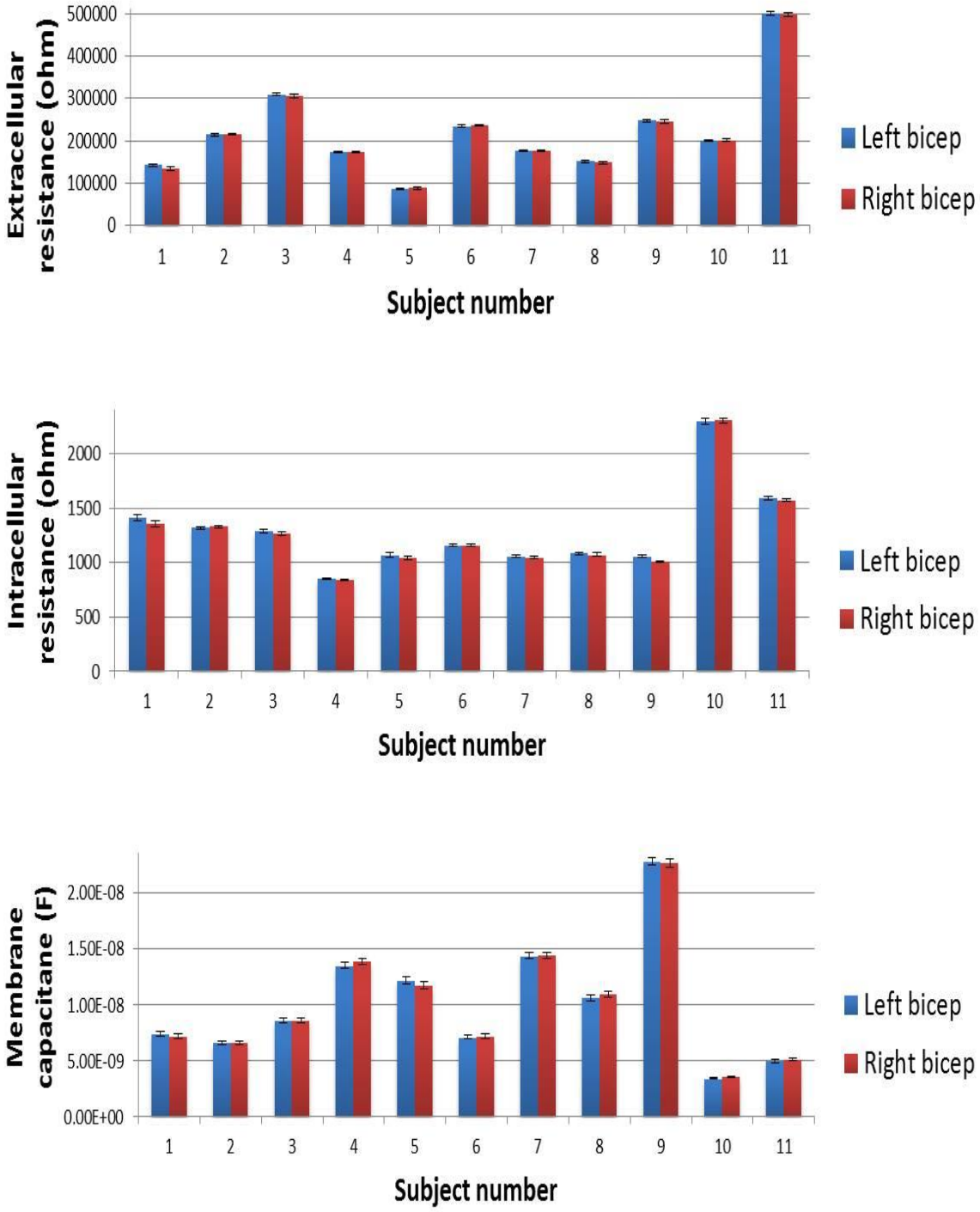

Figure 5.3. Comparison of the electrical parameters of right and left bicep of healthy subjects

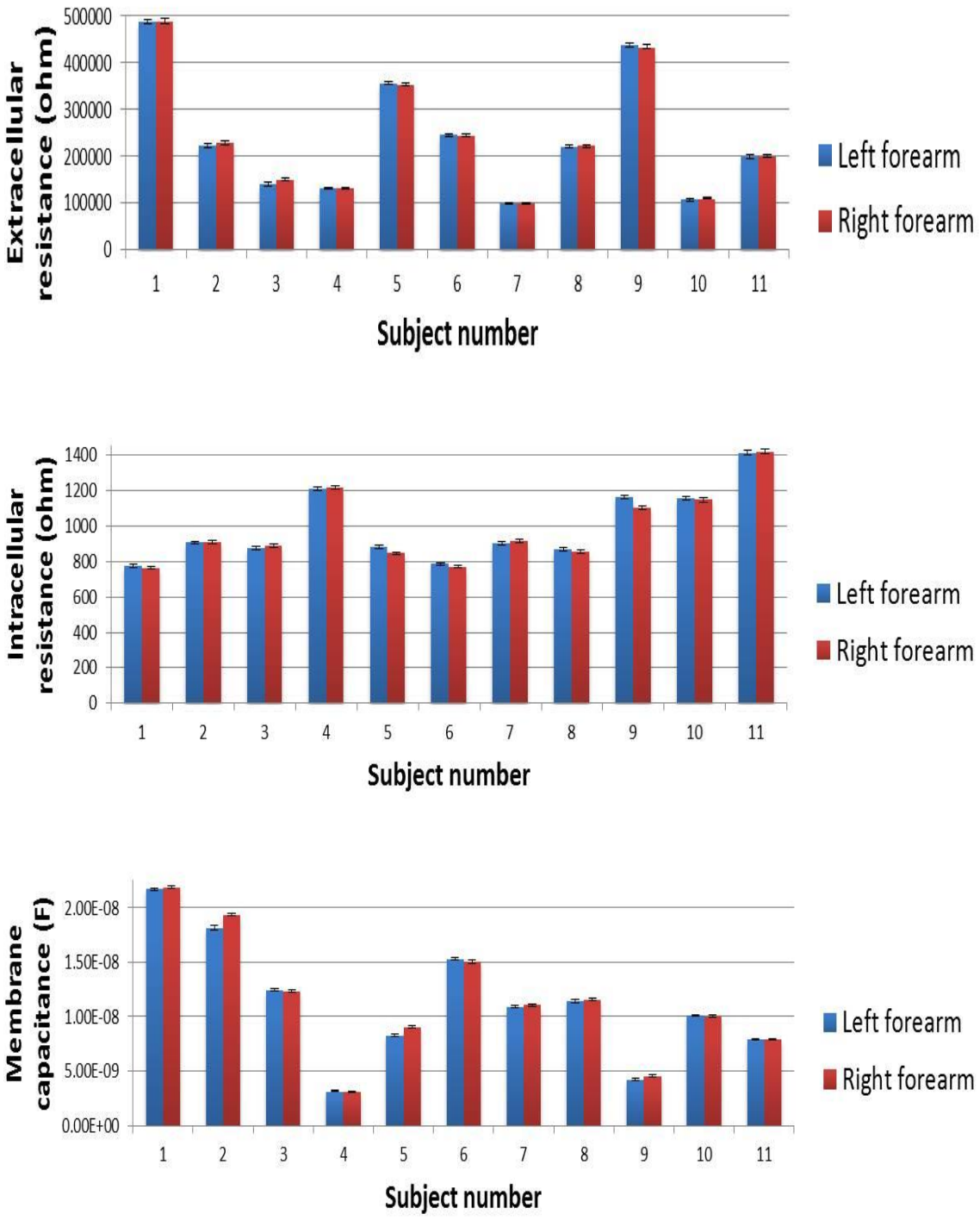

Figure 5.4. Comparison of the electrical parameters of right and left forearm of healthy subjects

5.1.3. Admittance results of contralateral sites in tumorous subjects

In this section of the study, the admittance results of 10 tumorous subjects are presented. The electrical impedance measuring probe was tested on the tumorous part of the patients as well as its contralateral healthy site. In order to have consistency with the healthy subjects' results, 2.5N force was applied to the measuring probe while taking the measurements by wearable PPS pressure sensors. The same procedure in presenting the healthy subjects' data was incorporated in this part; the imaginary part of admittance of each subject is plotted versus the real part of admittance, thus the Nyquist plot of each subject can be obtained. In order to compare the differences in admittances of tumorous and healthy tissues, the admittance of the tumorous part of each patient and the admittance of its contralateral healthy site were presented in the same plot and in the form of Nyquist plot. Thereafter, the raw data were fitted into the Cole-Cole model and the corresponding electrical parameters were calculated. In Figure 5.5, the Nyquist plots of the tumorous body parts of ten tumorous subjects as well as their contralateral healthy sites are illustrated and the results can be compared visually.

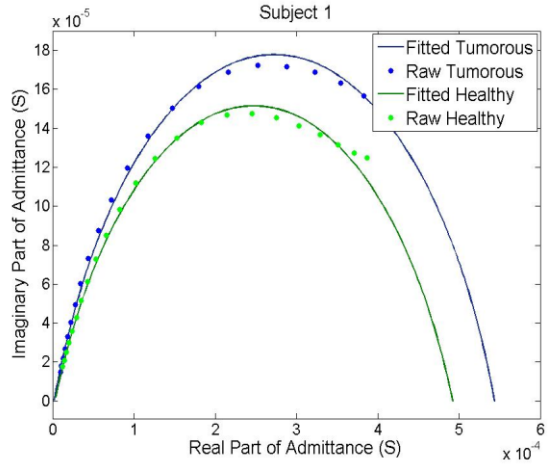
Subject 1
x 10^-5
Fitted Tumorous
Raw Tumorous
Fitted Healthy
Raw Healthy
Imaginary Part of Admittance (S)
Real Part of Admittance (S)
x 10^-4

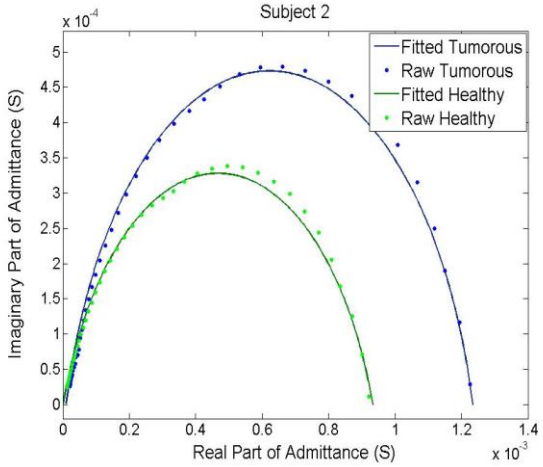
Subject 2
x 10^-4
Fitted Tumorous
Raw Tumorous
Fitted Healthy
Raw Healthy
Imaginary Part of Admittance (S)
Real Part of Admittance (S)
x 10^-3

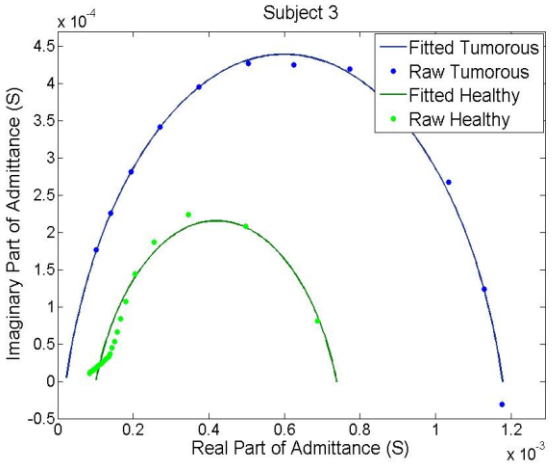
Subject 3
x 10^-4
Fitted Tumorous
Raw Tumorous
Fitted Healthy
Raw Healthy
Imaginary Part of Admittance (S)
Real Part of Admittance (S)
x 10^-3

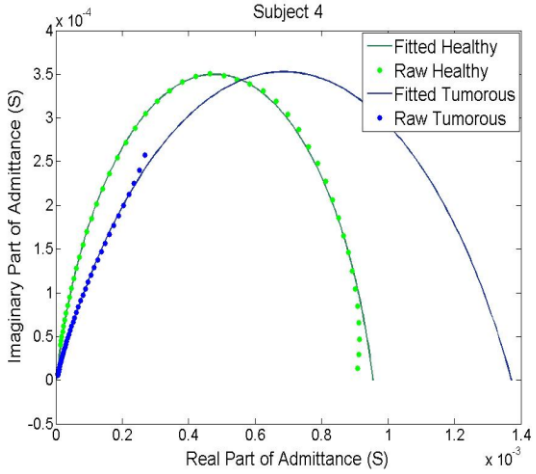
Subject 4
x 10^-4
Fitted Healthy
Raw Healthy
Fitted Tumorous
Raw Tumorous
Imaginary Part of Admittance (S)
Real Part of Admittance (S)
x 10^-3

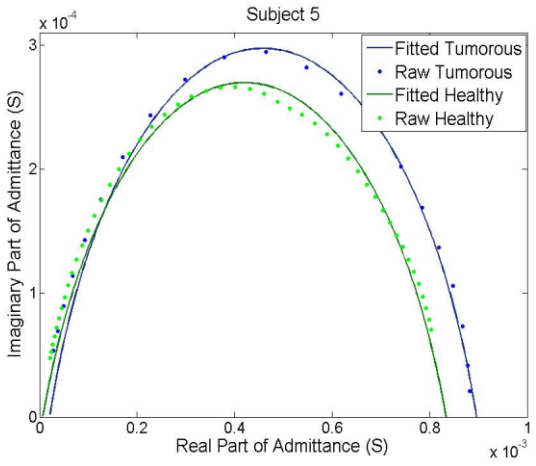
Subject 5
x 10^-4
Fitted Tumorous
Raw Tumorous
Fitted Healthy
Raw Healthy
Imaginary Part of Admittance (S)
Real Part of Admittance (S)
x 10^-3

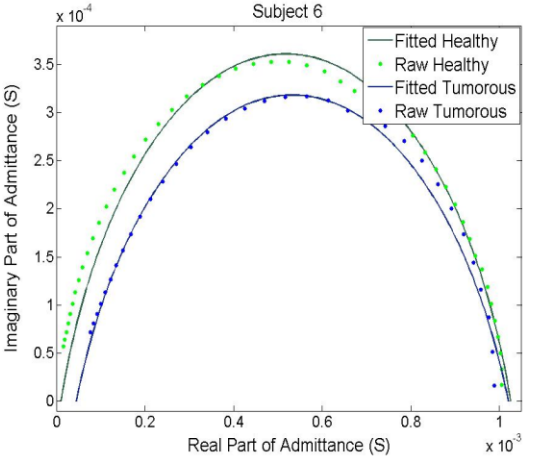
Subject 6
x 10^-4
Fitted Healthy
Raw Healthy
Fitted Tumorous
Raw Tumorous
Imaginary Part of Admittance (S)
Real Part of Admittance (S)
x 10^-3

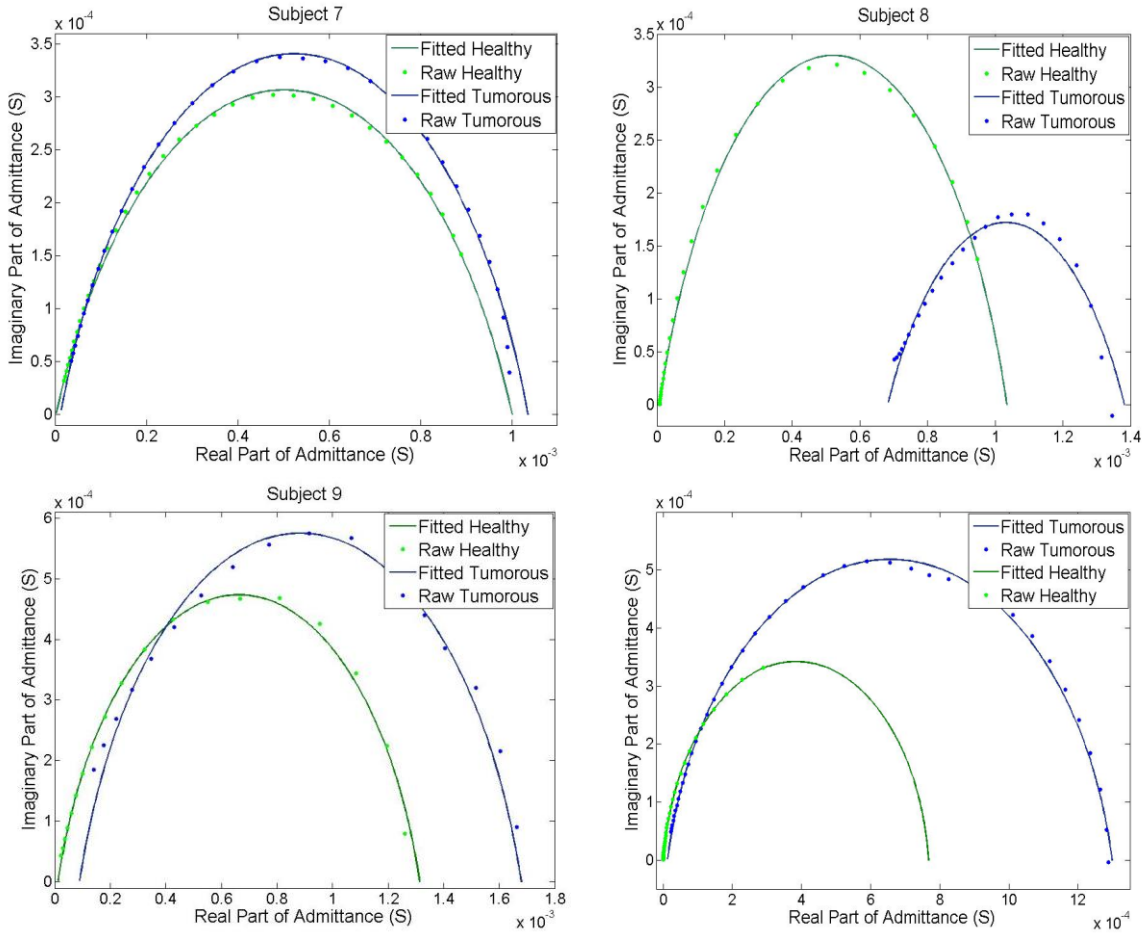

Figure 5.5. Admittance plot of the tumorous subjects and the contralateral healthy part

Comparing figures Figure 5.1, Figure 5.2 and Figure 5.5 reveals that the admittance Nyquist plots of contralateral sites in healthy subjects are almost the same, however, the admittance Nyquist plots of contralateral sites in tumorous subjects significantly vary. These results support the proposed idea of this research that the contralateral sites of body should have the same electrical properties unless there is a malignancy in one of the sites. For a more detailed comparison, the electrical properties of contralateral sites are extracted and compared in section 5.1.4.

5.1.4. Assessing the use of contralateral extracted electrical features of tumorous subjects

The visual comparison of Nyquist plots of admittances of the tumorous part and its contralateral site of ten tumorous subjects were illustrated in section 5.1.3. For a more detailed comparison, the electrical properties of each subject are extracted and compared according to the statistical analysis methods in this section.

The normality of the electrical parameters of tumorous subjects is checked in the same way as was explained in section 5.1.2. The calculated skewness and kurtosis z-values were in the desired range (between -1.96 and +1.96). The data are a little skewed and kurtotic, but they do not differ significantly from normality. The p-values obtained from the Shapiro-Wilk's test [72] [73] were above 0.05. Therefore, according to this test the data are normally distributed. Finally the visual inspection of their histograms, normal Q-Q plots and box plots showed that the electrical properties were approximately normally distributed. According to the normality of the data and comparing two groups of data, the independent sample t-test was chosen for this study.

Being normally distributed, an independent t-test was conducted to see if there is a significant difference in the electrical properties of the tumorous part of patient and its contralateral part, also to see if the contralateral site can be used as the control. The null hypothesis was: there is no significant difference in the mean electrical properties of the tumorous tissue and its contralateral site in each tumorous subject. In order to see if this null hypothesis is rejected or not, an independent t-test was performed on each subject's electrical properties extracted from each measurement individually in SPSS. The t-test results on each subject's 3 electrical properties showed p-values below 0.05 which rejected the null hypothesis and confirmed that there is a significant difference between the mean electrical properties of tumorous site and its contralateral healthy site. Therefore, the contralateral sites of tumorous subjects can be considered as the control.

The extracted electrical properties of each tumorous subject are illustrated in Figure 5.6. In these figures the electrical properties of the left and right tissues of each subject, i.e. the electrical properties of the tumorous and its contralateral healthy sites are plotted side by side in order to compare the results.

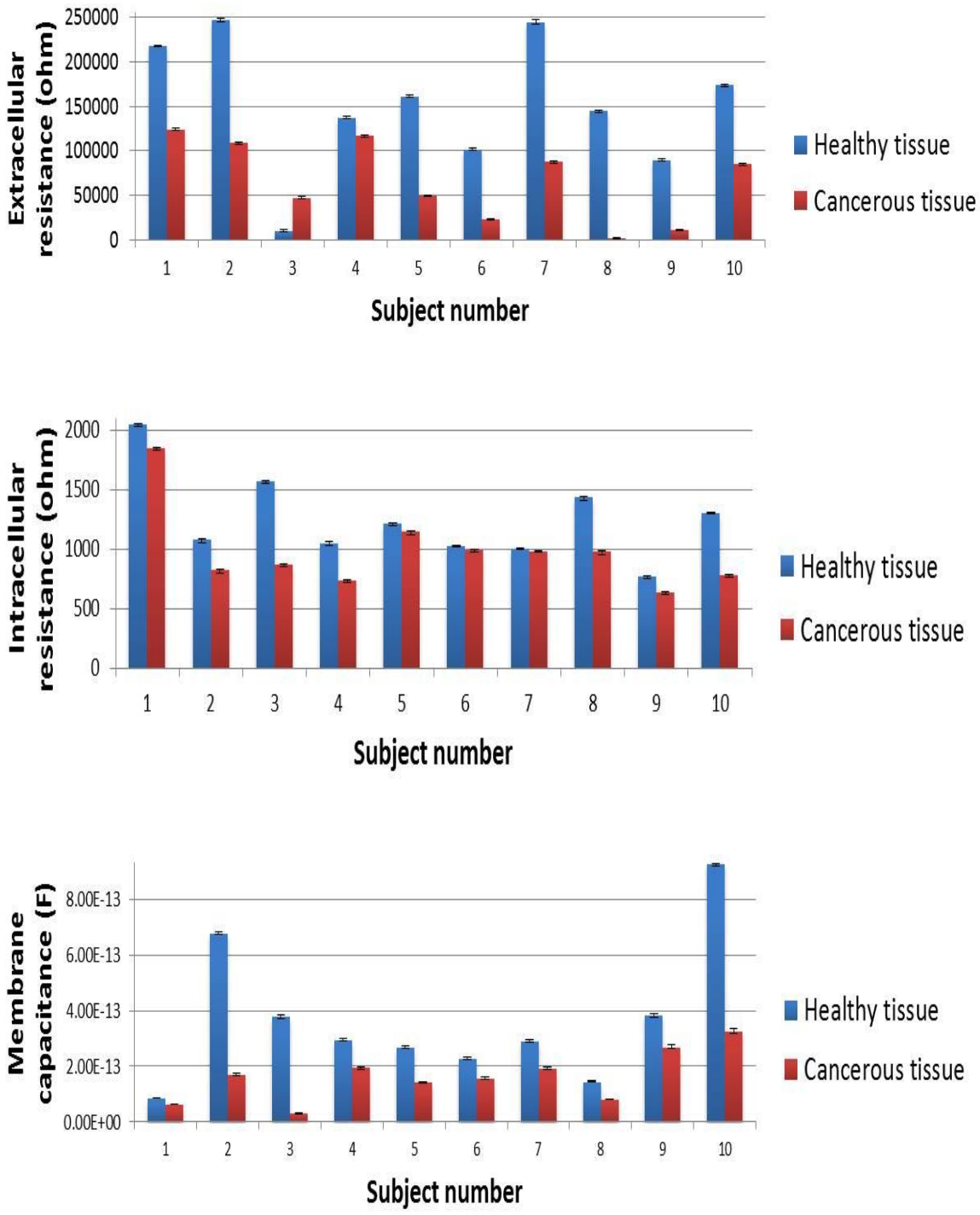

Figure 5.6. Comparison of the electrical parameters of the tumorous tissue and its contralateral healthy tissue in cancerous subjects

Due to the high inter-subject variations in the electrical properties of human subjects, there was a need to have a normalization method in order to have a better interpretation of results. Comparison of Figure 5.1 to Figure 5.6 confirms the idea proposed by this study that the contralateral sites of human body can be used for normalizing the electrical properties of each person. The results suggest that although there is a significant difference in electrical properties between subjects, there is no significant difference within the contralateral tissues of healthy subjects, unless there is a malignancy in one of the tested tissues. Thus in the classification methods performed in section 5.2, the contralateral sites of each tested tissue will be used as the control and for normalization.

5.2. Classification methods

As shown in this study, the use of electrical impedance of contralateral parts of body can be used as the control when performing tumor detection in human tissue. In this section, the electrical impedance spectra, which were measured from 10 histologically analyzed lesions and 22 healthy subjects, are used to train classification methods for automatic detection of malignancy. Three classification methods are implemented on the raw data, the extracted features as well as the normalized features. Thereafter, the performance of each classification method on both raw and processed data are compared.

Three different classifier techniques were used in this study: Naïve Bayes classifier with Gaussian distribution, Naïve Bayes classifier with Kernel distribution and support vector machine (SVM). Using electrical bioimpedance spectra of *in-vivo* tissue, the human subjects are classified into two classes: cancerous and healthy classes.

In the first step, the raw admittance data of the 32 subjects, 10 cancerous subjects and 22 healthy subjects, are classified by Naïve Bayes classifier methods and SVM. These data, which are the raw admittance of subjects at 50 frequencies, are complex numbers illustrated in Figure 5.7. As explained in section 3.3, because of the small number of subjects, cross validation method has been utilized in order to have a more reliable result. Thus 10-fold cross validation, which is a popular choice of cross

validation, was performed on the data. 10-fold cross validation randomly separates the training data into 10 disjoint subsets. Each subset has roughly equal size and equal class proportions as in the training set. In the 10-fold cross validation, one subset is removed and the other 9 subsets are used for training, then the trained model is used to classify the removed subset. This process is repeated by removing each of the 10 subsets one at a time.

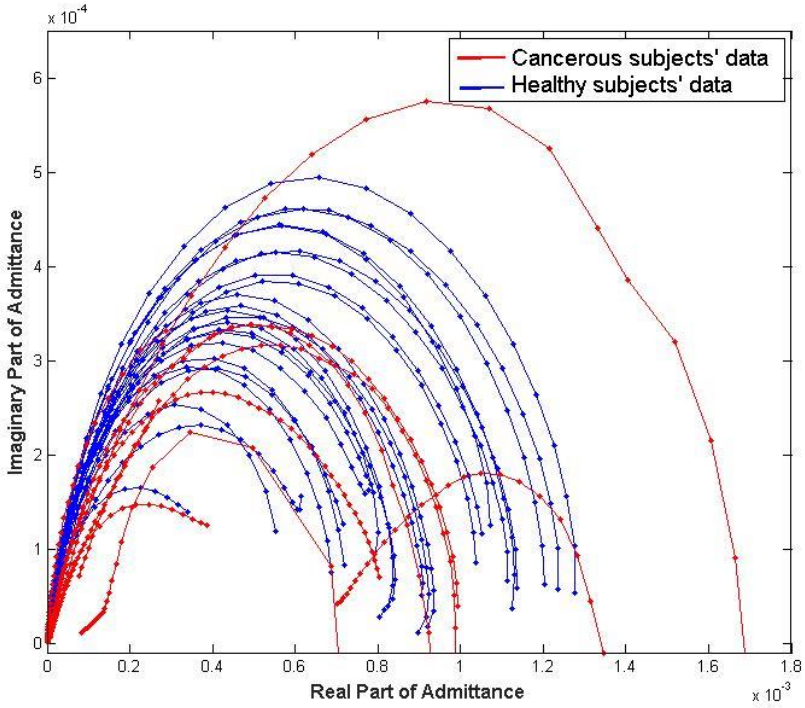

Figure 5.7. The raw admittance data of healthy and cancerous subjects

In the next step, the three classification methods were applied on the extracted electrical features of the healthy and cancerous subjects. The 3 extracted data of 32 subjects (22 healthy subjects and 10 cancerous subjects) are illustrated in Figure 5.8. Each axis represents one of the extracted electrical features. The axes in 3D plot show the extracellular resistance, intracellular resistance and membrane capacitance. The purpose of these plots is to show that there is a significant overlap between the extracted features of malignant and healthy subjects. By normalizing the extracted features with their contralateral value in each subject. Representing the normalized extracted electrical features in a 3D plot (see Figure 5.9), shows that the cancerous and

healthy data are separated. Separating the data by normalization results in a better performance of the classification methods.

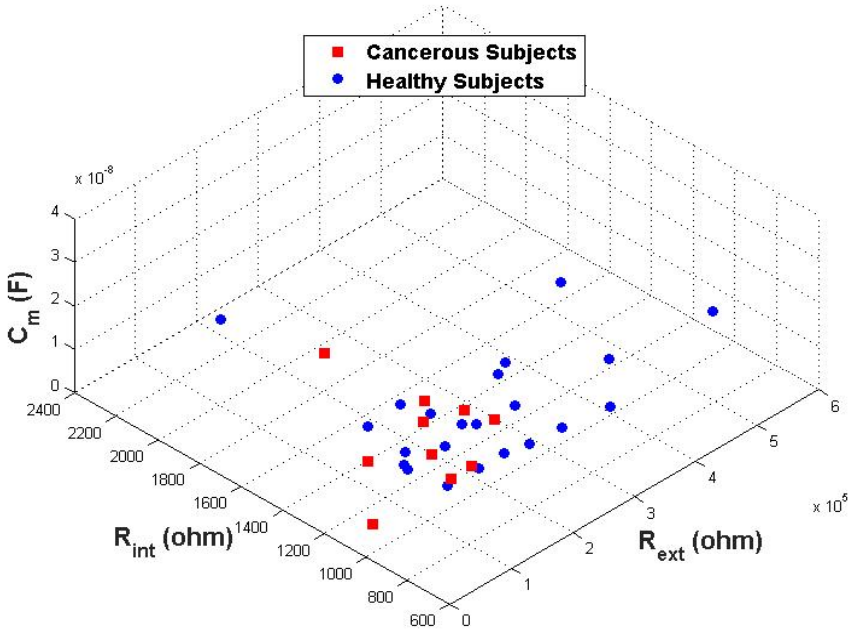

Figure 5.8. The representation of three extracted electrical properties of 32 subjects (22 healthy subjects and 10 cancerous subjects). Each axis indicates one of the electrical parameters

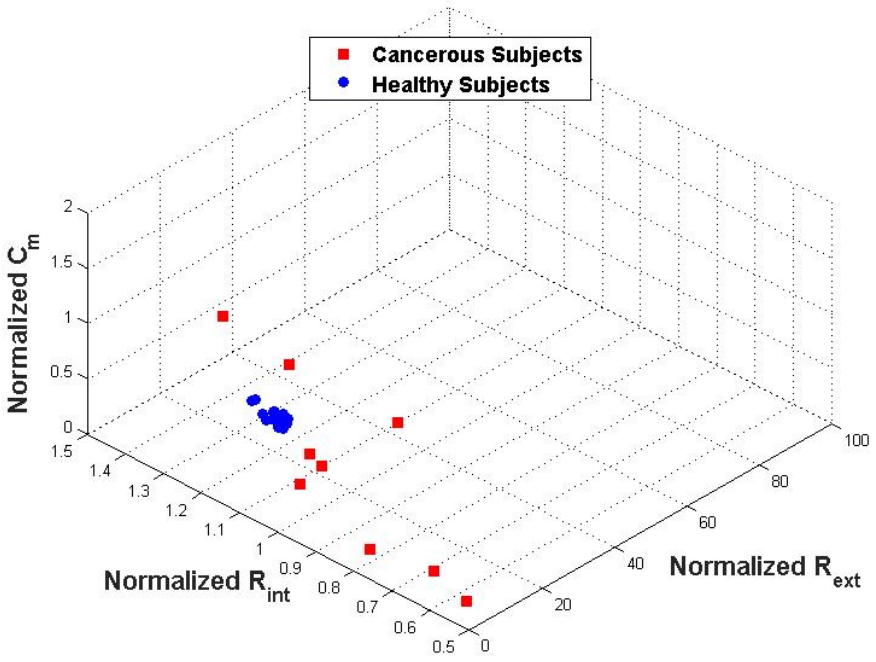

Figure 5.9. The representation of three normalized extracted electrical properties of 32 subjects (22 healthy subjects and 10 cancerous subjects). Each axis indicates one of the normalized electrical parameters to its contralateral values

A program was written in MATLAB for training and testing of NB classifiers (with Gaussian and Kernel distribution) and SVM classifier. The three classification methods have been applied on the raw data, the extracted features and the normalized extracted features. The accuracy, sensitivity, specificity, cross validation error and the misclassification error or resubstitution error of each method are illustrated in Table 5.1.

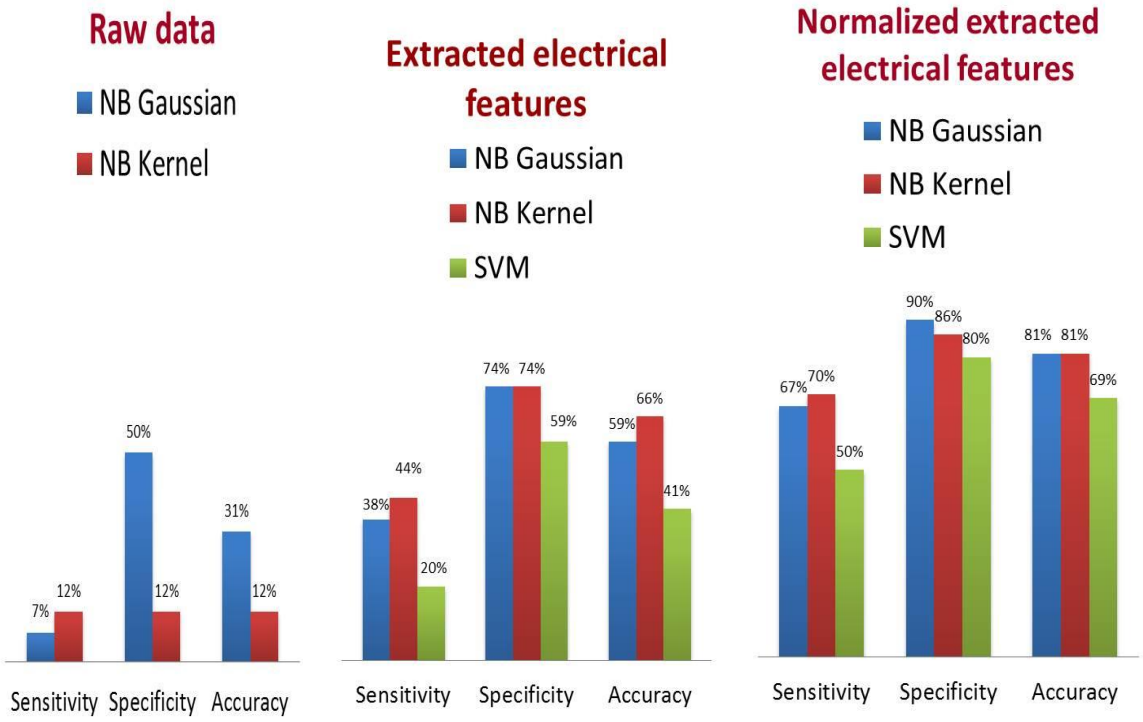

Figure 5.10. Comparison of the performance of 3 classification methods on the data

Table 5.1. The performance of various classification methods on raw and processed data

		Sensitivity %	Specificity %	Accuracy %	Resubstitution Error %	Cross Validation Error %
Raw Data	**NB Gaussian**	7.14	50	31.25	68.75	54.17
	NB Kernel	12.5	12.5	12.5	87.5	87.5
Extracted Features	**NB Gaussian**	38.46	73.68	59.38	40.63	31.2
	NB Kernel	44.44	73.91	65.63	34.38	33.3
	SVM	20	58.82	40.63	59.38	53.12
Normalized Extracted Features	**NB Gaussian**	66.67	90	81.25	18.75	16.67
	NB Kernel	70	86.36	81.25	18.75	13.12
	SVM	50	80	68.75	31.25	18.75

Chapter 6.

Discussion

The present study has primarily focused on two purposes. The first purpose of this study was to quantify the effect that compression has on the bioimpedance of soft tissue, both *in-vitro* and *in-vivo*. The second purpose of this study was to perform tissue classification for differentiate healthy subjects from subjects with lesions and examine various decision making methods for cancer detection.

For the first purpose of this study, two types of experiments were performed, *in-vitro* and *in-vivo*. In the *in-vitro* experiments, 20 chicken breast samples and 2 rat breast samples were electrically and mechanically tested and the correlation of the electrical properties and the mechanical properties of two types of tissue was sought. In the *in-vivo* study, two body parts of eleven human subjects were tested and again the effect of pressure on the electrical properties of tissues was acquired. The results of this study showed a linear correlation between the changes of the electrical properties of tissue and its displacement in both *in-vivo* and *in-vitro* results. The Pearson products of the linear relationships ($0.918 < p < 0.999$) indicated that the electrical properties of soft tissue correlate well to the mechanical changes as samples and subjects are compressed. The difference in the slopes and intercepts of the fitted models to the chicken, rat and human tissue data (Figure 4.6 to Figure 4.11 and Table 4.5) indicates that each type of tissue responds differently to the compression, suggesting that the electro-mechanical relation of tissue may be affected by its type and structure.

While the compression-induced alternations in bioimpedance of rat and chicken tissues have the same trend, the changes in both tissue types have different values. The changes of the normalized bioimpedance properties in rat tissue are much less than chicken tissue. This difference suggests that the cell structure of the rat breast is

different from the chicken breast and thus the extracellular and intracellular properties in rat tissue change less than the same properties of chicken tissue. In the experiments based upon *in-vivo* tissue testing, the same trend was observed as a result of the applied pressure. The slope of the changes in the bicep is more than that of the forearm which shows different tissue structure in these two types of body tissue.

Because of high impedance of cell's membrane in lower frequencies, current flows between the cells and through the extracellular space, therefore the resistivity measured at lower frequencies is mostly an indicator of the extracellular resistance. While at higher frequencies, permeability of cells' membrane increases which allows current cross the cell membrane, and therefore both intracellular and extracellular resistances of tissue influence the measured resistivity. The Cole-Cole model of the biological tissue also supports this idea by the fact that at lower frequencies, open circuit occurs at the branch containing capacitance. Therefore, current flows only through the resistor called the extracellular resistance and at higher frequencies, the capacitor short circuit occurs and thus current flows through both resistances in parallel. Accordingly, at higher frequencies, the equivalent resistance is comprised of two parallel resistors, so the total equivalent resistance has a lower value compared to each resistor's value. Therefore, in general, the value of resistance at higher frequencies is less than lower frequencies regardless of type of tissue. This has also been observed in previous experiments by Boris-Reymond [74] and in the current study, by the fact that the equivalent resistances at lower frequencies in chicken and rat breast are 537.85Ω and 565.54Ω and at higher frequencies are 262.39Ω and 307.89Ω respectively.

Based on the values of the extracellular resistances in this study, it is postulated that the higher extracellular resistance reflects a narrower extracellular space in any type of tissue. Koshini *et al.* also explained the increase in R_{ext} as a result of reduction in the extracellular volume [75]. The values at the first pressure level listed in Table 4.1 indicate that the extracellular resistance of the rat tissue is higher compared to chicken tissue. According to this postulation, it may be caused by the lower extracellular area between the rat cells where current faces less space to travel through. This idea is supported by another experimental observation in which squamous epithelium tissue

with more tightly packed cells showed higher resistivity in lower frequencies compared to columnar and transitional epithelia which have wider extracellular space [44].

The idea that the value of the extracellular resistance is influenced by the space between cells, may infer that applying pressure reduces the extracellular space and subsequently the extracellular resistance of tissue increases. This hypothesis is reflected in the extracellular behavior under compression in both *in-vivo* and *in-vitro* results (part a's of Figure 4.6 to Figure 4.11).

Another finding of this study was that while the changes in extracellular resistance have the same pattern in both *in-vivo* and *in-vitro* tests, the intracellular resistance and membrane capacitance show different behavior in *in-vivo* and *in-vitro* experiments. The *in-vivo* intracellular resistance increases as pressure is increased. The reason for this increase in R_{int} could be the reduced intracellular space, since the reduced intracellular space resists the current flowing cross the cells. This difference between the *in-vivo* and the *in-vitro* results may be due to the fact that in the *in-vitro* tests, the samples are collected after the animals' death while in the *in-vivo* study the subjects are alive and blood flow exists. When the blood supply is cut off in a tissue, the activity of ion pumps reduces and thus the distribution of ions and fluids between intracellular and extracellular spaces changes which leads to cell swelling [76]. Cell swelling increases the intracellular volume which could be a reason for reduction in the intracellular resistance in the *in-vitro* study. Cell swelling also reduces the extracellular pathways and makes them narrower, which is further evidence for the increase in the extracellular resistance [77]. Cell swelling and also release of lysosomal enzymes in the cell, causes rupture in cell membrane [78]. In the post-mortem specimens the cell membrane starts to deteriorate. Thus the cytosol leaves the cell and is mixed with the extracellular fluid [77]. This procedure is accelerated by applying pressure. The reduction in the intracellular fluid and the increase of the extracellular fluid (mixing the intracellular and extracellular fluid at the extracellular space) caused by deterioration of cell membrane and applying pressure might be further explanation of reduction in R_{int} and increase in R_{ext}. Also Demou has mentioned the possibility of reshaping of cells from spherical to oblong orientation which may result in an increase or decrease in electrical properties of tissue [79].

Membrane capacitance in *in-vitro* experiments increases. The value of capacitance is proportional to the area of cell membranes and inversely proportional to the separation between sheets. Cell swelling and applying pressure increases the surface [76] and cell membrane becomes thinner as a result of inflation [75]. Thus a possible explanation for the increase in membrane capacitance might be the decreased distance between two sheets of cell membrane and increased surface of these sheets. However, membrane capacitance decreases as the applied pressure to the *in-vivo* subjects is increased, which according to Dodde *et al.* might be the result of contacting the cell membranes [43].

In this study, the changes in electrical properties of living tissue were also compared contra laterally. The results illustrate the same behavior and the same linear correlation in contralateral parts of human subjects. This observation suggests that the correlation of electrical-mechanical properties of one part of the body is the same as its contralateral part, unless there is an abnormality in one of the contralateral parts. This comparison of electrical-mechanical correlation of contralateral parts of the body can be considered as a method for diagnosis of tumor or any abnormalities within tissue.

The results of *in-vivo* and *in-vitro* strengthen the fact that EIS measurements of *in-vitro* experiments do not represent an exact *in-vivo* environment. This idea strengthens the need to perform more experiments *in-vivo* rather than *in-vitro* in order to get more reliable results in the field of electrical impedance spectroscopy. One possibility for different behavior of *in-vivo* and *in-vitro* results would be the blood flow in the *in-vivo* case. The flowing blood in the living tissue is the most important factor influencing the tissue impedance. Since there is no blood flowing in dead tissue, the changes of its impedance properties do not follow the same pattern as the living tissue.

However, the findings of the current study do not fully support the previous research by Dodde [43]. The reason for this inconsistency may arise from the difference in the experiment protocols of these two studies, thus this is an important issue for future research. Further study should be performed to investigate the effect of pressure on electrical properties of tissue both *in-vivo* and *in-vitro*.

This study also suggests modifying the Cole-Cole model. In the Cole-Cole model, the tissue equivalent resistance and capacitance values are constant; while, according to this study a modified Cole-Cole model should be used in which the parameters are dependent on tissue displacement and elasticity. Knowing the dependency of the Cole-Cole model on the applied pressure, in the second part of this study, the same amount of pressure was applied to all tested tissues for having consistency in the results.

The strong correlation between the electrical properties and mechanical displacements of soft tissue eliminated the need for adding displacement sensors in the final setup. As a result this enables one, by knowing the correlation between the electrical properties and the mechanical displacements of the tissue, to measure the displacement of the tissue when pressure is applied to the tissue without incorporating any displacement sensors.

There were also some limitations in this study which should be eliminated during further experiments. In the *in-vitro* experiment the tissues were tested on a firm foundation and also the samples were not supported by surrounding tissue and bone. However, the same conditions were not present in the *in-vivo* tests. Another limitation of this study is that all the experiments were performed at the room temperature and there is the possibility that the room temperature was not constant during the experiments. As shown by Schwan and Foster, the electrical conductivity of tissue is dependent on temperature [80]. In addition, in the *in-vivo* experiments, a probe was designed for the EIS measurements and pressure was applied to the probe by means of a pressure sensor. The existence of a probe between the pressure sensor and tissue results in transferring pressure to tissue indirectly and thus the applied pressure might not be transferred to the tissue completely. Therefore in the future studies, the design of the probe should be optimized and this error should be reduced as much as possible and finally be eliminated.

In the second part of this study, which involves cancer detection by means of various classification techniques, 32 subjects (22 healthy body positions of 11 subjects and 10 cancerous subjects) were recruited for this study. The electrical admittance spectra of the 32 subjects were measured by a probe containing Ag/AgCl electrodes.

The most commonly used bioimpedance model, Cole-Cole model was then fitted to the data and the 3 electrical properties of the tested tissues were calculated.

Due to high inter subject variation in the electrical properties, it was proposed in this study to normalize the electrical properties of each subject. Since the electrical properties of biologic tissue are significantly dependent on the tissue structure [81], it was postulated in this study that the electrical properties of any tissue with exact structure should be approximately the same. Since each subject's left and right body parts have almost the same tissue structure, it was suggested that their multi-frequency admittance data and, therefore their electrical properties should not be significantly different, unless there is a malignancy in one of the body parts. This hypothesis was statistically tested and the results were promising. The results of section 5.1 revealed that the admittances and the Cole-Cole circuit equivalent electrical parameters of the contralateral sites in healthy subjects are not significantly different, however, the admittances and the Cole-Cole circuit equivalent electrical parameters of the lesions and their contralateral healthy sites are significantly different.

On the basis of the admittance measurements, modeling the lesions and healthy tissue by means of Cole-Cole circuit, the equivalent electrical properties of them were measured and their comparison indicated that extracellular resistance, the intracellular resistance and the cell membrane capacitance were significantly lower in the malignant tissue than the healthy tissue. These results were in line with the previous studies which have shown that the electrical conductivity is significantly higher in tumors than in the healthy tissues [10], [82]–[86]. This could be due to the higher amount of water in the extracellular space in the tumor and also the lower cell membrane density as a result of necrosis [10]. It is also known that the concentration of blood flow is higher in the tumorous area. The more water content and the more blood flow in the tumorous area increases the conductivity of that area. In other words, the resistances in these areas are decreased due to higher amount of water and blood. However, these findings are not supported by the findings of Morimoto *et al.* who have reported a much higher intracellular and extracellular resistances and much lower capacitance in the breast tumors than the healthy breasts [81]. These observations reported by Morimoto have been found by fitting the Cole-Cole model to the impedances in the frequency range of 0

to 200 kHz. However, the Cole-Cole model is usually used for β-dispersion region (5kHz-1MHz). The findings of the current study was in the β-dispersion region, while Morimoto's study wasn't performed in that region, thus this may result in different observations in these two studies.

The postulation of this study was that the electrical properties in the contralateral sites of the body should not be significantly different, unless there is a malignancy in one of the body parts. This postulation was tested statistically and the results were promising. Therefore, the electrical properties of each body part of each subject were normalized with its contralateral properties. Afterwards, three classification techniques were implemented on raw data, extracted features and the normalized extracted features in order to have a comparison.

The three methods were compared in terms of the percentages of accuracy, sensitivity, specificity, resubstitution error and cross validation error. Naïve Bayes classifier with Gaussian distribution in comparison to Naïve Bayes classifier with Kernel distribution in classification of raw data showed a higher specificity and accuracy. It resulted in a lower resubstitution error and cross validation error while the sensitivity of the latter was higher than the former. This may suggest that the Naïve Bayes classifier with Gaussian distribution might be a better classification method in classification of raw admittance data.

In the classification of the extracted features, NB with Kernel distribution showed the highest value of sensitivity, specificity and accuracy and lowest resubstitution error among the three classification methods. On the other hand, NB with Gaussian distribution showed the lowest cross validation error, while SVM showed the weakest performance among all the three classifiers.

After normalizing the extracted features, it was observed that the amount of overlap in the extracted features reduced significantly (see Figure 5.8 and Figure 5.9). Thereafter, the classification methods were applied on the normalized features and the following results were obtained. NB with Kernel distribution showed the highest sensitivity and the lowest cross validation error. Whereas, the NB with Gaussian distribution resulted in a higher specificity. However, the accuracy and resubstitution

error of both NB classifiers were the same. In addition, SVM had the weakest performance among these three classification methods.

Considering each classification method, a significant development was observed in the sensitivity, specificity and the accuracy of them when implemented on the extracted features and then on the normalized features. This result confirmed that the theory of dimension reduction by means of fitting a model to the large data points was a practical idea to increase the performance of classification methods. Moreover, the idea of normalizing each subject's body part's electrical properties by its contralateral properties made a significant improvement in the performance of classification techniques and reduced the errors resulted from the high inter subjects variability of the data. It was also observed that the NB with Kernel distribution which is a more flexible nonparametric technique in comparison to NB with Gaussian distribution may be a better classification technique for these types of data.

Although this study and method was developed for breast cancer detection, the experiments were conducted on biceps and forearms of healthy subjects and subjects with skin cancer. There were lots of limitations in performing human studies on healthy and cancerous breasts. High sensitivity, which was involved in the breast cancer patients, made us perform the experiments on skin cancer patients. Based on a study performed by Grewal *et al*., the electrical bioimpedance of bicep and forearm is the closest electrical bioimpedance to the breast tissue [87]. Therefore, the experiments were conducted on the biceps and forearms of healthy subjects.

One of the challenges in this study was the depth of tumors; the tumors in skin cancer patients are not deep and they are usually on the surface of skin, while the tumors in breast cancer patients are deep inside the body. The depth that the electrical current can penetrate to the tissue is half the distance between the electrodes [57]. Thus, for the purpose of testing the technology on skin cancer patients, a small distance between the electrodes was designed, so that most of the electrical current flowed through the tumor on the skin and the amount of penetration of current to the tissue was small. The probe can be redesigned and the distance between the electrodes can be increased in order to use the probe on breast tissue.

The concepts and results of this study can translate to breast cancer, since the concept of this study was to use the contralateral side of the body as the control. This concept was tested on the skin and can be expanded to any type of tissue including breast tissue. This research group will validate this technology on breast cancer patients in near future.

Chapter 7.

Conclusion and future work

The aim of this study is to benefit from electrical impedance spectroscopy for cancer detection purposes. In the first part of this study, through a widespread experimental investigation, it was observed that EIS is affected by the amount of pressure applied to the soft tissue. Thus, the use of EIS by various physicians is considerably operator and pressure dependent. In the previous studies on EIS for cancer detection, this issue was not considered. However, the aim of this study was to evaluate the effect of pressure on the EIS results.

In the first part of this study, various experimental studies were performed on the different *in-vivo* and *in-vitro* tissues and the correlation of the electrical-mechanical properties of various types of tissues were obtained. In the second part of this study, in order to eliminate the pressure dependency of EIS and have consistent results, the same amount of pressure was applied to the measuring probe while the data were collected from the subjects. However, this pressure was not applied to the electrodes directly and was applied to the probe. Consequently, the pressure might not be transferred completely to the electrodes due to the design of the probe. The design of the probe should be optimized for future studies in order to make sure the pressure is applied to the tissue below the electrodes completely. Moreover, since the electrodes used in this study were pre-gelled electrodes, the pressure applied on the electrodes might change the contact between the electrodes and tissue. In future studies, either the types of electrodes should be changed or a threshold should be defined for the applied pressure, so that the effect of pressure on the contact between the electrodes and tissue would have no significant effect on the correlations of the electrical properties and mechanical displacements.

Although the number of subjects of this study was extremely limited, the outputs of the classification methods are very promising and encourage us to expand this study by increasing the number of both healthy and cancerous subjects in future. Therefore, the long term purpose of this research is to increase the number of subjects and improve the diagnostic accuracy of EIS by developing a computer aided diagnosis (CAD) system besides EIS measurements. It was further observed in the experiments in this group and previous literature that age, gender and even the location on the same body being tested causes a significant difference in the electrical impedance properties of human soft tissue [88]. Thus, combining the electrical impedance data of subjects as well as the mechanical properties of the tested tissues, besides some information about the age, gender and the location of tested tissue by means of a highly complicated decision making system such as neuro-fuzzy algorithms will increase the accuracy of cancer detection by EIS.

The decision making approaches are classified as mathematical model-based methods and flexible model-based techniques [89]. Because of the nonlinearity and variability of human body, deriving an accurate numerical model is difficult, thus the flexible model-based technique will be a better option in this research. Neural networks and fuzzy logic are among the flexible model-based classifiers. Diagnostic knowledge from expertise as well as using the linguistic rules of fuzzy logic and its concept of formulation of expert knowledge in fuzzy IF-THEN rules in a way to mimic human brain in forecasting tasks, make the fuzzy system an appropriate method. Although, fuzzy systems are not capable of learning, the fuzzy membership functions (MFs) can be optimized by means of NNs. Incorporating adaptive neuro-fuzzy approaches in the decision making process gets benefit from the advantages of both NNs and FL.

Data that have been collected through this research and the concept of comparison of anomaly to its contralateral site have fuzziness in nature and their definitions are quite vague. The IF-THEN rules will be determined by experience based on the comparison of the extracted features of the anomaly and its contralateral site; concurrently the NNs optimize the fuzzy MF parameters.

In order to have a well-trained neuro-fuzzy system, sufficient data sets are needed. The number of data sets must be at least five times the number of the parameters to be updated [90]. Thus the bio-impedance measurements will be tested on a number of healthy as well as cancerous subjects, in order to provide a sufficient number of data sets to the neuro-fuzzy classifier system in future.

References

[1] C. A. Muro-Cacho, K. Rosario-Ortiz, S. Livingston, and T. Muñoz-Antonia, “Defective transforming growth factor beta signaling pathway in head and neck squamous cell carcinoma as evidenced by the lack of expression of activated Smad2.,” *Clin. Cancer Res.*, vol. 7, pp. 1618–1626, 2001.

[2] R. C. Laver, M. W. Reed, B. J. Harrison, and P. D. Newton, “The management of women with breast symptoms referred to secondary care clinics in Sheffield: implications for improving local services.,” *Ann. R. Coll. Surg. Engl.*, vol. 81, no. 4, pp. 242–7, Jul. 1999.

[3] S. Laufer and B. Rubinsky, “Tissue characterization with an electrical spectroscopy SVM classifier,” *IEEE Trans. Biomed. Eng.*, vol. 56, pp. 525–528, 2009.

[4] M. Wu and D. E. Burstein, “Fine Needle Aspiration,” Sep. 2004.

[5] B. D. Florentine, C. J. Cobb, K. Frankel, T. Greaves, and S. E. Martin, “Core needle biopsy. A useful adjunct to fine-needle aspiration in select patients with palpable breast lesions.,” *Cancer*, vol. 81, no. 1, pp. 33–9, Mar. 1997.

[6] A. B. Nover, S. Jagtap, W. Anjum, H. Yegingil, W. Y. Shih, W.-H. Shih, and A. D. Brooks, “Modern breast cancer detection: a technological review.,” *Int. J. Biomed. Imaging*, vol. 2009, p. 902326, Jan. 2009.

[7] C. Di Maggio, “State of the art of current modalities for the diagnosis of breast lesions,” in *Breast Cancer: Nuclear Medicine in Diagnosis and Therapeutic Options*, 2008, pp. 99–126.

[8] B. Cady and M. Chung, “Mammographic Screening: No Longer Controversial.,” *American Joutrnal of Clinical Oncology*, 2005. .

[9] T. Morimoto, S. Kimura, Y. Konishi, K. Komaki, T. Uyama, Y. Monden, D. Y. Kinouchi, and D. T. Iritani, “A Study of the Electrical Bio-impedance of Tumors,” Jul. 2009.

[10] S. Laufer, A. Ivorra, V. E. Reuter, B. Rubinsky, and S. B. Solomon, “Electrical impedance characterization of normal and cancerous human hepatic tissue.,” *Physiol. Meas.*, vol. 31, pp. 995–1009, 2010.

[11] B. S. Kim, D. Isaacson, H. Xia, T.-J. Kao, J. C. Newell, and G. J. Saulnier, “A method for analyzing electrical impedance spectroscopy data from breast cancer patients.,” *Physiol. Meas.*, vol. 28, pp. S237–S246, 2007.

[12] A. Keshtkar, A. Keshtkar, and R. H. Smallwood, “Electrical impedance spectroscopy and the diagnosis of bladder pathology.,” *Physiol. Meas.*, vol. 27, pp. 585–596, 2006.

[13] Y. Zou and Z. Guo, “A review of electrical impedance techniques for breast cancer detection,” *Medical Engineering and Physics*, vol. 25. pp. 79–90, 2003.

[14] H. Fricke and S. Morse, “The Electric Capacity of Tumors of the Breast,” *J. Cancer Res.*, vol. 10, no. 3, pp. 340–376, Oct. 1926.

[15] J. Jossinet, “Variability of impedivity in normal and pathological breast tissue,” *Med. Biol. Eng. Comput.*, vol. 34, pp. 346–350, 1996.

[16] B. H. Brown, J. Tidy, K. Boston, A. D. Blackett, and F. Sharp, “Tetrapolar measurement of cervical tissue structure using impedance spectroscopy,” *Proc. 20th Annu. Int. Conf. IEEE Eng. Med. Biol. Soc. Vol.20 Biomed. Eng. Towar. Year 2000 Beyond (Cat. No.98CH36286)*, vol. 6, 1998.

[17] C. Gonzalez-Correa, C. A. González-Correa, B. H. Brown, R. H. Smallwood, D. C. Walker, and K. D. Bardhan, “Electrical bioimpedance readings increase with higher pressure applied to the measuring probe.,” *… Meas.*, vol. 26, no. 2, pp. 39–47, 2005.

[18] K. Cole, “PERMEABILITY AND IMPERMEABILITY OF CELL MEMBRANES FOR IONS,” *Cold Spring Harb. Symp. Quant. Biol.*, vol. 8, 1940.

[19] R. Liu, X. Dong, F. Fu, F. You, X. Shi, Z. Ji, and K. Wang, “Multi-frequency parameter mapping of electrical impedance scanning using two kinds of circuit model.,” *Physiol. Meas.*, vol. 28, no. 7, pp. 85–100, 2007.

[20] H. P. SCHWAN, “Electrical properties of tissue and cell suspensions.,” *Adv. Biol. Med. Phys.*, vol. 5, pp. 147–209, Jan. 1957.

[21] U. Birgersson, “Electrical Impedance of Human Skin and Tissue Alterations : Mathematical Modeling and Measurements,” 2012.

[22] J. Harris, M. Lippman, C. Osborne, and M. Morrow, *Diseases of the Breast*. 2012.

[23] a a Fischer, “Pressure algometry over normal muscles. Standard values, validity and reproducibility of pressure threshold.,” *Pain*, vol. 30, pp. 115–126, 1987.

[24] P. Wellman and R. Howe, “Breast tissue stiffness in compression is correlated to histological diagnosis,” *Harvard BioRobotics …*, pp. 1–15, 1999.

[25] A. P. Sarvazyan, A. R. Skovoroda, and Y. P. Pyt’ev, “Mechanical introscopy-a new modality of medical imaging for detection of breast and prostate cancer,” *Proc. Eighth IEEE Symp. Comput. Med. Syst.*, 1995.

[26] A. Galea, “Mapping Tactile Imaging Information: Parameter Estimation and Deformable Registration,” Harvard University, 2004.

[27] B. S. Garra, E. I. Cespedes, J. Ophir, S. R. Spratt, R. A. Zuurbier, C. M. Magnant, and M. F. Pennanen, “Elastography of breast lesions: initial clinical results.,” *Radiology*, vol. 202, pp. 79–86, 1997.

[28] T. L. Chenevert, A. R. Skovoroda, M. O’Donnell, and S. Y. Emelianov, “Elasticity reconstructive imaging by means of stimulated echo MRI,” *Magn. Reson. Med.*, vol. 39, pp. 482–490, 1998.

[29] M. Zhang, Y. P. Zheng, and A. F. T. Mak, “Estimating the effective Young’s modulus of soft tissues from indentation tests—nonlinear finite element analysis of effects of friction and large deformation,” *Med. Eng. Phys.*, vol. 19, no. 6, pp. 512–517, Sep. 1997.

[30] R. Muthupillai, D. J. Lomas, P. J. Rossman, J. F. Greenleaf, A. Manduca, and R. L. Ehman, “Magnetic resonance elastography by direct visualization of propagating acoustic strain waves.,” *Science*, vol. 269, pp. 1854–1857, 1995.

[31] W. C. Hayes, L. M. Keer, G. Herrmann, and L. F. Mockros, “A mathematical analysis for indentation tests of articular cartilage.,” *J. Biomech.*, vol. 5, pp. 541–551, 1972.

[32] T. A. Krouskop, T. M. Wheeler, F. Kallel, B. S. Garra, and T. Hall, “Elastic moduli of breast and prostate tissues under compression,” *Ultrason. Imaging*, vol. 20, no. 4, pp. 260–274, 1998.

[33] Y. C. Fung, *Biomechanics: Mechanical Properties of living tissues*. New York: New York: Springer-Verlag., 1993.

[34] J. P. A. Arokoski, J. Surakka, T. Ojala, P. Kolari, and J. S. Jurvelin, “Feasibility of the use of a novel soft tissue stiffness meter.,” 2005.

[35] T. Lyyra, J. Jurvelin, P. Pitkanen, U. Vaatainen, and I. Kiviranta, “Indentation instrument for the measurement of cartilage stiffness under arthroscopic control,” *Med. Eng. Phys.*, vol. 17, pp. 395–399, 1995.

[36] T. Krouskop, T. Wheeler, and F. Kallel, “Elastic moduli of breast and prostate tissues under compression,” *Ultrason. Imaging*, vol. 20, no. 4, pp. 260–274, 1998.

[37] J. J. O’Hagan and A. Samani, “Measurement of the hyperelastic properties of tissue slices with tumour inclusion.,” *Phys. Med. Biol.*, vol. 53, no. 24, pp. 7087–106, Dec. 2008.

[38] J. Jossinet, “The impedivity of freshly excised human breast tissue,” *Physiol. Meas.*, vol. 19, no. 1, pp. 61–75, 1998.

[39] F. Kallel and J. Ophir, “Tissue mechanical attributes imaging: principles and methods,” in *… -Based Medical Systems, 2000. CBMS 2000. …*, 2000, pp. 147–159.

[40] J. Bercoff, S. Chaffai, and M. Tanter, “In vivo breast tumor detection using transient elastography,” *Ultrasound Med. …*, vol. 29, no. 10, pp. 1387–1396, 2003.

[41] A. Surowiec and S. Stuchly, “Dielectric properties of breast carcinoma and the surrounding tissues,” *… , IEEE Trans.*, vol. 35, no. 4, pp. 257–263, 1988.

[42] H. Fricke and S. Morse, “The electric capacity of tumors of the breast,” *J. Cancer Res.*, vol. 10, pp. 340–376, 1926.

[43] R. Dodde, J. Bull, and A. Shih, “Bioimpedance of soft tissue under compression,” *Physiol. Meas.*, vol. 33, pp. 1095–1109, 2012.

[44] C. Gonzalez-Correa, “Electrical bioimpedance readings increase with higher pressure applied to the measuring probe,” *… Meas.*, vol. 26, no. 2, pp. 39–47, 2005.

[45] B. Belmont, R. Dodde, and A. Shih, “Impedance of tissue-mimicking phantom material under compression,” *J. Electr. Bioimpedance*, vol. 4, pp. 2–12, 2013.

[46] R. Liu, X. Dong, F. Fu, F. You, and X. Shi, “Multi-frequency parameter mapping of electrical impedance scanning using two kinds of circuit model,” *Physiol. …*, vol. 28, no. 7, pp. 85–100, 2007.

[47] K. Cole and R. Cole, “Dispersion and absorption in dielectrics I. Alternating current characteristics,” *J. Chem. Phys.*, vol. 9, pp. 341–351, 1941.

[48] C. Tronstad and A. H. Pripp, “Statistical methods for bioimpedance analysis,” *J. Electr. Bioimpedance*, vol. 5, no. 1, pp. 14–27, Apr. 2014.

[49] J. Estrela da Silva, J. P. Marques de Sá, and J. Jossinet, “Classification of breast tissue by electrical impedance spectroscopy,” *Medical & Biological Engineering & Computing*, vol. 38. pp. 26–30, 2000.

[50] B. Zheng, D. Lederman, J. H. Sumkin, M. L. Zuley, M. Z. Gruss, L. S. Lovy, and D. Gur, “A Preliminary Evaluation of Multi-probe Resonance-frequency Electrical Impedance Based Measurements of the Breast,” *Acad. Radiol.*, vol. 18, pp. 220–229, 2011.

[51] Bharathi, “Efficient Classification of Cancer using Support Vector Machines and Modified Extreme Learning Machine based on Analysis of Variance Features,” *American Journal of Applied Sciences*, vol. 8. pp. 1295–1301, 2011.

[52] M. R. Daliri, “Combining extreme learning machines using support vector machines for breast tissue classification.,” *Comput. Methods Biomech. Biomed. Engin.*, 2013.

[53] A. Al Amin, S. Parvin, M. a Kadir, T. Tahmid, S. K. Alam, and K. Siddique-E Rabbani, “Classification of breast tumour using electrical impedance and machine learning techniques.,” *Physiol. Meas.*, vol. 35, pp. 965–74, 2014.

[54] Y. Wu and S. C. Ng, “Combining neural learners with the naive bayes fusion rule for breast tissue classification,” in *ICIEA 2007: 2007 Second IEEE Conference on Industrial Electronics and Applications*, 2007, pp. 709–713.

[55] S. Zaeimdar, “Mechanical Characterization of Breast Tissue Constituents for Cancer Assessment.” 25-Feb-2014.

[56] B. Rigaud, L. Hamzaoui, M. R. Frikha, N. Chauveau, and J.-P. Morucci, “In vitro tissue characterization and modelling using electrical impedance measurements in the 100 Hz-10 MHz frequency range,” *Physiol. Meas.*, vol. 16, no. 3A, pp. A15–A28, Aug. 1995.

[57] O. Martinsen and S. Grimnes, *Bioimpedance and bioelectricity basics*. 2011, pp. 1–471.

[58] Y. Yang, W. Ni, and Q. Sun, “Improved Cole parameter extraction based on the least absolute deviation method,” *Physiol. …*, vol. 34, no. 10, pp. 1239–1252, 2013.

[59] K. Chen, Z. Ying, H. Zhang, and L. Zhao, “Analysis of least absolute deviation,” *Biometrika*, vol. 95, no. 1, pp. 107–122, 2008.

[60] W. . Hayes, L. . Keer, G. Herrmann, and L. . Mockros, “mathematical analysis for indentation tests of articular cartilage,” *J. Biomech.*, vol. 5, no. 5, pp. 541–551, 1972.

[61] R. Dua, D. G. Beetner, W. V Stoecker, and D. C. Wunsch, “Detection of basal cell carcinoma using electrical impedance and neural networks.,” *IEEE Trans. Biomed. Eng.*, vol. 51, no. 1, pp. 66–71, Jan. 2004.

[62] P. Sangitab and S. R. Deshmukh, “Use of Support Vector Machine, decision tree and Naive Bayesian techniques for wind speed classification,” in *2011 International Conference on Power and Energy Systems, ICPS 2011*, 2011.

[63] I. Rish, “An empirical study of the naive Bayes classifier,” *IJCAI 2001 Work. Empir. methods AI*, pp. 41–46, 2001.

[64] T. Mitchell, *Machine Learning*. McGraw-Hill, 1997.

[65] A. Gelbukh and C. A. Reyes-Garcia, Eds., *MICAI 2006: Advances in Artificial Intelligence*, vol. 4293. Berlin, Heidelberg: Springer Berlin Heidelberg, 2006.

[66] E. Parzen, “On Estimation of a Probability Density Function and Mode on JSTOR,” *The Annals of Mathematical Statistics*, 1962. .

[67] Y. Murakami and K. Mizuguchi, “Applying the Naive Bayes classifier with kernel density estimation to the prediction of protein-protein interaction sites,” *Bioinformatics*, vol. 26, pp. 1841–1848, 2010.

[68] J. P. Morucci and B. Rigaud, “Bioelectrical impedance techniques in medicine. Part III: Impedance imaging. Third section: medical applications.,” *Crit. Rev. Biomed. Eng.*, vol. 24, no. 4–6, pp. 655–77, Jan. 1996.

[69] K. R. Foster and H. P. Schwan, “Dielectric properties of tissues and biological materials: a critical review.,” *Crit. Rev. Biomed. Eng.*, vol. 17, no. 1, pp. 25–104, Jan. 1989.

[70] D. Cramer and D. L. Howitt, *The SAGE Dictionary of Statistics: A Practical Resource for Students in the Social Sciences*. SAGE Publications, 2004, p. 208.

[71] D. Doane and L. Seward, “Measuring skewness: a forgotten statistic,” *J. Stat. Educ.*, 2011.

[72] S. Shapiro and M. Wilk, “An analysis of variance test for normality (complete samples),” *Biometrika*, 1965.

[73] N. Razali and Y. Wah, “Power comparisons of shapiro-wilk, kolmogorov-smirnov, lilliefors and anderson-darling tests,” *J. Stat. Model. Anal.*, 2011.

[74] E. McAdams and J. Jossinet, “Tissue impedance: a historical overview,” *Physiol. Meas.*, vol. 16, pp. A1–A13, 1995.

[75] Y. Konishi, T. Morimoto, Y. Kinouchi, T. Iritani, and Y. Monden, “Electrical properties of extracted rat liver tissue,” vol. 195, pp. 183–192, 1995.

[76] D. Haemmerich, R. Ozkan, S. Tungjitkusolmun, J. Z. Tsai, D. M. Mahvi, S. T. Staelin, and J. G. Webster, “Changes in electrical resistivity of swine liver after occlusion and postmortem.,” *Med. Biol. Eng. Comput.*, vol. 40, no. 1, pp. 29–33, Jan. 2002.

[77] D. Miklavacic, N. Pavselj, and F. X. Hart, *Wiley encyclopedia of biomedical engineering*. 2006, pp. 1–12.

[78] J. L. Farber, K. R. Chien, and S. J. Mittnacht, “The Pathogenesis of irreversible cell Injury in Ischemia,” vol. 102, pp. 271–281, 1981.

[79] Z. Demou, “Gene expression profiles in 3D tumor analogs indicate compressive strain differentially enhances metastatic potential,” *Ann. Biomed. Eng.*, vol. 38, no. 11, pp. 3509–3520, 2010.

[80] H. Schwan and K. Foster, “RF-field interactions with biological systems: electrical properties and biophysical mechanisms,” *Proc. IEEE*, vol. 68, no. 1, pp. 104–113, 1980.

[81] T. Morimoto, S. Kimura, Y. Konishi, K. Komaki, T. Uyama, Y. Monden, Y. Kinouchi, and T. Iritani, “A study of the electrical bio-impedance of tumors.,” *J. Invest. Surg.*, vol. 6, pp. 25–32, 1993.

[82] S. R. Smith, K. R. Foster, and G. L. Wolf, “Dielectric Properties of VX-2 Carcinoma Versus Normal Liver Tissue,” *IEEE Transactions on Biomedical Engineering*, vol. BME-33. pp. 522–524, 1986.

[83] D. Haemmerich, S. T. Staelin, J. Z. Tsai, S. Tungjitkusolmun, D. M. Mahvi, and J. G. Webster, “In vivo electrical conductivity of hepatic tumours.,” *Physiol. Meas.*, vol. 24, pp. 251–260, 2003.

[84] P. R. Stauffer, F. Rossetto, M. Prakash, D. G. Neuman, and T. Lee, “Phantom and animal tissues for modelling the electrical properties of human liver,” *Int. J. Hyperth.*, vol. 19, pp. 89–101, 2003.

[85] A. P. O’Rourke, M. Lazebnik, J. M. Bertram, M. C. Converse, S. C. Hagness, J. G. Webster, and D. M. Mahvi, “Dielectric properties of human normal, malignant and cirrhotic liver tissue: in vivo and ex vivo measurements from 0.5 to 20 GHz using a precision open-ended coaxial probe.,” *Phys. Med. Biol.*, vol. 52, pp. 4707–4719, 2007.

[86] D. Haemmerich, D. J. Schutt, A. W. Wright, J. G. Webster, and D. M. Mahvi, “Electrical conductivity measurement of excised human metastatic liver tumours before and after thermal ablation.,” *Physiol. Meas.*, vol. 30, pp. 459–466, 2009.

[87] F. Golnaraghi and P. K. Grewal, “Pilot study: electrical impedance based tissue classification using support vector machine classifier,” *IET Sci. Meas. Technol.*, vol. 9, Jun. 2014.

[88] I. Nicander, M. Nyren, L. Emtestam, and S. Ollmar, “Baseline electrical impedance measurements at various skin sites - related to age and sex,” *Ski. Res. Technol.*, vol. 3, no. 4, pp. 252–258, Nov. 1997.

[89] R. Isermann, “Supervision, fault-detection and fault-diagnosis methods — An introduction,” *Control Eng. Pract.*, vol. 5, no. 5, pp. 639–652, May 1997.

[90] W. Wang, F. Ismail, and F. Golnaraghi, “A neuro-fuzzy approach to gear system monitoring,” *Fuzzy Syst. IEEE …*, vol. 12, no. 5, pp. 710–723, 2004.

Appendix A.

Standard operation procedures- preparation of animal tissue samples

Simon Fraser University

Standard Operating Procedure

Preparation of Animal Tissue Samples

Date: November 2013

Author: Sepideh Mohammadi Moqadam

Principle Investigator: Dr. Farid Golnaraghi

Summary: The following SOP explains how to prepare animal samples.

Key Words: Sample dissection

Materials:

Latex gloves, lab coat, protective goggles, bleach, clear disposal bags, red sharp apparatus container, masks, labels, paper towels, cutter, permanent marker, plastic storage container, digital caliper, flat plate, ruler, sponge

Preparing required apparatus:

Place clear disposal bags, red sharp apparatus containing cutters, paper towels, marker, digital caliper and flat plate on the counter.

Preparing test samples:

1. Place animal tissue on flat plate.
2. Using marker and ruler, mark a rectangular shape in the wanted size on the tissue.
3. Using cutter, make the cuts on the marked area into the target tissue.
4. Separate the parallel faced cut from the rest of the tissue and prepare rectangular specimens by cutting rectangular cross sections.
5. Measure sample sizes using digital caliper, three times each sample, and record the averages.
6. Place the final test samples into small clear bags with labels (showing name and dimensions).

Clean up:

1. Package all unused tissue into clear bags with labels showing name, species and date, and keep in freezer.
2. Wipe all used surfaces with soaped sponge and water, and clean finally by bleach spraying.
3. Place all working tools in water and bleach solution (90:10) for 20 minutes.
4. Rinse tools in hot water tank using a sponge, and dry them with paper towel.
5. Return sharp tools to the red container.

Appendix B.

Standard operating procedures-performing electrical impedance spectroscopy measurements as well as compression testing on animal tissue specimens

Simon Fraser University

Standard Operating Procedure

Performing Electrical Impedance Spectroscopy Measurements as well as Compression Testing on Animal Tissue Specimens

Date: November 2013

Author: Sepideh Mohammadi Moqadam

Principle Investigator: Dr. Farid Golnaraghi

Summary: The following SOP describes how to set up the HF2IS Zurich Instrument as well as the FingerTPS wearable force sensors for performing EI measurements and compression testing of animal samples.

Key Words: Electrical Impedance Spectroscopy, Compression testing, Animal

Materials:

HF2IS Electrical Impedance Spectroscope, FingerTPS wearable force sensors by PPS, latex gloves, lab coat, protective goggles, ethanol, bleach, clear disposal bags, red sharp apparatus container, masks, labels, paper towels, plastic storage container, sponge

Preparing test setup:

1. Switch on the HF2IS Zurich Instrument and attach the cables to it for EIS measurements.
2. Switch on the load sensor and the customized software “Chameleon TVR”, available with PPS sensors
3. Wear three FingerTPS force sensors over your fingers
4. Calibrate the finger wearable sensors by the software “Chameleon”.
5. Attach the disposable pre-gelled Ag/AgCl electrodes to the top and bottom of the animal samples.
6. Attach the two cables from the HF2IS to the two electrodes.
5. Run the MATLAB code and collect the data.

Test Protocol:

1. Dissect and organize testing samples following SOP of Preparation of Animal Tissue Samples.
2. Pick up sample from clear bag and place on a flat plate.
3. Prepare the test setup and attach the electrodes as explained.
4. Place the force sensors worn over your fingers on top of the upper electrode attached to the sample.
5. Apply pressure to the electrode and sample by the finer force sensors.
6. Keep the pressure constant by monitoring the amount of pressure presented in the available software.
7. Run the MATLAB code and start data acquisition at one pressure level.
8. Once the data acquisition is completed at one pressure level, increase the amount of pressure and redo the experiment.
9. When the experiment is completed, detach the electrodes.
10. Place the electrodes inside waste clear bag with proper label.
11. Place the tested specimen inside waste clear bag with proper label.
12. Repeat steps 1 to 12 to test all samples.

Clean up:

1. Switch off the HF2IS, load sensor and the computer used in the experiment.
2. Remove all the cables and electrodes from HF2IS.
3. Dispose of all unused tissue and phantoms
4. Place all working tools in a 10% bleach solution for 20 minutes.
5. Clean up all the working surfaces using sponge soaked with water.
6. Store collected data in a flash drive.